

LIVING RADICAL POLYMERIZATION OF HYDROXYETHYL
METHACRYLATE AND ITS BLOCK COPOLYMERIZATION WITH
POLY(DIMETHYL SILOXANE) MACROAZOINITIATOR

A THESIS SUBMITTED TO
THE GRADUATE SCHOOL OF NATURAL AND APPLIED SCIENCES
OF
MIDDLE EAST TECHNICAL UNIVERSITY

BY

ELİF VARGÜN

IN PARTIAL FULFILLMENT OF THE REQUIREMENTS
FOR
THE DEGREE OF DOCTOR OF PHILOSOPHY
IN
POLYMER SCIENCE AND TECHNOLOGY

JUNE 2009

Approval of the thesis:

**LIVING RADICAL POLYMERIZATION OF HYDROXYETHYL
METHACRYLATE AND ITS BLOCK COPOLYMERIZATION WITH
POLY(DIMETHYL SILOXANE) MACROAZOINITIATOR**

submitted by **ELİF VARGÜN** in partial fulfillment of the requirements for the degree
of **Doctor of Philosophy in Polymer Science and Technology Department, Middle
East Technical University** by,

Prof. Dr. Canan Özgen _____
Dean, Graduate School of **Natural and Applied Sciences**

Prof. Dr. Cevdet Kaynak _____
Head of Department, **Metallurgical and Materials Engineering**

Prof. Dr. Ali Usanmaz _____
Supervisor, **Chemistry Dept., METU**

Examining Committee Members:

Prof. Dr. Zuhâl Küçükyavuz _____
Chemistry Dept., METU

Prof. Dr. Ali Usanmaz _____
Chemistry Dept., METU

Prof. Dr. Duygu Kısakürek _____
Chemistry Dept., METU

Prof. Dr. Serpil Aksoy _____
Chemistry Dept., Gazi University

Prof. Dr. Kemal Alyürük _____
Chemistry Dept. METU

Date: 11/06/2009

I hereby declare that all information in this document has been obtained and presented in accordance with academic rules and ethical conduct. I also declare that, as required by these rules and conduct, I have fully cited and referenced all material and results that are not original to this work.

Name, Last name: Elif Vargün

Signature:

ABSTRACT

LIVING RADICAL POLYMERIZATION OF HYDROXYETHYL METHACRYLATE AND ITS BLOCK COPOLYMERIZATION WITH POLY(DIMETHYL SILOXANE) MACROAZOINITIATOR

Vargün, Elif

Ph.D., Department of Polymer Science and Technology

Supervisor: Prof. Dr. Ali Usanmaz

June 2009, 145 pages

Hydrophilic poly(2-hydroxyethyl methacrylate), PHEMA, and hydrophobic poly(dimethyl siloxane), PDMS, segments containing copolymers have been widely used as a biomaterial. These amphiphilic copolymers also used as an emulsifying agent in polymer solutions and compatibilizer in polymer blends. In this case, solution polymerizations of HEMA by radiation, ATRP and RAFT methods were studied. The thermal degradation mechanism of PHEMA, which was prepared in aqueous solution by gamma radiation technique, was studied in detail. The DSC, TGA and Mass Spectroscopy analyses revealed that the degradation is linkage and depolymerization with a combination of monomer fragmentation. The ATRP of HEMA was performed with ethyl-2-bromoisobutyrate (EBriB) initiator and CuCl/bipyridine catalyst in MEK/1-propanol solvent mixture. Cu(II) complexes and PHEMA obtained via ATRP were characterized by UV-vis, FTIR and ¹H-NMR analysis. The RAFT polymerization of HEMA with different [RAFT]/[AIBN] ratios were also investigated in three solvents

(methyl ethylketone, ethyl acetate and toluene). The controlled polymerization of HEMA with the ratio of [RAFT]/ [AIBN]=18 at 80 °C in MEK and ethyl acetate, shows the first-order kinetic up to the nearly 40 % conversion Macroazoinitiator PDMS-MAI was synthesized from bifunctional PDMS and then copolymerized with MMA, EMA, HEMA and TMS-HEMA monomers Different characterization methods such as FTIR, ¹H-NMR, solid state NMR, GPC, XPS, SEM, DSC, etc. have been used for the characterization of block copolymers. P(DMS-b-TMSHEMA) was converted to the P(DMS-b-HEMA) block copolymer by deprotection of TMS groups. The phase separated morphology was observed for the P(DMS-b-HEMA) copolymer, which was different from P(DMS-b-MMA) and P(DMS-b-EMA) copolymers.

Keywords: Poly(hydroxyethyl methacrylate), thermal degradation, ATRP, RAFT, PDMS macroazoinitiator

ÖZ

HİDROKSİETİL METAKRİLATIN YAŞAYAN RADİKAL POLİMERLEŞMESİ VE POLİ(DİMETİL SİLOKSAN) MAKROBAŞLATICI İLE BLOK KOPOLİMERLEŞMESİ

Vargün, Elif

Doktora, Polimer Bilimi ve Teknolojisi Bölümü

Tez Yöneticisi: Prof. Dr. Ali Usanmaz

Haziran 2009, 145 sayfa

Hidrofilik poli(2-hidroksietil metakrilat), PHEMA, ve hidrofobik poli(dimetil siloksan), PDMS segment içeren kopolimerler biyomalzeme olarak sıklıkla kullanılır. Bu amfifilik kopolimerler ayrıca polimer çözeltilerinde emülsiyonlaştırıcı ve polimer karışımlarında uyum sağlayıcı olarak kullanılmaktadır. Bu amaçla, HEMA'nın radyasyonla çözelti polimerleşmesi, ATRP ve RAFT metotları çalışıldı. Radyasyonla sulu çözelti polimerleşmesi ile elde edilen PHEMA'nın ısıl bozunma mekanizması detaylıca çalışıldı. DSC, TGA ve Kütle Spektroskopisi analizleri bozunmanın, bağlanma ve monomer parçalanması ile depolimerleşme şeklinde olduğunu gösterdi. HEMA'nın ATRP polimerleşmesi etil-2-bromoizobutirat (EBriB) başlatıcı ve CuCl/bipiridin katalizörü ile MEK/1-propanol çözücü karışımında yapıldı. Cu(II) kompleksleri ve ATRP ile elde edilen PHEMA polimerleri UV-vis, FTIR and ¹H-NMR teknikleriyle karakterize edildi. Ayrıca, HEMA RAFT yöntemiyle farklı [RAFT]/[AIBN] oranlarında ve üç farklı çözücüde (metil etilketon, etil asetat ve toluen) polimerleştirildi. HEMA'nın [RAFT]/ [AIBN]= 18 oranında, 80 °C de MEK ve etil asetat çözücülerinde kontrollü polimerleşmesi yüzde 40 dönüşüme kadar birinci

dereceden kinetik göstermiştir. Makrobařlatıcı PDMS-MAI iki fonksiyonlu PDMS'den sentezlenmiş ve daha sonra MMA, EMA, HEMA and TMS-HEMA monomerleri ile kopolimerleştirilmiştir. Blok kopolimerlerin karakterizasyonunda FTIR, ¹H-NMR, katı faz NMR, GPC, XPS,SEM ve DSC gibi farklı yöntemler kullanılmıştır. P(DMS-b-TMSHEMA) kopolimeri P(DMS-b-HEMA) blok kopolimerine silil grupların uzaklaştırılması yoluyla dönüřtürülmüřtür. P(DMS-b-MMA) ve P(DMS-b-EMA) kopolimerlerinden farklı olarak P(DMS-b-HEMA) kopolimerinde fazlara ayrılmış bir morfoloji görülmüřtür.

Anahtar Kelimeler: Poli(2-hidroksietil metakrilat), ısıl bozunma, ATRP, RAFT, PDMS makrobařlatıcı .

To My Family

ACKNOWLEDGEMENTS

I would like to express my gratitude to my supervisor Prof. Dr. Ali Usanmaz for his guidance, encouragement, and support throughout the research. He supplied all opportunities in his laboratory. He always has a practical and a positive thinking and this approach will be a model in my future life.

I would like to express my acknowledgements to Prof. Dr. Duygu Kısakürek and Prof. Dr. Serpil Aksoy for their valuable suggestions, comments and discussions during progress of the study. These meetings influenced my research plan deeply and organized me. I would also like to thank all the excellent Professors at METU whose courses forced me to think the structure-property relationship in polymer synthesis.

I would like to thank to Bengi Aran and Elif Kemeröz for being my good friends. Memories, shared funny times in laboratory and their helps have never been forgotten.

I would like to express my appreciations to METU Central Laboratory specialists Dr. Eda Ayşe Aksoy, Dr. Selda Keskin and Leyla Molu. They showed great patience and assistance to me during characterization experiments.

My sincere appreciation goes to my labmate and PST-502 Lab. colleague Selin Kozanoğlu for her help and understanding during this study. I would like to thank to my last PST-502 Lab. colleagues Dr. Güralp Özkoç and Olcay Mert for their helps. I am also grateful to Mrs. Suzanne M. Usanmaz for spell checking during the writing of thesis. Also I would like to thank to Dr. Seha Tirkeş for supporting me morally.

All the members of Chemistry Department, B-36,37,39 Lab. members and technician Osman Yaslıtaş are greatfully acknowledged.

I would also like to thank to Muğla University for the financial support during my thesis in Faculty Development Program (ÖYP).

Finally, I would like to thank to my warm family, my mother, my father and my brother, for their endless love and patience. I will always feel your love in my heart and I know how lucky I am with having such an excellent family.

TABLE OF CONTENTS

| | |
|--|-----|
| ABSTRACT | iv |
| ÖZ..... | vi |
| ACKNOWLEDGEMENTS..... | ix |
| TABLE OF CONTENTS..... | xi |
| LIST OF TABLES | xv |
| LIST OF FIGURES..... | xvi |
| ABBREVIATIONS..... | xx |
| CHAPTERS..... | 1 |
| 1. INTRODUCTION..... | 1 |
| 1.1 Polymerization and/or copolymerization of HEMA with different techniques..... | 3 |
| 1.1.1 Free Radical Aqueous Polymerization of HEMA | 4 |
| 1.1.2 Atom Transfer Radical Polymerization (ATRP)..... | 6 |
| 1.1.3 Literature Review on ATRP polymerization of HEMA | 11 |
| 1.1.4 Reversible Addition Fragmentation Chain Transfer (RAFT) Polymerizn.... | 12 |
| 1.1.5 Literature Review of RAFT polymerization of HEMA | 14 |
| 1.2 Block Copolymer Synth. of Polymethacrylates with PDMS Macroazoinitiator . | 16 |
| 1.3 The Aim of This Study | 19 |
| 2. EXPERIMENTAL | 20 |
| 2.1 Aqueous Solution Polymerization of HEMA by Gamma Radiation..... | 20 |
| 2.2 Atom Transfer Radical Polymerization of HEMA | 20 |
| 2.2.1 Materials for the synthesis of PHEMA by ATRP | 20 |
| 2.2.2 Synthesis of Cu(I) and Cu(II) complexes..... | 21 |
| 2.2.3 Method for PHEMA Synthesis via ATRP | 22 |
| 2.2.4 Synthesis of 2-[(trimethylsilyl)oxy]ethyl methacrylate (TMS-HEMA) and its polymerization and copolymerization with PDMS via ATRP..... | 23 |

| | |
|--|----|
| 2.3. Reversible Addition-Fragmentation Chain Transfer Polymerization of HEMA | 24 |
| 2.3.1 Materials for the synthesis of RAFT agent and PHEMA..... | 25 |
| 2.3.2 Preparation of RAFT Agent (2-phenylprop-2-yl dithiobenzoate , CDB) | 25 |
| 2.3.3 Method for PHEMA Synthesis via RAFT | 27 |
| 2.3.4 Method for P(HEMA-b-DMS) block copolymer synthesis (RAFT) | 27 |
| 2.4 Block Copolymer Synthesis using PDMS Macroazoinitiator..... | 27 |
| 2.4.1 Materials for Synth. of PDMS Macroazoinitiator and Block Copolymers... | 27 |
| 2.4.2 Synthesis of Macroazoinitiator, PDMS-MAI | 28 |
| 2.4.3 Method for Block Copolymers with PDMS Macroazoinitiator..... | 30 |
| 2.5 Polymer Characterization Methods | 34 |
| 2.5.1 Fourier Transform Infrared Spectroscopy (FTIR)..... | 34 |
| 2.5.2 Nuclear Magnetic Resonance Spectroscopy (¹ H-NMR)..... | 35 |
| 2.5.3 Gas Chromatography Mass Spectrometry(GC-MS) | 35 |
| 2.5.4 Solid State NMR..... | 35 |
| 2.5.5 Gel Permeation Chromatography (GPC) | 36 |
| 2.5.6 Film Preparation for XPS and SEM Analysis..... | 36 |
| 2.5.7 X-Ray Photoelectron Spectroscopy (XPS) | 37 |
| 2.5.8 Scanning Electron Microscopy (SEM)..... | 37 |
| 2.5.9 Differential Scanning Calorimetry (DSC) | 37 |
| 2.5.10 Thermogravimetric Analysis (TGA) | 38 |
| 2.5.11 Pyrolysis Mass Spectroscopy..... | 38 |
| 2.5.12 Viscosity Measurements | 38 |
| 3. RESULTS and DISCUSSION | 39 |
| 3.1 Aqueous solution polymerization of HEMA by gamma-radiation..... | 39 |
| 3.1.1 FTIR Analysis of gamma irradiated PHEMA | 40 |
| 3.1.2 DSC Analysis of gamma irradiated PHEMA | 41 |
| 3.1.3 Thermal Degradation of PHEMA..... | 41 |
| 3.2 Atom Transfer Radical Polymerization of HEMA | 55 |

| | |
|---|-----|
| 3.2.1 UV-Vis and FTIR results of Cu (II) complexes | 56 |
| 3.2.2 UV-Vis results of Cu (I) complexes..... | 61 |
| 3.2.3 FTIR results of polymers prepared by ATRP..... | 63 |
| 3.2.4 ¹ H-NMR analysis of polymers prepared by ATRP | 64 |
| 3.3 RAFT Polymerization of HEMA..... | 70 |
| 3.4 Block Copolymer Synthesis by PDMS Macroazoinitiator..... | 80 |
| 3.4.1 FTIR Analysis of Block Copolymers..... | 82 |
| 3.4.1.1 P(DMS-b-MMA) | 82 |
| 3.4.1.2 P(DMS-b-EMA) | 83 |
| 3.4.1.3 P(DMS-b-TMSHEMA)..... | 85 |
| 3.4.2 ¹ H-NMR Analysis of Block Copolymers..... | 86 |
| 3.4.2.1 P(DMS-b-MMA) | 86 |
| 3.4.2.2 P(DMS-b-EMA) | 86 |
| 3.4.2.3 P(DMS-b-TMSHEMA)..... | 86 |
| 3.4.3 Solid State NMR Studies | 90 |
| 3.4.3.1 P(DMS-b-MMA) | 90 |
| 3.4.3.2 P(DMS-b-TMSHEMA) and P(DMS-b-HEMA) Block Copolymers..... | 92 |
| 3.4.4 GPC Analysis of P(DMS-b-MMA) & P(DMS-b-EMA) Block Copolymers..... | 95 |
| 3.4.5 XPS Results of Copolymers..... | 97 |
| 3.4.5.1 P(DMS-b-MMA) | 97 |
| 3.4.5.2 P(DMS-b-EMA) | 103 |
| 3.4.5.3 P(DMS-b-TMSHEMA)..... | 105 |
| 3.4.5.4 P(DMS-b-HEMA) | 107 |
| 3.4.6 SEM Analysis of Block Copolymers | 109 |
| 3.4.6.1 P(DMS-b-MMA) | 109 |
| 3.4.6.2 P(DMS-b-EMA) | 111 |
| 3.4.6.3 P(DMS-b-TMSHEMA) and P(DMS-b-HEMA) | 112 |
| 3.4.7 DSC of Block Copolymers | 115 |

| | |
|---|-----|
| 3.4.7.1 P(DMS-b-MMA) | 115 |
| 3.4.7.2 P(DMS-b-EMA) | 116 |
| 3.4.7.3 P(DMS-b-TMSHEMA)..... | 118 |
| 4. CONCLUSIONS | 119 |
| REFERENCES | 124 |
| APPENDICES | 129 |
| A. UV-Vis Spectra of Cu(II) Complexes | 129 |
| B. GPC MW Distribution Plots | 132 |
| C. XPS Results of copolymers | 134 |
| CURRICULUM VITAE..... | 144 |

LIST OF TABLES

TABLES

| | |
|---|-----|
| Table 2.1 The recipe of materials used for the synthesis of catalysts | 21 |
| Table 2.2 The recipe of ATRP of HEMA..... | 23 |
| Table 2.3 Recipe for copolymerization of PDMS-MAI and MMA..... | 31 |
| Table 2.4 Recipe for copolymerization of PDMS-MAI and EMA..... | 32 |
| Table 2.5 Recipe for copolymerization of PDMS-MAI and TMSHEMA | 33 |
| Table 3.1 Mass spectral fragments at different stage of degradation..... | 49 |
| Table 3.1 Continued | 50 |
| Table 3.2 Conversion % data for ATRP of PHEMA | 65 |
| Table 3.3 Conversion % and intrinsic viscosity results for the RAFT polymerization of HEMA in MEK, ([RAFT]= 0.018 M, [AIBN]= 0.001M at 80 °C)..... | 72 |
| Table 3.4 Conversion % and intrinsic viscosity results for the RAFT polymerization of HEMA in ethyl acetate, ([RAFT]= 0.018 M, [AIBN]= 0.001M at 80°C)..... | 74 |
| Table 3.5 Conversion % and intrinsic viscosity results for the RAFT polymerization of HEMA in toluene, ([RAFT]= 0.018 M, [AIBN]= 0.001M at 80°C)..... | 75 |
| Table 3.6 %Conversion-time and IV results for the HEMA polymerization with different [CTA]/[AIBN] ratios in three different solvents..... | 78 |
| Table 3.7 Solubility test for copolymers at room temperature..... | 96 |
| Table 3.8 Surface atomic ratio of Si/C, wt % of PDMS and PMMA in dif. samples.. | 100 |
| Table 3.9 Surface atomic ratio of Si/C, wt % of PDMS and PEMA in diff. samples.. | 104 |
| Table 3.10 Surface atomic ratio of Si/C, wt % of PDMS and PTMSHEMA in different samples..... | 106 |
| Table 3.11 Surface atomic ratio of Si/C, wt % of PDMS and PHEMA in different samples..... | 108 |

LIST OF FIGURES

FIGURES

| | |
|---|----|
| Figure 1.1 The general mechanism of ATRP [22] | 7 |
| Figure 1.2 Proposed Cu(I) and Cu(II) species [21]..... | 10 |
| Figure 1.3 The RAFT Mechanism [37] | 12 |
| Figure 1.4 Different types of RAFT agents [22] | 13 |
| Figure 1.5 Synthesis of PDM-MAI [50]..... | 18 |
| Figure 1.6 Polymerization of St and MMA using PDM-MAI [50] | 18 |
| Figure 2.1 Schematic representation of dithiobenzoate salt preparation | 25 |
| Figure 2.2 Acidification of dithiobenzoate..... | 26 |
| Figure 2.3 Synthesis of Cumyl Dithiobenzoate..... | 26 |
| Figure 2.4 The chemical structure of DPTS | 28 |
| Figure 2.5 Mechanism of synthesis of PDMS-MAI | 29 |
| Figure 2.6 Synthesis of Block Copolymers | 34 |
| Figure 3.1 Conversion – Time graph for γ -radiation polymerization of HEMA | 39 |
| Figure 3.2 FTIR spectrum of (a) HEMA and (b) polymer of HEMA..... | 40 |
| Figure 3.3 DSC thermogram of PHEMA | 41 |
| Figure 3.4 GC-MS spectrum of HEMA..... | 42 |
| Figure 3.5 Schematic representation of fragmentation | 43 |
| Figure 3.6 TGA thermogram of γ -irradiated PHEMA..... | 45 |
| Figure 3.7 FTIR spectrum of decomposition gases from TGA analysis | 46 |
| Figure 3.8 FTIR spectra of PHEMA after pyrolysis at different temperatures | 48 |
| Figure 3.9 Mass thermogram of PHEMA..... | 51 |
| Figure 3.10 Fragments of PHEMA obtained at (a)48°C, (b)365°C..... | 52 |
| Figure 3.10 continued for (c) 420°C and (d) 520°C | 53 |
| Figure 3.11 Schematic representations of main fragments in last two stages | 54 |

| | |
|--|----|
| Figure 3.12 Simplified ATRP mechanism for PHEMA macroinitiator and P(HEMA-b-DMS) copolymer..... | 55 |
| Figure 3.13 UV-Vis spectrum of Cu(II)01 complex..... | 57 |
| Figure 3.14 UV-Vis spectrum of Cu(II)02 complex..... | 58 |
| Figure 3.15 FTIR spectrum of Cu(II)02 complex..... | 59 |
| Figure 3.16 FTIR spectrum of Cu(II)05 complex..... | 60 |
| Figure 3.17 UV-Vis spectrum of Cu(I)A complex..... | 61 |
| Figure 3.18 UV-Vis spectrum of Cu(I)B complex..... | 62 |
| Figure 3.19 FT-IR spectra of (a)HEMA and (b)PHEMA (by ATRP method)..... | 63 |
| Figure 3.20 ¹ H-NMR spectrum of PHEMA via ATRP..... | 64 |
| Figure 3.21 FTIR spectra of TMSHEMA (a) monomer (b) polymer via ATRP..... | 67 |
| Figure 3.22 ¹ H-NMR spectra of TMSHEMA and its homopolymer..... | 68 |
| Figure 3.23 ¹ H-NMR spectrum of P(HEMA-b-DMS)..... | 69 |
| Figure 3.24 ¹ H-NMR spectrum of RAFT Agent..... | 71 |
| Figure 3.25 ¹³ C-NMR spectrum of RAFT Agent..... | 71 |
| Figure 3.26 ln([M] ₀ /[M] _t) vs. time graph for the RAFT polymerization of HEMA in MEK, ([RAFT]= 0.018 M, [AIBN]= 0.001M at 80 °C)..... | 73 |
| Figure 3.27 ln([M] ₀ /[M] _t) vs. time graph for the RAFT polymerization of HEMA in ethyl acetate, ([RAFT]= 0.018 M, [AIBN]= 0.001M at 80 °C)..... | 74 |
| Figure 3.28 ln([M] ₀ /[M] _t) vs. time graph for the RAFT polymerization of HEMA in toluene, ([RAFT]= 0.018 M, [AIBN]= 0.001M at 80 °C)..... | 76 |
| Figure 3.29 Comparison of three conversion – time graphs for the RAFT polymerization of HEMA, [RAFT]= 0.018 M, [AIBN]= 0.001M at 80 °C..... | 77 |
| Figure 3.30 ¹ H-NMR spectrum of P(HEMA-b-DMS) copolymer via RAFT polymerization..... | 80 |
| Figure 3.31 Schematic representation of copolymer synthesis..... | 81 |
| Figure 3.32 FTIR Spectra of PDMS , P(DMS-b-MMA) and PMMA..... | 83 |
| Figure 3.33 FTIR Spectra of PDMS, P(DMS-b-EMA) and PEMA..... | 84 |

| | |
|--|-----|
| Figure 3.34 FTIR Spectra of PDMS, P(DMS-b-TMSHEMA) and PHEMA..... | 85 |
| Figure 3.35 ¹ H-NMR spectra of PDMS, PDMS-MAI & P(DMS-b-MMA) copolymer | 87 |
| Figure 3.36 ¹ H-NMR spectra of PDMS, PDMS-MAI & P(DMS-b-EMA) copolymer. | 88 |
| Figure 3.37 ¹ H-NMR spectra of PDMS, PDMS-MAI, P(DMS-b-TMSHEMA) and P(DMS-b-HEMA) | 89 |
| Fig. 3.38 ¹³ C CPMAS NMR spectrum of P(DMS-b-MMA)..... | 90 |
| Figure 3.39 Solid-state ²⁹ Si MAS NMR spectrum of P(DMS-b-MMA)..... | 91 |
| Fig. 3.40 ¹³ C CPMAS NMR spectra of P(DMS-b-TMSHEMA) & P(DMS-b-HEMA) | 93 |
| Figure 3.41 ²⁹ Si MAS NMR spectra of P(DMS-b-TMSHEMA)& P(DMS-b-HEMA) | 94 |
| Figure 3.42 Full scan XPS of P _{14,3} M(12) copolymer on glass side..... | 98 |
| Figure 3.43 C1s XPS spectra of P ₄ M(12) (a air side, b glass side) and P _{14,3} M(12).... | 102 |
| (c air side, d glass side) copolymers..... | 102 |
| Figure 3.45 Full scan XPS of P _{8,7} TH(12) copolymer on glass side..... | 105 |
| Figure 3.46 Full scan XPS of P _{4,6} H(8) copolymer on air side..... | 107 |
| Figure 3.47 SEM micrographs of (a) P ₄ M(12) _{air} , (b) P _{7,7} M(12) _{air} and (c) P _{14,3} M(12) _{air} | 109 |
| Figure 3.47 (cont'n)..... | 110 |
| Figure 3.47 (cont'n)..... | 110 |
| Figure 3.48 SEM micrographs of (a) P _{1,8} E(12) _{glass} and (b) P _{3,5} E(12) _{glass} | 111 |
| Figure 3.48 (cont'n)..... | 112 |
| Figure 3.49 SEM micrographs of (a) P _{4,6} TH(12) _{air} and (b) P _{8,7} TH(12) _{air} | 113 |
| Figure 3.49 (cont'd)..... | 113 |
| Figure 3.50 SEM micrographs of (a) P _{4,6} H(8) _{air} and (b) P _{16,1} H _{air} (after deprotection of trimethyl silyl groups)..... | 114 |
| Figure 3.50 (cont'd)..... | 114 |
| Figure 3.51 DSC thermogram of P _{7,7} M(8) copolymer..... | 115 |
| Figure 3.52 DSC thermogram of P _{14,3} M(8) copolymer..... | 116 |
| Figure 3.53 DSC thermogram of P _{6,8} E(8) copolymer..... | 117 |
| Figure 3.54 DSC thermogram of P _{8,7} TH(8) copolymer..... | 118 |

| | |
|--|-----|
| Figure A.1 UV-Vis spectrum of Cu(II)03 complex | 129 |
| Figure A.2 UV-Vis spectrum of Cu(II)04 complex | 130 |
| Figure A.3 UV-Vis spectrum of Cu(II)05 complex | 131 |
| Figure B.1 Molecular weight distribution plot of P _{7.7} M(8) copolymer | 132 |
| Figure B.2 Molecular weight distribution plot of PDMS-MAI macroazoinitiator | 133 |
| Figure B.3 Molecular weight distribution plot of P _{6.8} E(4) copolymer | 133 |
| Figure C.1 Full scan XPS of P _{14.3} M(12) copolymer on air side | 134 |
| Figure C.2 Full scan XPS of P _{14.3} M(12) copolymer on glass side | 134 |
| Figure C.3 Full scan XPS of P _{6.8} E(12) copolymer on air side | 135 |
| Figure C.4 Full scan XPS of P _{6.8} E(12) copolymer on glass side | 135 |
| Figure C.5 C1s XPS spectra of P _{1.8} E(12) (a air side, b glass side) and P _{6.8} E(12) (c air side, d glass side) copolymers | 137 |
| Figure C.6 Full scan XPS of P _{4.6} TH(12) copolymer on air side | 138 |
| Figure C.7 Full scan XPS of P _{4.6} TH(12) copolymer on glass side | 138 |
| Figure C.8 C1s XPS spectra of P _{4.6} TH(12) (a air side, b glass side) and P _{8.7} TH(12). (c air side, d glass side) copolymers..... | 140 |
| Figure C.9 Full scan XPS of P _{16.1} H copolymer (after deprotection) on air side | 141 |
| Figure C.10 Full scan XPS of P _{16.1} H copolymer (after deprotection) on glass side | 141 |
| Figure C.11 C1s XPS spectra of P _{4.6} H(8) (a air side, b glass side) and P _{16.1} H(8)..... | 143 |
| (c air side, d glass side) copolymers..... | 143 |

ABBREVIATIONS

| | |
|-------|--|
| ACPA | 4,4'-azobis-4-cyanopentanoic acid |
| AIBN | azoisobutyronitrile |
| ATRP | Atom Transfer Radical Polymerization |
| BPY | 2,2'-bipyridine |
| CDB | Cumyl dithiobenzoate |
| CL | Contact Lens |
| CPMAS | Cross Polarization Magic Angle Spinning |
| CTA | Chain Transfer Agent |
| DCC | N,N'-dicyclohexylcarbodiimide |
| DMAP | 4-(Dimethylamino) pyridine |
| DMF | N,N'-dimethyl formamide |
| DPTS | 4-(Dimethylamino)pyridinium 4-Toluenesulfonate |
| DSC | Differential Scanning Calorimetry |
| EBriB | Ethyl-2-bromoisobutyrate |
| EMA | Ethyl methacrylate |
| FTIR | Fourier Transform Infrared Spectroscopy |
| GPC | Gel Permeation Chromatography |
| IPN | Interpenetrating Polymer Networks |
| LRP | Living Radical Polymerization |
| MEK | Methyl ethyl ketone |
| MMA | Methyl methacrylate |
| MS | Mass Spectroscopy |
| MWD | Molecular Weight Distribution |
| NMP | Nitroxide Mediated Polymerization |

| | |
|--------------|--|
| NMR | Nuclear Magnetic Resonance |
| P(DMS-b-MMA) | Poly(dimethylsiloxane-block-methyl methacrylate) copolymer |
| PDMS-MAI | Poly(dimethyl siloxane) Macroazoinitiator |
| PHEMA | Poly(hydroxyethyl methacrylate) |
| PMDETA | N,N,N',N',N''-pentamethyldiethylene triamine |
| PTSA | P-toluenesulfonic acid |
| RAFT | Reversible Addition Fragmentation Chain Transfer |
| SEM | Scanning Electron Microscope |
| TGA | Thermogravimetric Analysis |
| TMSHEMA | 2-[(trimethylsilyl)oxy]ethyl methacrylate |
| XPS | X-ray Photoelectron Spectroscopy |

CHAPTER 1

INTRODUCTION

Poly(2-hydroxyethyl methacrylate), PHEMA, has great interest due to hydrophilicity (hydroxyl functional group), readily polymerized or copolymerized and used in many applications. PHEMA is the most widely used hydrogel because the water content is similar to that of living tissues, bio- and blood-compatibility and resistance to degradation [1]. PHEMA based soft contact lenses (CL) and intraocular lenses (IOL) are the most important application area of this polymer due to high oxygen permeability, good mechanical properties and favourable refractive index value. Currently, daily disposable soft CLs based on HEMA and continuous wear soft CLs based on a silicon containing material are rapidly gaining market share [2]. Silicone polymers are also used in CLs but the main disadvantage is its hydrophobicity. Despite their high oxygen permeability, the silicone lenses develop deposit of mucous and proteins quite easily and the major complication is adherence to the cornea. Compared to PHEMA, silicone soft CLs are somewhat uncomfortable during wear due to their higher modulus of elasticity and poorer wetting characteristics.

In recent years, to dissipate these drawbacks, improve wettability and tear strength, surface modification of silicone CLs were carried out. This was achieved by plasma induced graft copolymerization with HEMA and acrylic acid. Hsiue et. al. [3-4] developed a highly biocompatible membrane as an artificial cornea. Surface properties were characterized and results indicated that PHEMA grafted silicone rubber (SR) were completely covered with corneal epithelial cells (CEC) three weeks after implantation into the host cornea. They also examined the effect of the amount of HEMA grafted on Ar-plasma-treated and graft copolymerization for various parameters of power,

pressure, reaction time and concentration of HEMA aqueous solution. Characterization was done by ATR-FTIR, ESCA, contact angle and SEM [5-6].

Deposition of plasma-polymerized HEMA on silicone in presence of Ar-plasma was also studied by Bodas et. al. [7] at deposition time of 10 and 40 min. films of thicknesses ~800 and ~2000 Å, were obtained and confirmed from AFM results.

Abbasi and Mirzadeh [8-9] compared the properties of surface- and bulk-modified PDMS. Laser-induced surface grafting of PHEMA and a sequential method for preparation interpenetrating polymer networks (IPNs) of PDMS/PHEMA were prepared. Both of systems were characterized by ATR-FTIR, DMA, SEM and water contact angle measurements. It can be concluded that surface grafting results in a modified surface having higher hydrophilicity, while the IPN method results in the hydrophile/hydrophobe surface the ratio of which can be controlled by regulating the PHEMA content in the IPN. Also, laser treatment followed by surface grafting cannot affect the T_g of PDMS. But in IPN system there were 2 T_g's, meaning that this multicomponent system is a two-phase polymeric system.

Another approach to obtain soft CLs is silanization of hydrophilic polymers. Deng et. al. [10] studied the surface reactions of PHEMA and the copolymer of poly(HEMA-methacrylic acid) with methyltrimethoxysilane, ethyltrimethoxy silane and phenyltrimethoxy silane.

In addition to the surface modification of PHEMA type hydrogels, various types of bulk modifications have been examined to obtain a perfect biomaterial. Their poor mechanical strength, mainly in the swollen state, has been settled by blending, copolymerization, functionalization or crosslinking. These hydrogels can be reinforced also by gaining the hydrophobic/hydrophilic balance with interpenetrating polymer networks. So, different copolymerization techniques have been used to synthesize a

well-defined amphiphilic block or graft copolymers with PDMS and PHEMA. Hou et. al. [11] generated graft copolymers poly(HEMA-g-DMS) by direct radical copolymerization. They also performed the anionic copolymerization of the same PDMS macromer with silyl-protected HEMA, namely, 2-(trimethylsiloxy)ethyl methacrylate. (SiEMA), produced graft copolymers, poly(SiEMA-g-DMS). Successive hydrolysis eliminated the protecting trimethylsilyl groups in the backbone to afford amphiphilic graft copolymers poly(HEMA-g-DMS) with a narrow MWD (1.09-1.16).

1.1 Polymerization and/or copolymerization of HEMA with different techniques

HEMA is polymerized by different methods such as free radicalic [12-13], anionic [14-15], and controlled/living polymerization [16-20]. For many years, free radical polymerization has been the simplest and most widely used technique on an industrial scale due to the simple radical generation and the applicability to various monomers containing different functional groups. There is no need for any sophisticated procedures or equipments. However, limitations are the diffusion-controlled termination reactions between growing radicals and little control molecular weight distribution (MWD), resulting in difficulties to control polymerization. The short life time of the generated radical does not permit some experimental modifications. In the 1980s, industrial and academic attention was focused on polymerization mechanisms that offered the control living radical polymerization. Recently, (co)polymerization of HEMA was achieved by living and/or controlled radical polymerization techniques. A living radical polymerization (LRP) can be defined simply as a synthetic method for preparing polymers with predetermined molecular weights, low polydispersity and controlled functionality. This method is more tolerant to functional groups on monomer and a variety of solvents than for conventional living polymerization technique. So, properties of controlled living radical polymerization (LRP) are between the conventional living and the free radical polymerizations. The principal of this method is the reversible deactivation (either by termination or transfer) of growing polymer

radicals. The mechanism is based on the rapid equilibrium between an active growing radicals and a dormant species [21]. The concentration of radicals was kept low enough to reduce the termination rate. This exchange also enables an extension of the average lifetime of propagating chain which provides various chain architectures (star, block copolymers etc.) [22]. Currently, the three most effective methods of LRP that have been used include nitroxide mediated polymerization (NMP), atom transfer radical polymerization (ATRP) and reversible addition-fragmentation chain transfer (RAFT) polymerization.

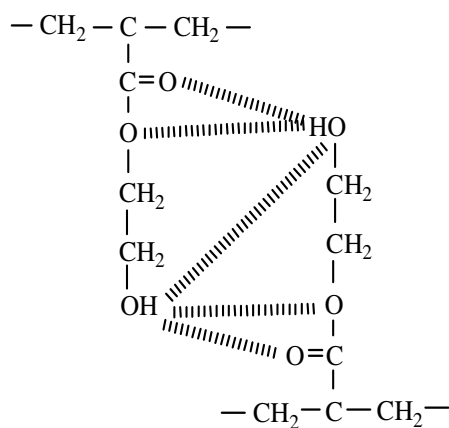
1.1.1 Free Radical Aqueous Polymerization of HEMA

Free radical polymerization of HEMA in aqueous solution was studied by several research groups. Kamakura et.al. [23] stated the effect of the viscosity of HEMA at temperatures near T_g (-96°C) on polymerization rate and they revealed that the presence of water in the monomer was important for the formation of a porous structure to immobilize enzymes and cells in a matrix. It was concluded that the polymerization of HEMA is accelerated by the addition of water and this acceleration effect increases with increasing temperature above T_g .

Kaetsu et.al. [24] showed that the initial polymerization rate initially decreased (at relatively high temperatures) with decreasing temperature, reached a minimum polymerization rate, increased to a maximum at vitrification temperature T_v and then decreased again in the low temperature region. It was also stated that no polymerization occurs when the temperature is lower than the T_g of the monomer. The increase in R_p above T_v with decreasing temperature was attributed to the marked viscosity increase as T_g is approached.

Despite the wide usage of PHEMA as a biomaterial, some undesired irritating compounds were observed during bio-application. Stol et.al investigated some model compounds assumed to be potential irritants (i.e. HEMA monomer and decomposition

products of the polymerization catalysts) and their toxic effects in vivo [25]. Results of the intradermal irritation tests revealed that at low concentrations of HEMA and sodium benzoate (up to 1 %) only a little irritation was recorded, while at higher levels (5% or more) a significant adverse reaction was detected. Hence, determination of decomposition or degradation products of PHEMA during processing conditions is very vital information, because such products may have toxic effects on living tissues. So, many researchers studied thermal degradation of PHEMA. Hill et. al. [26] examined the degradation of gamma radiated PHEMA by ESR. The high proportion of the $-CH-$ radical in irradiated PHEMA compared to other alkyl methacrylates is a reflection on their high thermal stability due to the hindered mobility of the main chain as a result of crosslinking and hydrogen bonding due to the presence of hydroxyl groups on the side chain. There are 3 types of H-bonding in the system which are the interaction between the H of the hydroxyl group of the side chain and (i) other hydroxyl groups, (ii) oxygen of the side chain and (iii) carbonyl oxygen of other monomeric units as follows:



The thermal degradation of PHEMA [27-28] reported to give monomer and some other pyrolysis products such as ethylene glycol dimethacrylate (EGDMA), methacrylic acid and acetaldehyde. Chandrasekhar and White [29] reported that GC/MS and pyrolysis-GC/FT-IR analyses of PHEMA at 500°C revealed that significant quantities of ethylene

glycol and ethyleneglycol dimethacrylate were formed along with some ethenol and methacrylic acid. They also showed by TG-MS analyses that ethylene glycol and methacrylic acid were produced at a temperature range of 350 - 450°C. According to Teijon et.al. [30], when the side chain of the polymer is hydrophilic, the formation of cyclic anhydrides is prevented. However Demirelli et. al. [31] suggested some products namely 1,3-dioxolane and anhydride rings, vinyl methacrylate 2-isopropenyloxyethyl methacrylate and ethyleneoxy methacrylate were also produced after degradation. They found from cold ring fractions (CRFs), the formation of monomer as the main fraction in thermal degradation at 25-400 °C due to depolymerization reaction. The side products arising from ester decomposition were a six-membered glutaric anhydride type ring, an oxolane type ring. The thermal properties of PHEMA were investigated with DSC and TGA by Çaykara et.al. [32]. The glass transition temperature (T_g) of PHEMA was found as 87°C. It was observed that the weight loss of PHEMA began at about 322°C and reached maximum at 361°C. The TG curve of PHEMA indicated one degradation stage which was reflected as a single peak in the DTG curve. Initial degradation temperature of PHEMA showed that the degradation was due to random chain scission.

1.1.2 Atom Transfer Radical Polymerization (ATRP)

ATRP is based on the generation of radicals by a reversible redox reaction of transition metal complex (M_t^n -Y/Ligand, where Y is a counterion). Transfer of an atom (usually halogen) from a dormant species to the metal results in an oxidized metal complex (X - M_t^{n+1} -Y/Ligand which is persistent species) and free radical (R^\bullet) Figure 1.1.

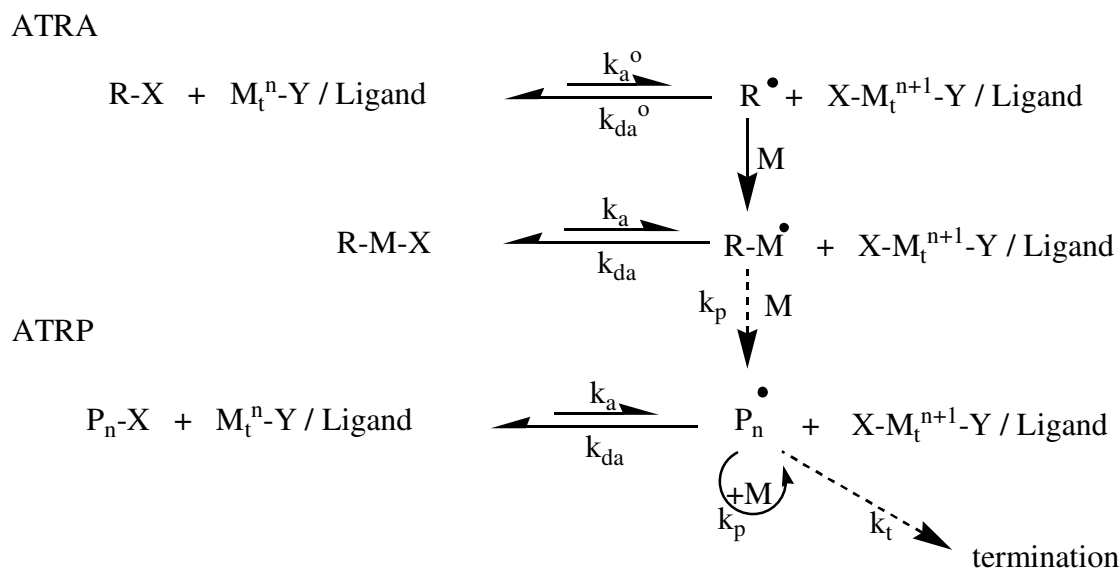


Figure 1.1 The general mechanism of ATRP [22]

The new radical can initiate the polymerization by adding a vinyl monomer, propagate, terminate by either combination or disproportionation or reversibly deactivated by the higher oxidation state metal complex. In a well controlled ATRP, no more than a small percent of the polymer chains undergo termination (persistent radical effect). During the initial, short, nonstationary stage of the polymerization the concentration of radicals decays by the unavoidable irreversible self termination, whereas, the oxidized metal complexes increases steadily as a persistent species. As time proceeds, the decreasing concentration of radicals causes the decrease in self termination and cross reaction with persistent species towards the dormant species [33]. So, the reduction in the stationary concentration of growing radicals contributes to decay the rate of termination which has a key role for the first order kinetic.

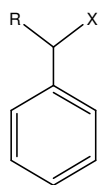
Initiation should be fast and be completed at low monomer conversion and also trapping of the product radical should be faster than the subsequent propagation step to achieve a uniform growth of all the chains. Radicals are formed reversibly and their

concentration is established by the balancing rates of activation and the deactivation. The exchange between the growing radicals and the dormant species is the most important feature of all LRP systems. The position and the dynamics of the equilibrium define the observed rates as well as affect molecular weights and polydispersities of the polymer [22].

The major components of ATRP are monomer, initiator with a transferable atom (halogen) and catalyst (transition metal with suitable ligands). Monomers can be styrenes, (meth)acrylates, (meth)acrylamides, dienes, acrylonitriles. Even using the same ATRP conditions (same catalyst and initiator), each monomer has its own unique atom transfer equilibrium constants for its active and dormant species. ($K_{eq} = k_{act}/k_{deact}$) The rate of polymerization depends on K_{eq} and if it is too small ATRP will occur slowly. On the contrary, if it is too big due to the high radical concentration, termination will occur and polymerization will be uncontrolled [21]. The stabilizing group (e.g. phenyl or carbonyl) on monomers produce sufficiently large atom transfer equilibrium constant.

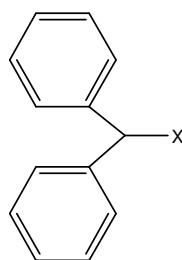
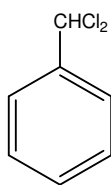
The homolytic cleavage of the alkyl halide bond by the metal complex generates the radical and so the role of the initiator is to determine the number of growing chains then the final molecular weight of polymer. The degree of polymerization is conversely related with the initial initiator concentration ($DP = [M]_0/[I]_0 \times \text{Conversion}$). The halide group, X (Br, Cl, I) must rapidly and selectively migrate between the growing chain and the transition metal complex. Also, the initiator side reactions should be minimized. ATRP initiators can be summarized as follows:

- a. Halogenated alkanes: CHCl_3 , CCl_4 , CCl_3Br .
- b. Benzylic halides: 1-phenylethyl chloride, benzhydryl chloride

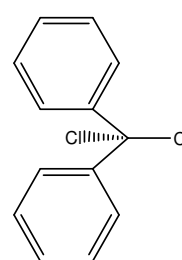


R=H,CH₃

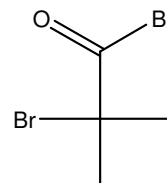
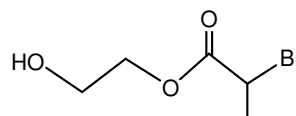
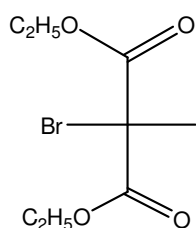
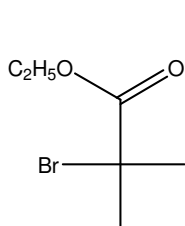
X=Br,Cl



X=Br,Cl



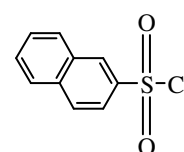
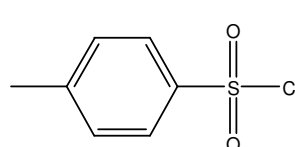
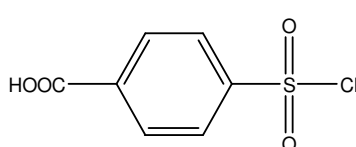
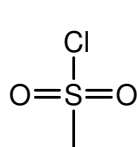
c. α -Haloesters: 2-Bromo isobutyrate



d. α -Haloketone: α -Bromo ketone, CCl₃C(=O)CH₃,

e. α -Halonitriles: 2-bromopropionitrile

f. Sulfonyl chloride:



The other component of ATRP medium is the catalyst and the utility of this depends on the metal (Mo, Cr, Re, Ru, Fe, Rh, Ni, Pd, Cu) and ligand (nitrogen or phosphorus). The metal center must have at least two oxidation states and has the affinity toward the halogen. Because some rearrangements in configuration and expansion of the

coordination sphere occur with added halogen atom [21]. Ligands used are bidentate (2,2'-bipyridine and bpy derivatives, N,N,N',N'-Tetramethylethylenediamine), tridentate (N,N,N',N'',N''-Pentamethyldiethylenetriamine, substituted terpyridine) and tetradentate (1,1,4,7,10,10-Hexamethyltriethylenetetramine, tris[2-(dimethylamino)ethyl]amine) [34]. Cu(I) prefers a tetrahedral or square planar configuration with tetradentate or two bidentate ligands, whereas, Cu(II) forms cationic trigonal bipyramidal structures. Cu-bpy complexes are represented by a tetrahedral Cu(I)(bpy)₂ and a trigonal bipyramidal XCu(II)(bpy)₂ (Figure 1.2).

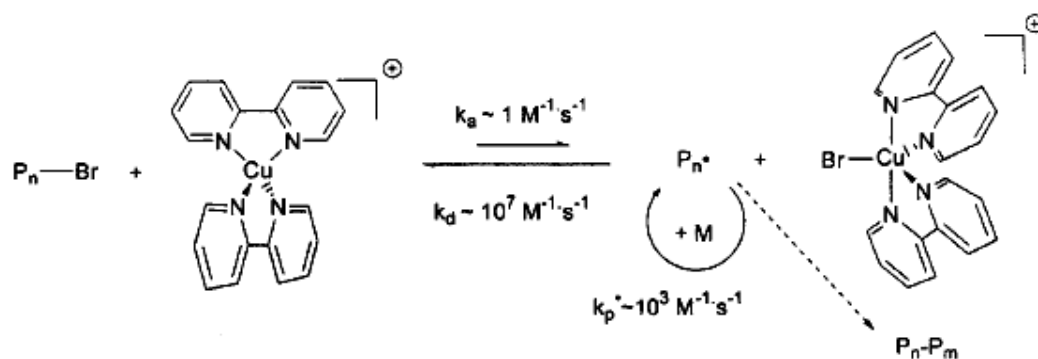


Figure 1.2 Proposed Cu(I) and Cu(II) species [21]

Matyjaszewski [22] summarized typical features of a living or controlled polymerization as follows:

- Reaction should be first order with respect to the monomer concentration (linear $\ln([M]_0/[M])$ vs. time plot)
- MW increases linearly with conversion and the polydispersity decreases with conversion.
- End functionality is not affected by slow initiation and exchange but is reduced when chain breaking reactions occur.

1.1.3 Literature Review on ATRP polymerization of HEMA

HEMA can not be polymerized by anionic and group transfer polymerizations due to the labile proton on the hydroxyl group. Little success has been accomplished in polymerization of methacrylates by NMP. Beers et. al. reported the controlled linear homopolymerization of HEMA and the preparation of a block copolymer with a MMA by ATRP [16]. Molecular weight data obtained by SEC for $M_n=26.000$. An alternating to preparing well-defined PHEMA is to protect the hydroxyl group with a trimethylsilyl group (HEMA-TMS) by ATRP. After hydrolyzation MW determined by SEC and $M_n=18.300$ ($M_w/M_n=1.10$).

Robinson [17] et. al. reported that the efficient ATRP of HEMA in either 50:50 methanol/water mixtures or in pure methanol at room temperature. Homopolymerization of HEMA in methanol at 20°C was rather slower than in the presence of water. Polymerization is first order with respect to HEMA up to 95% conversion. They also prepared comb architecture copolymers by the statistical copolymerization of HEMA with monomethoxy-capped poly(ethylene glycol) methacrylate [PEGMA; DP=45 ethylene glycol units].

Ethyl-2-bromopropionate (EPN-Br)/CuCl/bpy system was used successfully in bulk polymerization of HEMA. A monomer with a high value of dielectric constant would make it easy to form a catalyst active structure, $[Cu(I)bpy_2]X^-$. Wang and coworkers [35] also synthesized a block copolymer of HEMA with MMA.

Miller et. al. studied the ATRP of methacrylates from poly(dimethylsioxane) (PDMS) macroinitiators to synthesize inorganic/organic polymer hybrids. Allyl 2-bromoisobutyrate terminal groups on difunctional PDMS macroinitiator was obtained by anionic ring opening polymerization and then used in ATRP of HEMA-TMS monomer [36].

1.1.4 Reversible Addition Fragmentation Chain Transfer (RAFT) Polymerization

Reversible addition fragmentation chain transfer is another successful technique that utilizes dithioesters as chain transfer agents for the living character of polymer. Rates of addition and fragmentation are fast relative to the rate of propagation. RAFT agent deactivates the polymer chains to form a dormant species, resulting in a controlled polymerization. The mechanism is illustrated in Figure 1.3.

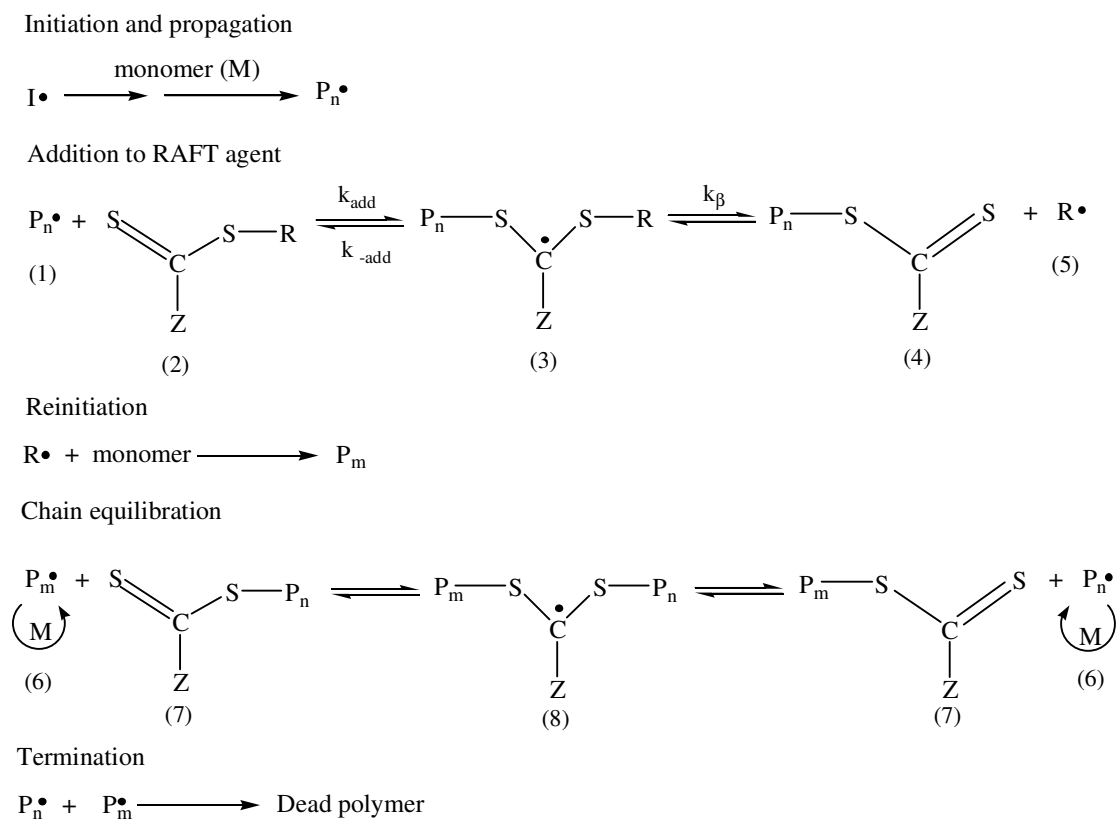


Figure 1.3 The RAFT Mechanism [37]

After the production of a propagating radical by a conventional way, a chain transfer agent (CTA) (2) reacts with a propagating macroradical (1) and form transient radical (3). This transient radical can fragment back to the original form or to the direction of another dormant chain (4) and produce a living group, R^\bullet (5). This leaving group should react with the monomer to reinitiate the polymerization, then a series of addition-fragmentation steps occur. The equilibrium between the active propagating species (6) and the dormant polymeric RAFT species (7) allows all chains to have an almost same opportunity to grow and controlled polymerization takes place. When the polymerization is complete, the end groups of the chains contain the thiocarbonylthio moiety [22].

The effectiveness of the RAFT agent depends on its transfer constant, which is determined by the stabilizing (Z) and leaving (R) groups [37]. Some examples of the different classes of RAFT agents can be seen in Figure 1.4.

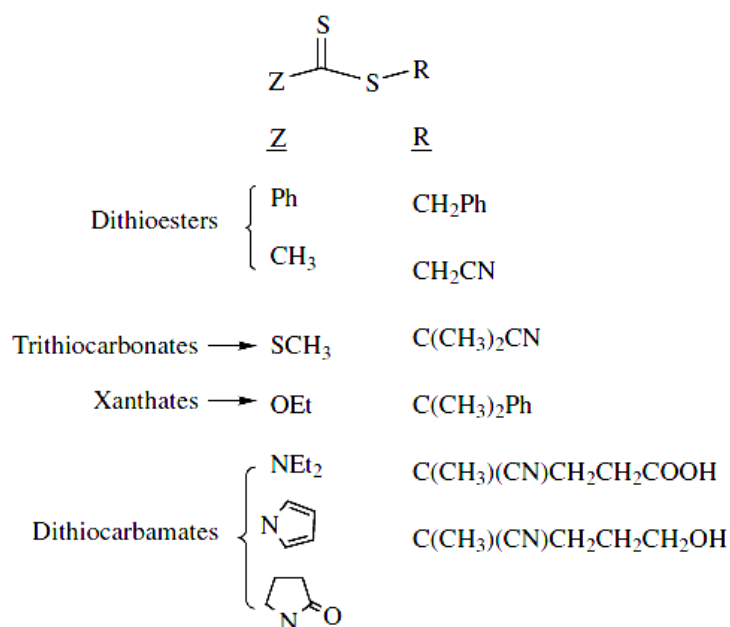


Figure 1.4 Different types of RAFT agents [22]

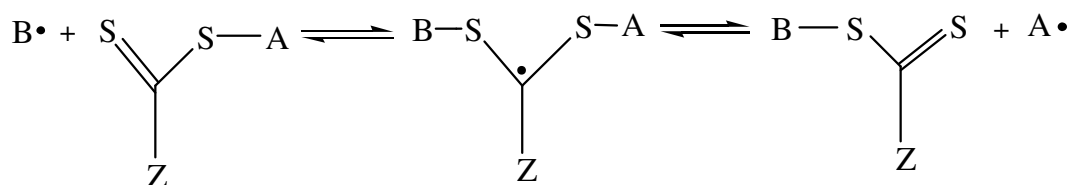
Choosing the most appropriate RAFT agent for the polymerization system (monomer, initiator and/or solvent) has the crucial role in well-controlled system. Otherwise, retardation takes places due to the slow fragmentation of the transient radical (3) or the incapability of addition of $R\bullet$ to the monomer. (e.g. cumyl dithibenzoate is a retarder in St polymerization). Z group in the RAFT agent influences the C=S bond character and Z should favor the radical addition to this double bond. For St polymerization, the chain transfer constants were found to decrease in the series where Z is aryl (Ph) >> alkyl (CH₃) ~ alkylthio (SCH₂Ph, SCH₃) ~ N-pyrrolo >> N-lactam > aryloxy (OC₆H₅) > alkoxy >> dialkylamino [22]. R group is also effective in molecular weight control and low polydispersity. R should be a good radical leaving group (polar and steric factors) and also $R\bullet$ should prefer to react with the monomer instead of the RAFT agent (e.g. triphenylmethyl is a perfect leaving group but not reactive toward the monomer due to the stability). For MMA polymerization, the effectiveness of RAFT agent decreases in the series where R is C(alkyl)₂CN ~ C(alkyl)₂Ph > C(CH₃)₂C(=O)OEt > C(CH₃)₂C(=O)NH(alkyl) > C(CH₃)₂CH₂C(CH₃)₃ ~ CH(CH₃)Ph > C(CH₃)₃ ~ CH₂Ph.

In RAFT polymerization, radical-radical termination reactions are unavoidable, but the fraction of dead chains is small. The amount of dead chains can be controlled by reducing the number of initiator-derived chains which can be achieved by using the appropriate amount of the RAFT agent.

1.1.5 Literature Review of RAFT polymerization of HEMA

There are numerous examples of utilizing the living nature of the RAFT process to prepare various AB, ABA, and ABC blocks. RAFT polymerization of methacrylates [38-40], styrenes [41], acrylates [42], acrylamides [43], vinyl esters [44] were studied by many groups. In 1998, Chiefari and coworkers [45] reported the copolymerization of HEMA with MMA by the RAFT process in ethyl acetate at 60°C, obtaining polydispersity index of 1.21.

The synthesis of block copolymers is easy by the feasibility of sequential monomer addition. Chong et. al. [46] reported different AB diblock and ABA triblock copolymer synthesis. In block copolymerization, the majority of chains in the product polymer possess the S=C(Z)S- group, polymerization can be continued in the presence of a second monomer to give a block copolymer. For the preparation of AB block copolymer in a batch polymerization, the first-formed polymeric macroRAFT (S=C(Z)S-A) should have a high transfer constant in the following copolymerization step to give the B block. The leaving group ability of propagating radical A• should be greater than that of the propagating radical B• under the reaction conditions as given below:



When A is a poly(acrylate ester) or a polystyrene chain, the transfer constants of S=C(Z)S-A in MMA polymerization appear to be very low. This is attributed to the styryl- or acrylyl-propagating radicals being poor leaving groups with respect to a methacrylyl propagating radical causing the adduct radical to partition strongly in favor of starting materials. When preparing a block copolymer, which block should be prepared firstly is an important consideration.

Chong et. al. also stated that in the absence of chain transfer (to solvent, initiator, or monomer), the total number of chains formed will be equal to (or less than) the moles of the dithio compound employed plus the moles of initiator-derived radicals. In block copolymer synthesis, these additional initiator-derived chains are a source of homopolymer impurity. For maximum purity, it is desirable to use low concentration of initiator and to choose solvents and initiators which give minimal chain transfer. As

with conventional radical polymerization, the rate of RAFT polymerization is determined by the initiator concentration. Besides the monomer reactivity ratios the composition of monomer feed has a vital role in creating a gradient or tapered copolymer. For example, copolymerization of a 1:0.91 (mole ratio) mixture of MMA and BA ($r_{\text{MMA}} \approx 1.7$ and $r_{\text{BA}} \approx 0.2$) in the presence of cumyl dithiobenzoate provides a narrow polydispersity copolymer with a gradient in composition of [MMA]/[BA] from ca. 1:0.45 to ca. 2:1.

Mayadunne et. al. [47] demonstrated the effectiveness of different trithiocarbonates in polymerization of St, MA and MMA. Several water-soluble RAFT agents based on dithiobenzoate were synthesized by Mertoglu et.al. By these RAFT agents controlled aqueous polymerizations of different (meth)acrylate, (meth)acrylamide and styrene were possible [48].

1.2 Block Copolymer Synthesis of Polymethacrylates with PDMS Macroazoinitiator

Block and graft copolymers have more complex and novel structures than their homopolymers or random copolymers. Although, it is more difficult to synthesize block copolymers, they possess characteristic physical properties of corresponding homopolymers simultaneously. Block and graft copolymers allow us to investigate the effects of segments on new morphologies and novel mechanical or solution properties. Anionic polymerization mechanism allows the synthesis of block copolymers with precise and predictable structures. Molecular weights of blocks can be predetermined and also the narrow MWD is possible with anionic living polymerization due to the lack of termination step. Despite the fact that the anionic method permits the copolymer formation in a well defined form, it has limited to some certain monomers. For example when methyl methacrylate is polymerized by anionic mechanism, the initiator (lithium alkyl) gives side reactions with pendant ester group. Also, the requirement of extremely pure reaction medium including monomer, initiator, solvent, etc. is not feasible for the

industry and economic considerations. Then researchers looked for alternative methods to synthesize block copolymer which display both the economical and the practical free radical polymerization and the well defined behavior of anionic mechanism. One technique has been developed to obtain copolymers by free radical mechanism with macroinitiator and this technique should also be applicable to a wide range of monomers. Thus, prepolymers with active end groups have been synthesized, which permit the coupling reactions with other polymer chains or acting as an initiator for subsequent copolymerization reaction. In the latter case, the prepolymer was named a “macroinitiator” which can be activated either by a thermal or a photochemical process to initiate the copolymerization. Based on the functionality of the macroinitiator, different types of block copolymers can be prepared (monofunctional for AB type and difunctional for ABA and $(AB)_n$ multiblock types).

This approach has been employed to prepare the PDMS-*b*-PMMA block copolymers by Chang et.al. [49]. Firstly, the 4,4'-azobis-4-cyanopentanoic acid were reacted with thionyl chloride to obtain 4,4'-azobis-4-cyanopentanoylchloride (ACPC). Then the azo group-containing polydimethylsiloxanes, macroazoinitiators, were prepared by polycondensation reaction of ACPC with hydroxybutyl terminated PDMS. Finally, PDMS-ACP macroazoinitiator was used as a precursor for the synthesis of PDMS-*b*-PMMA block copolymers. Deniz et. al. also used the same macroazoinitiator to synthesis poly(dimethylsiloxane-*b*-styrene) (PDMS-*b*-PSt) and poly(dimethylsiloxane-*b*-methyl methacrylate) (PDMS-*b*-PMMA) block copolymers [50] The polycondensation reaction between PDMS and ACPC was carried out for the synthesis of polydimethylsiloxane based macroazoinitiator, MAI, having a scissile azo-group and the reaction pathway can be seen in Figure 1.5.

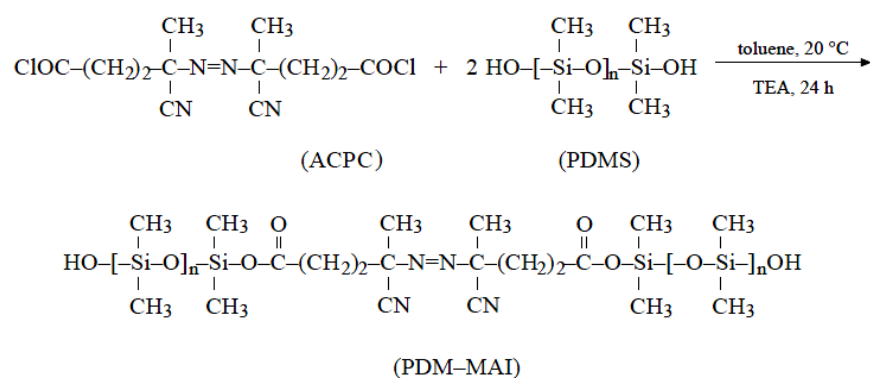


Figure 1.5 Synthesis of PDM-MAI [50]

The thermal dissociation of PDM-MAI generates free radicals to initiate the St or MMA polymerization (Figure 1.6).

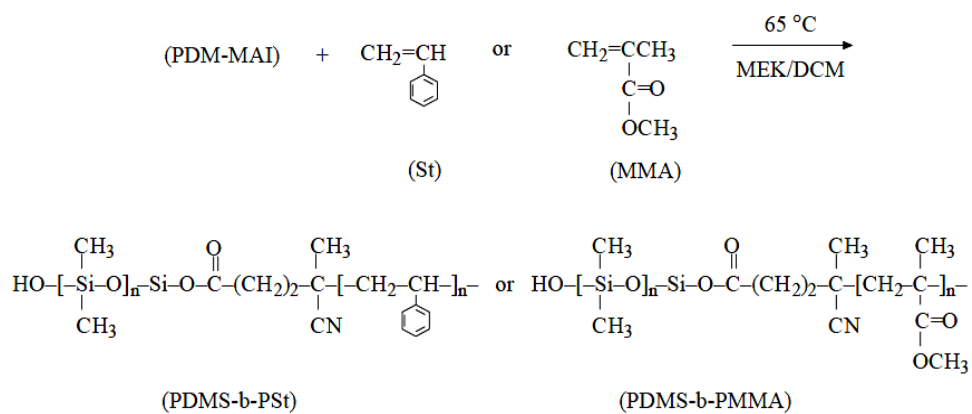


Figure 1.6 Polymerization of St and MMA using PDM-MAI [50]

1.3 The Aim of This Study

Amphiphilic block copolymers exhibit different morphologies and physical properties from their parent homopolymers, therefore they have a wide application areas. In this work, HEMA with the desired molecular weight and properties will be synthesized by appropriate methods. In this case, solution polymerization by radiation, ATRP and RAFT methods will be tried. The polymer obtained will be in the living nature for the copolymerization with PDMS and the molecular weight of PHEMA macronitiator is expected to be less than 5×10^4 to obtain a copolymer suitable to be used as membrane. Bifunctional PDMS (HO-PDMS-OH, $M_w=6000 \text{ g.mol}^{-1}$) is converted to PDMS-based macroazoinitiator (PDMS-MAI) by polycondensation of the ACPA in the presence of DCC and DPTS. After the characterization of PDMS-MAI, it will be used for block copolymerization of MMA, EMA, HEMA and TMS-HEMA. After removing the trimethyl silyl groups of TMSHEMA, P(DMS-b-HEMA) block copolymer will be obtained. Although, the synthesis of block copolymers containing DMS and HEMA sequences by group transfer polymerization has been reported in literature[51] this is the first time to synthesize P(DMS-b-EMA) and P(DMS-b-HEMA) block copolymer by PDMS macroazoinitiator method. Different characterization methods such as FTIR, NMR, UV-vis, GPC, DSC, MS, TGA, XPS, SEM etc. will be used for the characterization of products obtained under different conditions.

CHAPTER 2

EXPERIMENTAL

2.1 Aqueous Solution Polymerization of HEMA by Gamma Radiation

Hydroxyethyl methacrylate, HEMA, (Acros Organics, 98%, USA) was distilled under vacuum. About 5 mL of 40 % (v/v) aqueous solution of HEMA was placed in polymerization tubes and evacuated on a high vacuum system at 10^{-5} - 10^{-6} mm-Hg for about 5 hours then sealed by flame. The tubes were then irradiated in ^{60}Co γ source with a dose rate of 1.987 kGy/day at 25°C. After the desired irradiation period, tubes were broken open and the unpolymerized monomer was extracted with diethyl ether. Percent conversion was calculated gravimetrically.

2.2 Atom Transfer Radical Polymerization of HEMA

The systematic study of the synthesis and characterization of various Cu(I) and Cu(II) complexes were performed and then, the best conditions for the polymerization and copolymerization of HEMA and TMSHEMA via ATRP technique was determined. Homopolymers and copolymers were synthesized and characterized by FTIR and ^1H -NMR techniques.

2.2.1 Materials for the synthesis of PHEMA by ATRP

CuBr (98%, Aldrich), CuCl (90%, ACS Reagent, Aldrich), CuCl₂ (97%, Aldrich) for the metal center of the complex, 2,2'-bipyridyl (99+%, Aldrich), 4,4'-dimethyl-2,2'-bipyridyl (99%, Aldrich), N,N,N',N',N''-pentamethyldiethylene triamine (99 %, Aldrich) for the ligands of the complex, ethyl 2-bromoisobutyrate (98 %, Aldrich), 2-bromopropionyl bromide (97%, Aldrich), 2-bromo-2-methylpropionyl bromide (98%, Acros Organics), p-toluenesulfonyl chloride (98%, reagent grade, Aldrich) for the

initiators were all used as received. HEMA (98%, Acros Organics) was used after vacuum distillation. Solvents; methanol (99.8%, J.T.Baker), tetrahydrofuran (99%, J.T.Baker), acetonitrile (99.9%, Merck), 1-propanol (98%, Merck), methyl ethylketone (MEK, Atabay), diethyl ether (anhydrous, 99.5%, J.T.Baker) DMF (99.8%, analytical reagent, Lab-Scan) were used as received.

2.2.2 Synthesis of Cu(I) and Cu(II) complexes

Before polymerization, Cu(II) complexes with different ligands were synthesized to adjust the equilibrium toward the dormant species and to reduce the concentration of growing radicals. Complexes were prepared under N₂ atmosphere in different solvents by stirring for 2 hours and were characterized by UV-Vis and FT-IR techniques. All chemicals were grade and were not purified further. The recipes for the synthesis of catalysts were summarized in Table 2.1.

Table 2.1 The recipe of materials used for the synthesis of catalysts

| Name of complex | Metal (mmol) | Ligand (mmol) | Solvent | Temp. °C |
|-----------------|---------------------------|---|---------------------------------|----------|
| Cu(II)01 | CuCl ₂ (0.104) | Pentamethyldiethylene triamine (PMDETA) (0.519) | Methanol | 20 |
| Cu(II)02 | CuCl ₂ (0.372) | 4,4'-dimethyl bipyridine (dMbpy) (0.999) | 1:1 mixture of THF&Acetonitrile | 20 |
| Cu(II)03 | CuBr ₂ (0.224) | 2,2'-bipyridine (bpy) (1.178) | 1:1 mixture of THF&Acetonitrile | 20 |
| Cu(II)04 | CuBr ₂ (0.259) | Pentamethyldiethylene triamine (PMDETA) (0.519) | Methanol | 20 |
| Cu(II)05 | CuBr ₂ (0.559) | 4,4'-dimethyl bipyridine (dMbpy) (2.497) | 1:1 mixture of THF&Acetonitrile | 20 |
| Cu(IA) | CuCl (0.248) | 2,2'-bipyridine (bpy) (0.494) | 70:30 mixture of MEK/1-Propanol | 20 |
| Cu(IB) | CuCl (0.240) | 4,4-dimethyl bipyridine (dMbpy) (0.482) | 70:30 mixture of MEK/1-Propanol | 20 |

2.2.3 Method for PHEMA Synthesis via ATRP

In a 100 mL round bottom flask CuCl (0.0246g 0.24 mmol) and bipyridine (0.0772g 0.48 mmol) were added by purging Ar for 30 minutes. In another flask, HEMA (6 mL 48 mmol) was dissolved in a mixture of MEK/1-propanol (6 mL) (70/30 v/v) then added to the catalyst. Ethyl-2-bromoisobutyrate (EBriB) (35.6 μ L 0.24 mmol) was added dropwisely with a syringe. So that metal (M):ligand (L):monomer (H):initiator (I) ratio is 1:2:200:1. After the addition of the initiator, the temperature was raised to 70°C in an oil bath while stirring the mixture. After 2 h., the polymer was precipitated in diethyl ether and then dissolved in methanol then precipitated again in diethyl ether. The sample was dried in a vacuum desiccator at 35°C, then, the polymer molecular weight was determined relatively by viscosity measurement.

The same procedure with oxidized Cu(II) complexes was applied in the second type preparation method. In a 100 mL round bottom flask CuCl (0.0246g 0.248 mmol) and bipyridine (0.0772g 0.494 mmol) were added by bubbling Ar for 30 minutes. HEMA (6 mL 48 mmol) and Cu(II)O₂ complex (0.0120g 0.024 mmol) was dissolved in a mixture of MEK/1-propanol (6 mL) (70/30 v/v) then added to the reaction flask. Ethyl-2-bromoisobutyrate (EBriB) (35.6 μ L 0.24 mmol) was added dropwisely with a syringe. Polymerization took place at 70°C and the polymer was precipitated in diethyl ether. The molecular weight of the dried polymer was determined by viscosity. Table 2.2 shows the recipe of ATRP of HEMA.

Table 2.2 The recipe of ATRP of HEMA

| Run No | Metal (CuCl) (mmol) | Ligand (bpy) (mmol) | Initiator (μL) | HEMA (mmol) | Cu(II)O ₂ (mmol) |
|--------|---------------------|---------------------|-----------------------------|-------------|-----------------------------|
| 1 | 0.248 | 0.494 | (EBriB) 35.60 | 48 | 0 |
| 2 | 0.248 | 0.494 | (EBriB) 35.60 | 48 | 0.024 |
| 3 | 0.248 | 0.494 | (BrMPB) 29,66 | 48 | 0 |
| 4 | 0.248 | 0.494 | (BrMPB) 29,66 | 48 | 0.024 |
| 5 | 0.248 | 0.494 | (BrPB) 25.14 | 48 | 0 |
| 6 | 0.248 | 0.494 | (BrPB) 25.14 | 48 | 0.024 |

2.2.4 Synthesis of 2-[(trimethylsilyloxy)ethyl methacrylate (TMS-HEMA) and its polymerization and copolymerization with PDMS via ATRP

TMSHEMA was prepared according to Beers et.al. [16] procedure. Briefly, a 10 mL (76 mmol) of HEMA (98%, Acros Organics), 10.6 mL (76 mmol) of triethylamine (99.5%, Aldrich) and 250 mL diethyl ether (anhydrous, 99.5%, J.T.Baker) were mixed under argon atmosphere in a 500 mL round bottom flask. The mixture was cooled to 0°C and then, a 9.8 mL (76 mmol) of chlorotrimethyl silane (97%, Aldrich) was added dropwisely for 30 minutes. The solution was mixed at 0°C for 2 hours and then, filtered to remove white precipitates. The filtrate was washed with 100 mL deionized water for three times and dried with MgSO₄ and the ether phase was removed by rotary evaporator. Later the vacuum distillation was applied to the residual product for the ATRP of TMSHEMA. Characterization was done by FTIR and ¹H-NMR techniques.

TMSHEMA was copolymerized with poly(dimethylsiloxane), (PDMS, vinyl terminated Mw=25000 g.mol⁻¹, typical viscosity=850.000-1,150.000 cSt, Aldrich), by ATRP process. Briefly, two-necked reaction flask fitted with a condenser and rubber septa for the materials addition and argon purging. CuBr (0.0214g, 0,149 mmol) was purged with argon for 15 minutes and then, a mixture of 1.5 mL TMSHEMA and

ligand; PMDETA (0.0519g, 0.299 mmol) was injected into the flask and purged for extra 15 minutes. Initiator p-toluenesulfonyl chloride (0.0566g, 0.298 mmol) was dissolved in 1.5 mL TMSHEMA monomer and the mixture was added to the reaction flask dropwisely. So that metal (M):ligand (L):monomer (H):initiator (I) ratio is 1:2:100:2. Polymerization of TMSHEMA proceeded for 3 hours at 70°C. Later, a 0.5 mL hot toluene was added with a syringe to decrease the viscosity of the medium and then, a solution of CuBr (0.0054g, 0.038 mmol) in 1.5 mL toluene was added to the poly(TMSHEMA) solution. In a beaker a 0.5 mL of PDMS (vinyl terminated) and ligand; PMDETA (0.0131g 0.075 mmol) were dissolved in a 1.5 mL toluene and the solution was injected into the reaction flask for copolymerization. After finishing the sequential addition of PDMS, copolymerization proceeded for 4 hours at 70°C. Polymer was precipitated into the cold water and green color polymers (because of metal complexes) were dried in vacuum oven at 40°C. For deprotection of trimethylsilyl groups, 0.1091g copolymer (product) was dissolved in DMF. A few (6-7) drops of 1.5M HCl solution was added to this copolymer solution and mixed for 2 hours. P(HEMA-b-DMS) copolymer was precipitated in water and then, dried in vacuum oven. ¹H-NMR analysis was performed for the characterization.

2.3. Reversible Addition-Fragmentation Chain Transfer Polymerization of HEMA

The RAFT agent [2-phenylprop-2-yl dithiobenzoate (cumyl dithiobenzoate,CDB)] was synthesized according to the published procedures [52] and then used in HEMA homopolymerization in three different solvents (methyl ethyl ketone, ethyl acetate and toluene) with different RAFT agent contents. Both the RAFT agent and the PHEMA homopolymer were characterized by FTIR, ¹H-NMR and ¹³C-NMR spectroscopy techniques.

2.3.1 Materials for the synthesis of RAFT agent and PHEMA

Sulfur (reagent grade, powder, Aldrich), sodium methoxide (Sigma-Aldrich), benzyl chloride (99.5%, Acros Organics), α -methyl styrene (99%, Acros Organics), p-toluene sulfonic acid (98,5+%, ACS Reagent Aldrich), methanol (99.8%, J.T.Baker), diethyl ether (anhydrous, 99.5%, J.T.Baker), hexane (99%, Merck), HCl (37%, ACS Reagent Aldrich), MgSO₄ (97%, Acros Organics), hydroxyethyl methacrylate (HEMA, 98% Acros Organics), α,α' -azoisobutyronitrile (AIBN, 98%, Merck), methylethyl ketone (MEK, Atabay), ethyl acetate (EtOAc, 99.5%, Riedel-deHaen), toluene (99.5%, J.T.Baker) were used as received.

2.3.2 Preparation of RAFT Agent (2-phenylprop-2-yl dithiobenzoate , CDB)

In a round bottom flask, sulfur (3.2g, 0.012 mol), freshly prepared sodium methoxide solution (22.34g, 30%) and methanol (26.5g, 0.827 mol) were poured and benzyl chloride (6.4g, 0.051 mol) was added with dropping funnel (Figure 2.1). The mixture was mixed with a magnetic stirrer using a water bath to dissipate the heat of reaction, then changed with an oil bath to reflux it overnight.

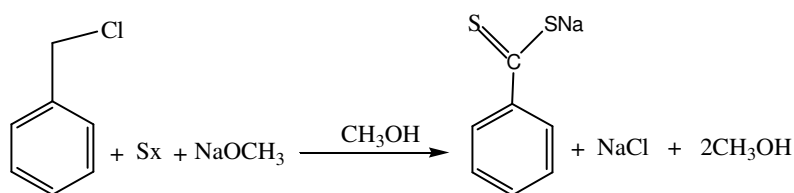


Figure 2.1 Schematic representation of dithiobenzoate salt preparation

On the second day a small amount of NaCl was added then filtered. Methanol was removed by rota-vap and 50 mL of distilled water was added. Extraction was done

three times with 30 mL diethyl ether and the top level was discarded. A further 30 mL of ether was added and acidified with HCl until the top level became purple and the bottom colorless (Figure 2.2).

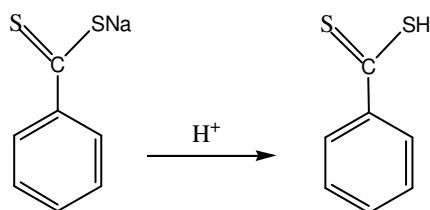


Figure 2.2 Acidification of dithiobenzoate

The product was in an organic phase (top level), then MgSO₄ was added and filtered. Residual ether was removed by rota-vap. α -methyl styrene (25 more than product as stoichiometrically) and 10 mg p-toluene sulfonic acid were added. On the third day, the product was purified by a silica gel chromatographic column with 5% solution diethyl ether in hexane (Figure 2.3).

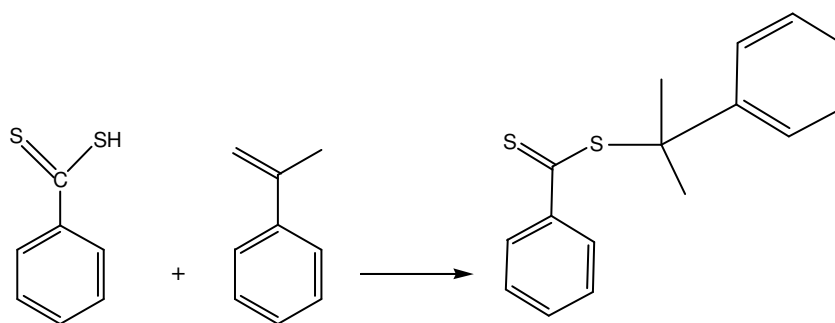


Figure 2.3 Synthesis of Cumyl Dithiobenzoate

2.3.3 Method for PHEMA Synthesis via RAFT

HEMA was distilled under vacuum before use. Aliquots (2.8 mL) of a stock solution of CDB, AIBN with HEMA in three different solvents (toluene, methyl ethyl ketone and ethyl acetate) were transferred to ampoules and they were degassed by three vacuum-freeze-thaw cycles, then flame sealed. Polymerization took place at 80°C for different time periods and the conversions were determined by gravimetrically. The effect of different [CTA]/[AIBN] ratios (9, 18 and 27) were also investigated in three solvents in order to optimum control of the polymerization of HEMA.

2.3.4 Method for P(HEMA-*b*-DMS) block copolymer synthesis (RAFT)

The RAFT polymerization of HEMA (2.5g) was performed in MEK (2.5g), ([RAFT]= 0.018 M, 0.0399g [AIBN]= 0.001M, 0.0009g) at 80 °C under argon atmosphere for 8 hours. Later, a 0.0009 g of AIBN was dissolved in 0.5g MEK and then, added to the flask. After the 10 minutes 0.5g of PDMS(vinyl terminated) was dissolved in 1.5 g of MEK and then added to the flask by syringe. The copolymerization continued for 4 hours and the product was precipitated in distilled water.

2.4 Block Copolymer Synthesis using PDMS Macroazoinitiator

2.4.1 Materials for Synthesis of PDMS Macroazoinitiator and Block Copolymers

Bis(hydroxyalkyl)-terminated PDMS (HO-PDMS-OH, $M_n=6000 \text{ g}\cdot\text{mol}^{-1}$, typical viscosity=1,000.000 cSt, Aldrich), 4-(Dimethylamino) pyridine (DMAP, 99%, Aldrich), p-toluenesulfonic acid (PTSA, 98.5% ACS Reagent Aldrich), N,N'-dicyclohexylcarbodiimide (DCC, 99% Aldrich), dichloromethane (99%, general purpose reagent, Lab-Scan), N,N'-dimethyl formamide (DMF, 99.8%, analytical reagent, Lab-Scan) methyl methacrylate (MMA, 99%, Acros Organics), ethyl methacrylate (EMA, 99%, Acros Organics), and hydroxyethyl methacrylate (HEMA,

98%, Acros Organics) were used as received. 4,4'-azobis-4-cyanopentanoic acid (ACPA, 98%) was purchased from Fluka and used without further purification. Hexane (99%, Merck), ethanol (99.5%, J.T.Baker), benzene (99.5%, Riedel deHaen) were used as received.

2.4.2 Synthesis of Macroazoinitiator, PDMS-MAI

4-(Dimethylamino)pyridinium 4-Toluenesulfonate (DPTS) was synthesized by the procedure of Moore et.al. [53] Briefly, an equimolar solution of DMAP in warm benzene was added to the anhydrous benzene solution of PTSA and mixed thoroughly. The resulting suspension was cooled to room temperature and the solid was collected by filtration (Figure 2.4). The product was purified by recrystallization from 1,2-dichloroethane, yielding white powder.

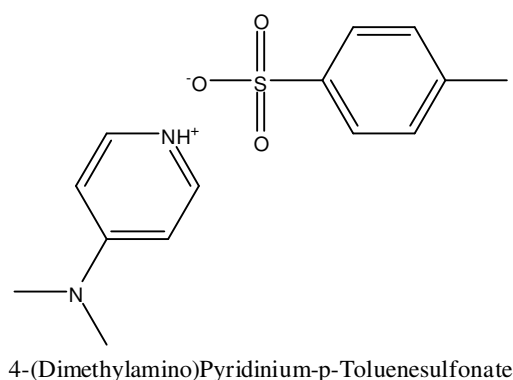


Figure 2.4 The chemical structure of DPTS

The PDMS-MAI was prepared with a direct polycondensation reaction between HO-PDMS-OH and ACPA by the procedure of Feng et.al. [54] HO-PDMS-OH (6 g, 1.0 mmol), ACPA (0.28 g, 1.0 mmol), and DPTS (0.1175 g, 0.4 mmol) were dissolved in a mixture of 20 g of dichloromethane and 3.25 g of DMF at room temperature. Later, the

DCC solution (0.62g, 3 mmol) (0.62 g of DCC dissolved in 6 g of dichloromethane) was added slowly and stirred at room temperature for 24 h. The resulting viscous suspension was filtered to eliminate the dicyclohexylurea (DCU) formed, which was washed with dichloromethane twice. The filtrate was slowly poured into a large volume of methanol to precipitate the polymer. The precipitation-dissolution procedure was repeated twice to purify the polymer. The residual volatiles in the viscous oily polymer were then removed in vacuum (Figure 2.5).

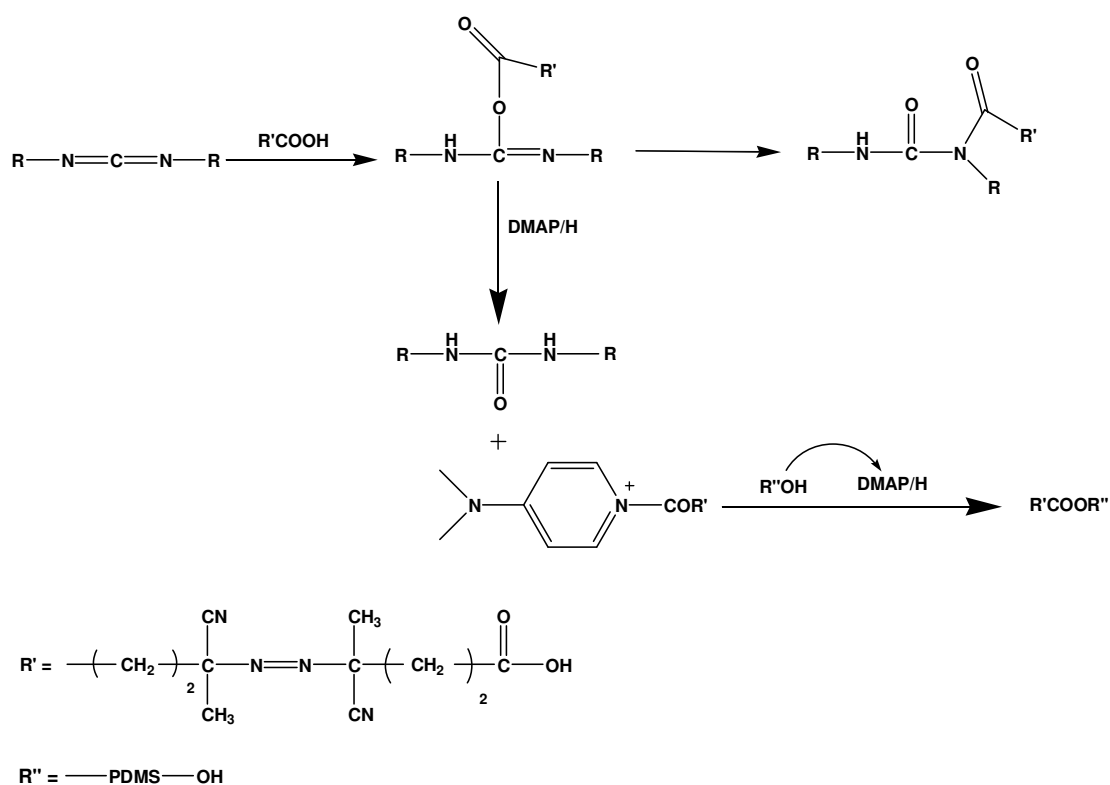


Figure 2.5 Mechanism of synthesis of PDMS-MAI

2.4.3 Method for Block Copolymers with PDMS Macroazoinitiator

A typical polymerization procedure was performed using: a 100 ml three-necked flask equipped with a magnetic stirrer, a condenser, an Ar inlet, a thermometer and an oil bath. Prescribed amounts of PDMS-MAI and MMA (or EMA, TMSHEMA) were dissolved in 32 g of benzene, and then polymerized at 75 °C for different time periods. As the polymerization proceeded the solution viscosity increased. The resulting block copolymers P(DMS-b-MMA) and P(DMS-b-EMA) were precipitated in ethanol and P(DMS-b-TMSHEMA) was precipitated into the cold water. Further purification of block copolymer is a crucial step for removing the homopolymer and other impurities. So the dissolution and the precipitation cycles were applied to different copolymers in different solvents and non-solvents. The final product was dried under vacuum at 50 °C for 24 h. The same polymerization procedure was applied to the other monomers (EMA, and TMS-HEMA). Table 2.3, 2.4 and 2.5 shows recipe for copolymerization of MMA, EMA and TMSHEMA, respectively.

Table 2.3 Recipe for copolymerization of PDMS-MAI and MMA

| Feed | | | | Copolymer | | | | | |
|-------------------------|--------|-------------------|---------|-----------|---------|---------------------|----------------|----------------|--------------------------------|
| Sample Code | Run No | PDMS-MAI weight % | MMA (g) | Time (h) | % Yield | *DMS units weight % | M _w | M _n | M _w /M _n |
| P ₄ M(4) | 1 | 4,00 | 7,485 | 4 | 23,1 | 18,92 | 183857 | 58949 | 3,12 |
| P ₄ M(8) | 2 | 4,00 | 7,485 | 8 | 23,8 | 18,71 | 148634 | 50690 | 2,93 |
| P ₄ M(12) | 3 | 4,00 | 7,485 | 12 | 24,0 | 11,18 | 165742 | 64543 | 2,57 |
| P _{7.7} M(4) | 4 | 7,69 | 7,485 | 4 | 18,8 | 7,85 | 52816 | 21749 | 2,43 |
| P _{7.7} M(8) | 5 | 7,69 | 7,485 | 8 | 25,1 | 6,89 | 120627 | 45996 | 2,62 |
| P _{7.7} M(12) | 6 | 7,69 | 7,485 | 12 | 30,1 | 5,59 | 134227 | 45541 | 2,95 |
| P _{14.3} M(4) | 7 | 14,29 | 7,485 | 4 | 27,9 | 10,29 | 117774 | 45776 | 2,57 |
| P _{14.3} M(8) | 8 | 14,29 | 7,485 | 8 | 30,6 | 9,09 | 99386 | 35822 | 2,77 |
| P _{14.3} M(12) | 9 | 14,29 | 7,485 | 12 | 33,5 | 8,47 | 114927 | 41327 | 2,78 |

*Calculated by ¹H-NMR

Table 2.4 Recipe for copolymerization of PDMS-MAI and EMA

| Feed | | | | Copolymer | | | | | |
|------------------------|--------|-------------------|---------|-----------|---------|---------------------|----------------|----------------|--------------------------------|
| Sample Code | Run No | PDMS-MAI weight % | EMA (g) | Time (h) | % Yield | *DMS units weight % | M _w | M _n | M _w /M _n |
| P _{1,8} E(4) | 1 | 1,79 | 8,5388 | 4 | 11,0 | 9,76 | 216635 | 100435 | 2,16 |
| P _{1,8} E(8) | 2 | 1,79 | 8,5388 | 8 | 17,0 | 6,28 | 130855 | 47409 | 2,76 |
| P _{1,8} E(12) | 3 | 1,79 | 8,5388 | 12 | 12,9 | 7,96 | 185650 | 66581 | 2,79 |
| P _{3,5} E(4) | 4 | 3,53 | 8,5388 | 4 | 19,4 | 10,29 | 190015 | 85875 | 2,21 |
| P _{3,5} E(8) | 5 | 3,53 | 8,5388 | 8 | 25,1 | 9,41 | 169774 | 62552 | 2,71 |
| P _{3,5} E(12) | 6 | 3,53 | 8,5388 | 12 | 28,2 | 7,59 | 164812 | 64568 | 2,55 |
| P _{6,8} E(4) | 7 | 6,81 | 8,5388 | 4 | 23,5 | 18,79 | 16113 | 44339 | 3,63 |
| P _{6,8} E(8) | 8 | 6,81 | 8,5388 | 8 | 27,1 | 11,83 | 223273 | 70652 | 3,16 |
| P _{6,8} E(12) | 9 | 6,81 | 8,5388 | 12 | 38,2 | 12,82 | 184749 | 62967 | 2,93 |

*Calculated by ¹H-NMR

Table 2.5 Recipe for copolymerization of PDMS-MAI and TMSHEMA

| Feed | | | | Copolymer | | |
|-------------------------|--------|-------------------|-------------|-----------|---------|---------------------|
| Sample Code | Run No | PDMS-MAI weight % | TMSHEMA (g) | Time (h) | % Yield | *DMS units weight % |
| P _{2,3} TH(4) | 1 | 2,34 | 6,5119 | 4 | 22,1 | 3,08 |
| P _{2,3} TH(8) | 2 | 2,34 | 6,5119 | 8 | 24,9 | 3,31 |
| P _{2,3} TH(12) | 3 | 2,34 | 6,5119 | 12 | 33,5 | 5,54 |
| P _{4,6} TH(4) | 4 | 4,57 | 6,5119 | 4 | 29,2 | 3,99 |
| P _{4,6} TH(8) | 5 | 4,57 | 6,5119 | 8 | 36,8 | 4,44 |
| P _{4,6} TH(12) | 6 | 4,57 | 6,5119 | 12 | 39,1 | 4,21 |
| P _{8,7} TH(4) | 7 | 8,74 | 6,5119 | 4 | 37,1 | 6,94 |
| P _{8,7} TH(8) | 8 | 8,74 | 6,5119 | 8 | 41,4 | 7,67 |
| P _{8,7} TH(12) | 9 | 8,74 | 6,5119 | 12 | 45,4 | 9,01 |
| P _{1,8} TH | 10 | 1,18 | 6,5119 | 8 | 8,3 | 1,68 |
| P _{16,1} TH | 11 | 16,08 | 6,5119 | 8 | 51,8 | 7,98 |

*Calculated by ¹H-NMR

The use of DCC as the activating agent and DPTS as the catalyst provided a convenient method to synthesize the PDMS-MAI by the direct polycondensation of ACPA with hydroxyl-terminated PDMS. The obtained PDMS-MAI was very effective in initiating the polymerization of P(DMS-b-MMA), P(DMS-b-EMA) and P(TMS-HEMA) copolymers. The whole process of MAI synthesis and its block copolymers were described in Figure 2.6.

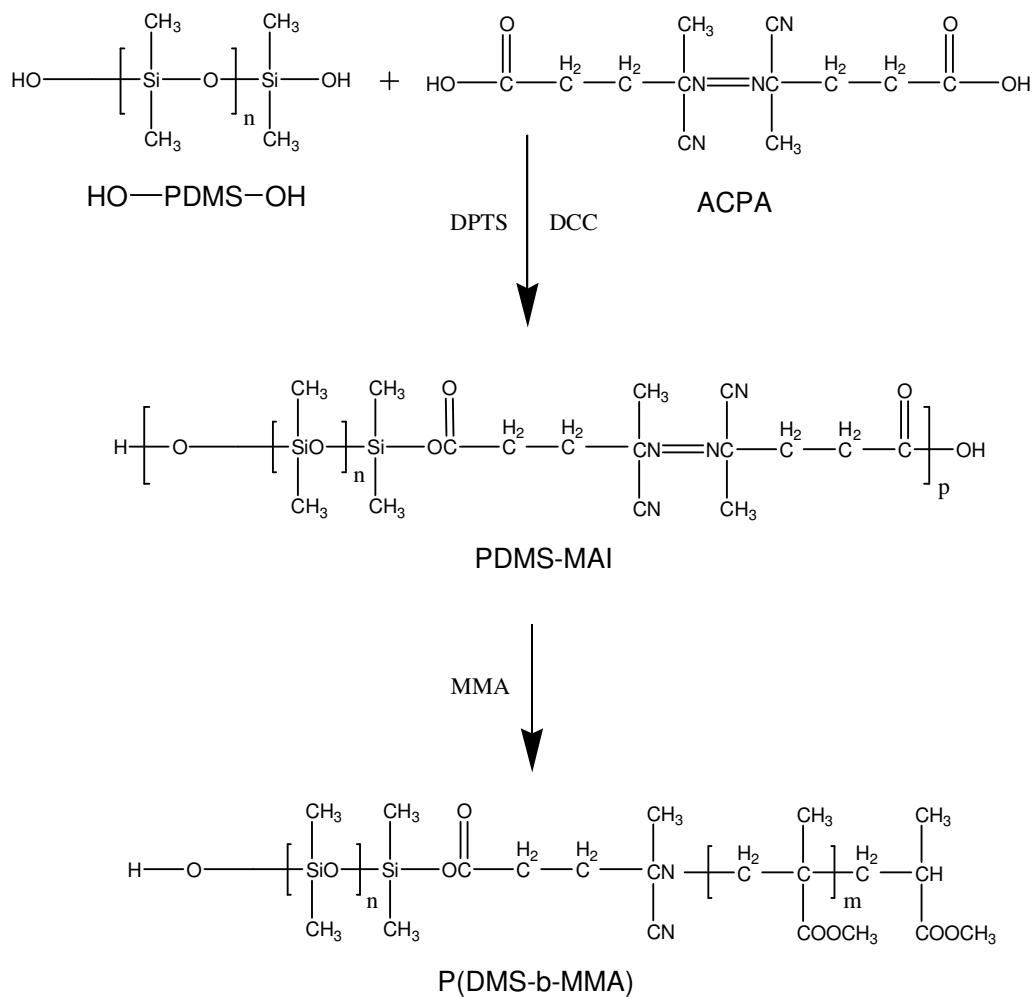


Figure 2.6 Synthesis of Block Copolymers

2.5 Polymer Characterization Methods

2.5.1 Fourier Transform Infrared Spectroscopy (FTIR)

- For ATRP, RAFT and Macroazoinitiator polymers: FTIR analyses were performed with Bruker Optics Tensor Series using IR-spectrometer (resolution

is 4 cm^{-1} and number of scan is 16 cm^{-1}). The data was processed by the OPUS computer program.

- For Gamma rad. polymers: Infrared spectra of the monomer and the polymers obtained were taken from KBr pellets by using a Perkin Elmer Spectrum-One FT-IR Spectrometer.

2.5.2 Nuclear Magnetic Resonance Spectroscopy (^1H -NMR)

^1H and ^{13}C NMR experiments were performed on all homopolymers and copolymers for polymer structural analysis. Bruker Avance DPX 400 and Avance III Ultrashield instruments were used. For ^1H - and ^{13}C -NMR measurements, 400 and 100 MHz frequencies were used, respectively. Measurements were done in deuterio-chloroform (CDCl_3) and deuterio-dimethyl sulfoxide ($\text{d}_6\text{-DMSO}$).

2.5.3 Gas Chromatography Mass Spectrometry(GC-MS)

- For Gamma rad. polymers: The monomer degradation was carried out by GC 2000 Trace Series, which was determined on a phenomenex Zebron ZB-5 capillary column (ThermoQuest Finnigan, Automass). $T_1= 50^\circ\text{C}$ $t=5\text{ min.}$, with $5^\circ\text{C}/\text{min}$ heating rate $T_2= 300^\circ\text{C}$ $t=5\text{ min.}$, $T_3= 300^\circ\text{C}$ $t=5\text{ min.}$ Right inlet temperature = 250°C and constant pressure was applied ($P=250\text{ kPa}$).

2.5.4 Solid State NMR

High-resolution solid-state NMR spectroscopy provides detailed information on the structure of solid polymers. A polymer chain has a large number of conformations because of the various possibilities of rotation around the chain bonds. Contrary to the solution NMR, solid-state NMR spectra are very broad due to the anisotropic or orientation-dependent interactions (internuclear dipolar broadening, chemical shift anisotropy, spin-spin relaxation and spin lattice relaxation). The degree of line

broadening as a function of temperature can provide important motional information about a polymer system. Line broadening in both deuterium and ^{13}C spectroscopy can be used for this purpose. A number of special techniques/equipment, including magic-angle spinning, cross polarization, special 2D experiments, enhanced probe electronics, etc., can provide the same type of information that is available from corresponding solution NMR spectra. ^{13}C CPMAS and ^{29}Si MAS analysis were performed and also ^{29}Si CP-MAS NMR experiments are valuable for assessing the nature of the polysiloxane systems and the local siloxane structures in the region of the pendant group attachments [55]. Solid state NMR spectra were recorded on a High Power Solid State 300 MHz NMR Spectrometer (Bruker, Superconducting FT.NMR Spectrometer AvanceTM, Germany) running ^{29}Si MAS and ^{13}C CPMAS analysis at a spin rate of 5000 Hz with a scan number of 10,000. Samples were ground to powders and packed into the 7 mm ZrO_2 rotors.

2.5.5 Gel Permeation Chromatography (GPC)

The molecular weight and the molecular weight distribution of macroazoinitiator and block copolymers were determined by gel permeation chromatography (GPC, Polymer Laboratories PL-GPC 220) with a 5 μm PL gel columns. Experiments were conducted in THF at 30°C with a 1mL/min. flow rate. Polystyrene universal calibration was applied.

2.5.6 Film Preparation for XPS and SEM Analysis

A required amount of copolymer was dissolved in proper solvent (chloroform for P(DMS-b-MMA), THF for P(DMS-b-EMA) and DMF for P(DMS-b-HEMA)) at 10 % concentration. The solution was cast on a glass plate and allowed for the evaporation of the solvent for three days at 20°C. Films were then dried in a vacuum at 40°C and their thickness was around 30 μm .

2.5.7 X-Ray Photoelectron Spectroscopy (XPS)

X-ray photoelectron spectroscopy (XPS or ESCA) provides information about the chemical composition of film surfaces. The XPS experiments were performed on a SPECS ESCA (Berlin, GERMANY) spectrometer equipped with a unmonochromatized Al K α X-ray source with a power of 250 W. EA 200 hemispherical electrostatic energy analyzer was used in the constant pass energy mode of 96 eV using 4 \times 7 mm² area. The pressure of the analyzer chamber was 10⁻⁸ to 10⁻⁹ torr. Binding energies were referenced to the carbon bond which was assigned a binding energy of 284.5 eV. Each spectrum was curve-fitted using the SpecsLab software.

2.5.8 Scanning Electron Microscopy (SEM)

The surface features and the topography of copolymers were imaged by SEM. SEM micrographs of the sample surfaces that were coated with 2 nm AuPd were taken on Quanta 400 microscope FEI Company (Netherlands) at a magnification of x1000, x2000 and x5000, respectively.

2.5.9 Differential Scanning Calorimetry (DSC)

- For Macroazoinitiator polymers: Thermal transition temperatures of copolymers were determined by Perkin Elmer Jade DSC at N₂ atmosphere. Samples were heated from -160 to 200°C with a 10°C/min. heating rate.
- For Gamma rad. polymers: DSC thermograms were taken on a Dupont Thermal Analyst 2000 Differential Scanning Calorimeter 910 S. All the measurements were done under N₂(g) atmosphere in a temperature range of 25°C to 400°C with 5°C/min heating rate.

- For ATRP polymers: The thermal analyses of the samples were recorded by a TA-DSC 910S differential scanning calorimeter. Heating rate 10⁰C/ min. from – 20⁰ C to 350⁰C under nitrogen gas atmosphere.

2.5.10 Thermogravimetric Analysis (TGA)

TGA in situ FT-IR thermogram for PHEMA was taken on a Perkin Elmer Pyris 1 TGA & Spectrum 1 FT-IR Spectrometer under N₂(g) atmosphere and the polymer was heated from 35⁰C to 720⁰C with a heating rate of 5⁰C/min.

2.5.11 Pyrolysis Mass Spectroscopy

The direct insertion probe pyrolysis mass spectrometry used for the thermal analyses consists of a 5973 HP quadruple mass spectrometer coupled to a JHP SIS direct insertion probe pyrolysis system. Polymer samples (0.01mg) were pyrolyzed in flared glass sample vials. The temperature was increased at a rate of 10⁰C/min and the scan rate was 2 scans/s.

2.5.12 Viscosity Measurements

Viscosity measurements were made in a thermostatic water bath at 30 °C using an Ubbelohde viscometer. A copolymer was dissolved in methanol, which had been exhaustively dried. For each polymer, the viscosity of four concentrations was measured. Multiple readings were made at each concentration. Intrinsic viscosity was obtained by extrapolation of a plot of specific viscosity/concentration vs concentration to infinite solution.

CHAPTER 3

RESULTS and DISCUSSION

3.1 Aqueous solution polymerization of HEMA by gamma-radiation

The time-conversion plot for radiation induced polymerization of HEMA at 25°C is given in Figure 3.1. The kinetic curve showed an autoacceleration character with a short induction period. The polymer obtained was brittle, transparent and insoluble in common organic solvents.

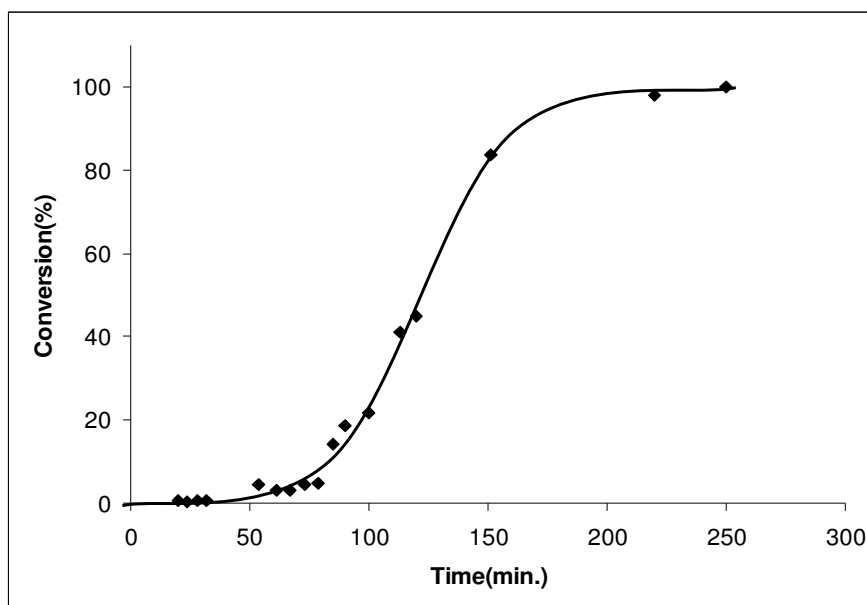


Figure 3.1 Conversion – Time graph for γ -radiation polymerization of HEMA

3.1.1 FTIR Analysis of PHEMA obtained by gamma radiation

The FT-IR spectra of HEMA and PHEMA are given in Figure 3.2. In the spectrum of monomer (Figure 3.2a) the -OH peak is broad in the range of $3300\text{-}3700\text{ cm}^{-1}$ indicating hydrogen bonding. It also was retained in the spectrum of polymer (Figure 3.2b). However, the shoulder at 3100 cm^{-1} ; peaks at 1637 , 933 and 816 cm^{-1} corresponding to -C=C- in the spectrum of monomer are not present in the polymer spectrum. The -C=O (1719 cm^{-1}), -C-O-C- ($1321\text{-}1032\text{ cm}^{-1}$), -CH_2 ($1404\text{-}1379\text{ cm}^{-1}$) are present in both spectrum. Thus, polymerization proceeds via the opening of double bonds.

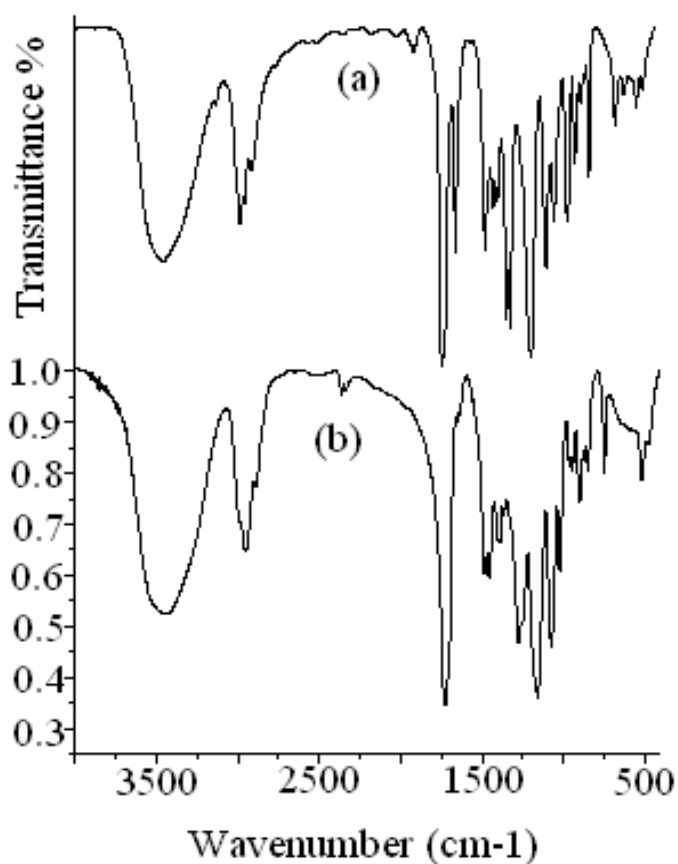


Figure 3.2 FTIR spectrum of (a) HEMA and (b) polymer of HEMA

3.1.2 DSC Analysis of PHEMA obtained by gamma radiation

The DSC thermogram of PHEMA is given in Figure 3.3. The detailed analysis of thermogram by a program showed that the T_g value is around 88°C and peak at 110-160 (maximize at 140 °C) corresponds to further polymerization which was not observed in the second run thermogram. The polymerization peak has the enthalpy of $\Delta H = -61.3 \text{ J/g}$.

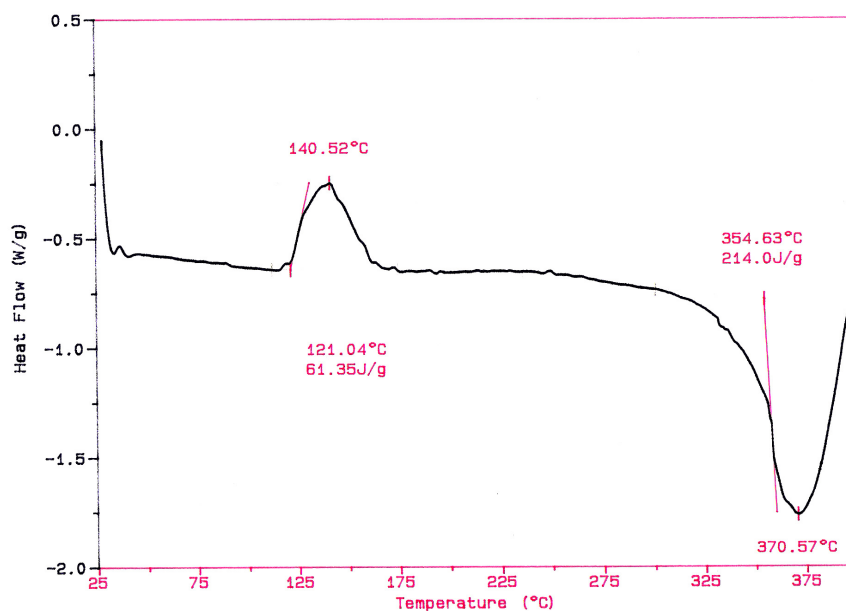


Figure 3.3 DSC thermogram of PHEMA

3.1.3 Thermal Degradation of PHEMA

The GC-MS results of the monomer, HEMA is shown in Figure 3.4. Monomer degradation is reached maximum at about 175°C. The main fragments at 175°C are

given in Figure 3.4b. The fragmentation is shown in Figure 3.5. Monomer is not observed in the spectrum. Therefore, monomer is not stable and gives fragments, which are also observed in the mass spectrum of polymer. The main fragments are $\text{CH}_2=\text{C}(\text{CH}_3)\text{CO}$ ($m/z=69$), $\text{CH}_2=\text{C}(\text{CH}_3)-$ ($m/z=41$) and $(\text{CH}_3)_2\text{CHCO}_2$ ($m/z=87$).

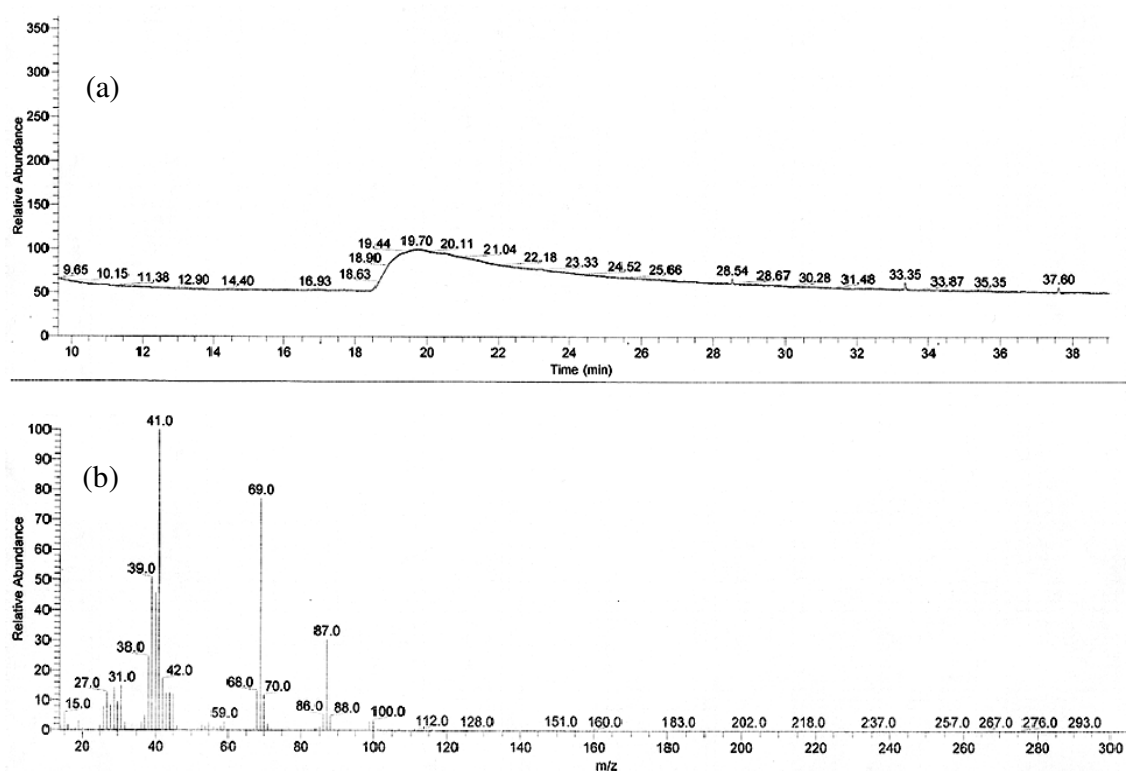


Figure 3.4 GC-MS spectrum of HEMA

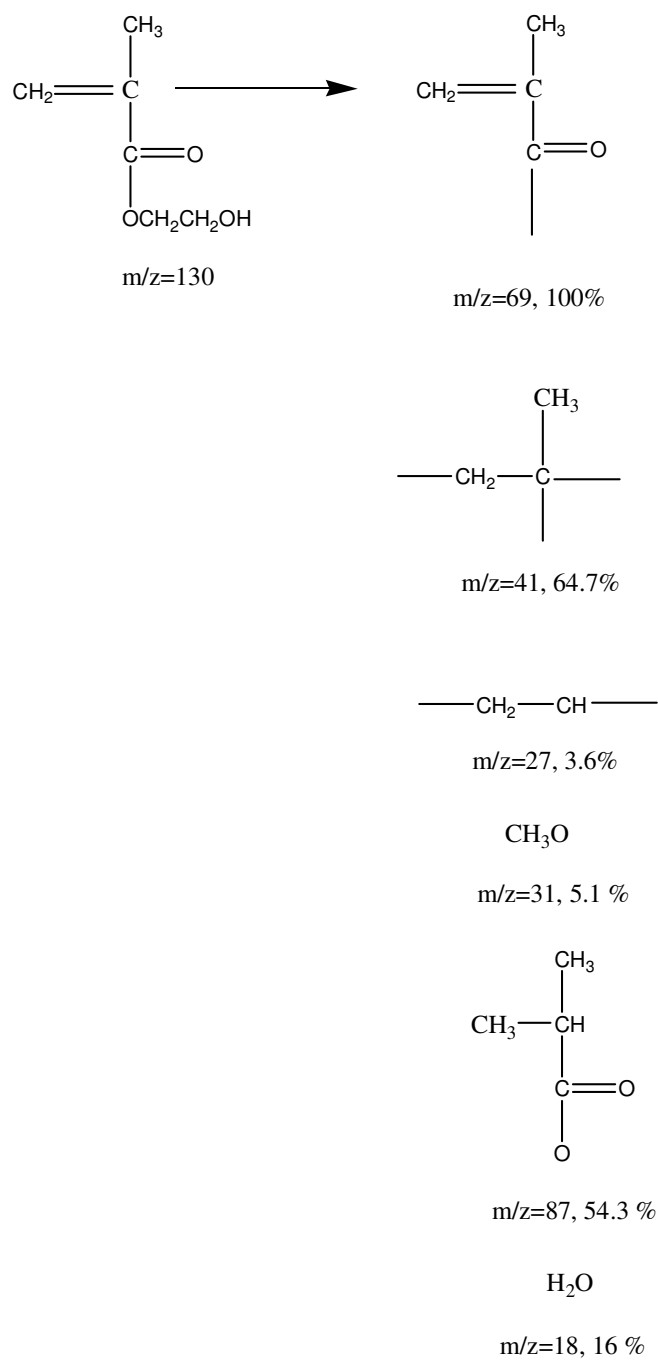


Figure 3.5 Schematic representation of fragmentation

The thermal degradation of PHEMA was investigated by TGA-FTIR and electron impact (70 eV) Mass Spectroscopy methods. The thermal stability of PHEMA was characterized by means of TGA from 35°C to 700°C in N₂ atmosphere as shown in Figure 3.6. The TGA thermogram showed depolymerization type degradation and derivative weight loss is a broad peak with a maximum at about 275°C. The activation energy of degradation was calculated according to Broido method [56] as 73,06 kJ/mol, which is smaller than the reported activation energy [31]. The thermal degradation of homogeneous system has following expression:

$$\frac{d\alpha}{dt} = k(T)f[\alpha(t)] \quad \text{Eq.1.1}$$

$$\alpha = (W_0 - W_t) / (W_0 - W_f) \quad \text{Eq.1.2}$$

where α is extent of sample being degraded and W_0, W_t and W_f are weight of sample before degradation, at time t and after complete degradation, respectively. $f(\alpha)$ represents the net results of elementary steps, as the polymer degradation are often chain reactions. For solid state reactions $f(\alpha) = (1 - \alpha)^n$, where n is the order of reaction (for many pyrolysis process $n=1$ is assumed). At a specific heating rate, $\beta = dT/dt$,

$$\frac{d\alpha}{dT} = (A/\beta)\exp(-E_a/RT)(1-\alpha)^n \quad \text{Eq.1.3}$$

According to Broido method for $n=1$

$$\log[-\log(1-\alpha)] = -(E_a/2.303R)[(1/T)+K] \quad \text{Eq.1.4}$$

So, in the $\log[-\log(1-\alpha)]$ versus $1/T$ plot the slope gives the $-E_a/2.303R$ value.

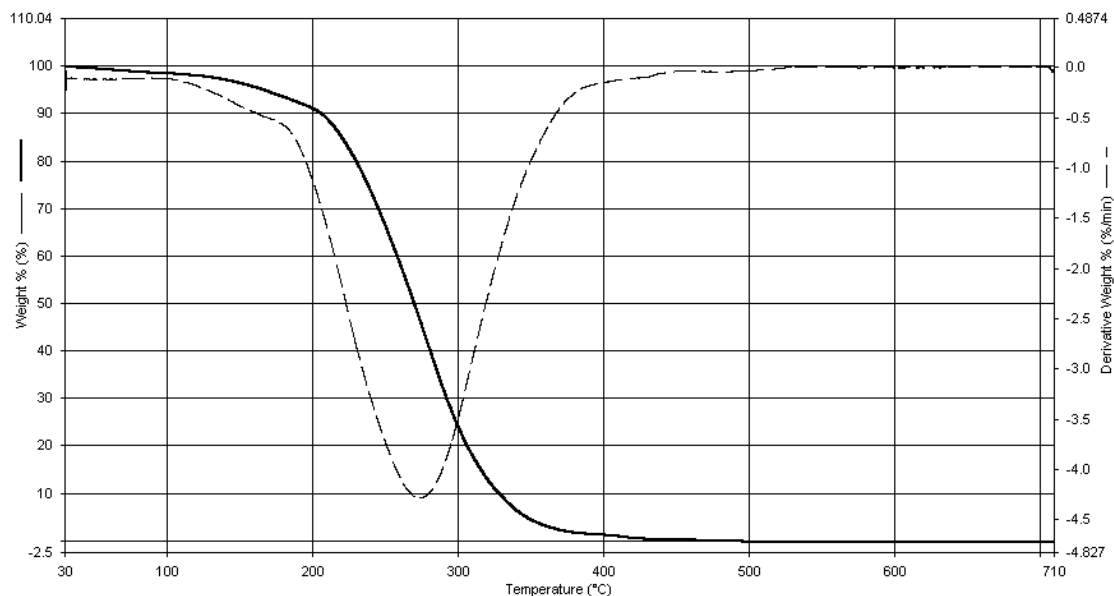


Figure 3.6 TGA thermogram of γ -irradiated PHEMA

Polymer was degraded completely at about 483°C. The evolved gas from the degradation was recorded by FT-IR spectra continuously. The FT-IR spectra of the degraded fragments at 197°C to 431°C are given in Figure 3.7. The FT-IR spectra for degradation from 125 to 293 °C are corresponding to that of monomer, which have been depolymerized or in oligomers. However the broad and strong peak of -OH in monomer FT-IR spectrum (Figure 3.2a) was not observed in these spectra. Therefore, there should be linkage type degradation in the early stage of degradation to remove HOCH₂CH₂- groups. The noisy peaks at 3800-3700 cm⁻¹, ~2400 cm⁻¹, 1400-1800 cm⁻¹ as transmitted correspond to H₂O and CO₂ backgrounds. The degradation is completed at 483°C. Thus, the TGA degradation of PHEMA is different from that of PMMA, which is a depolymerization type.

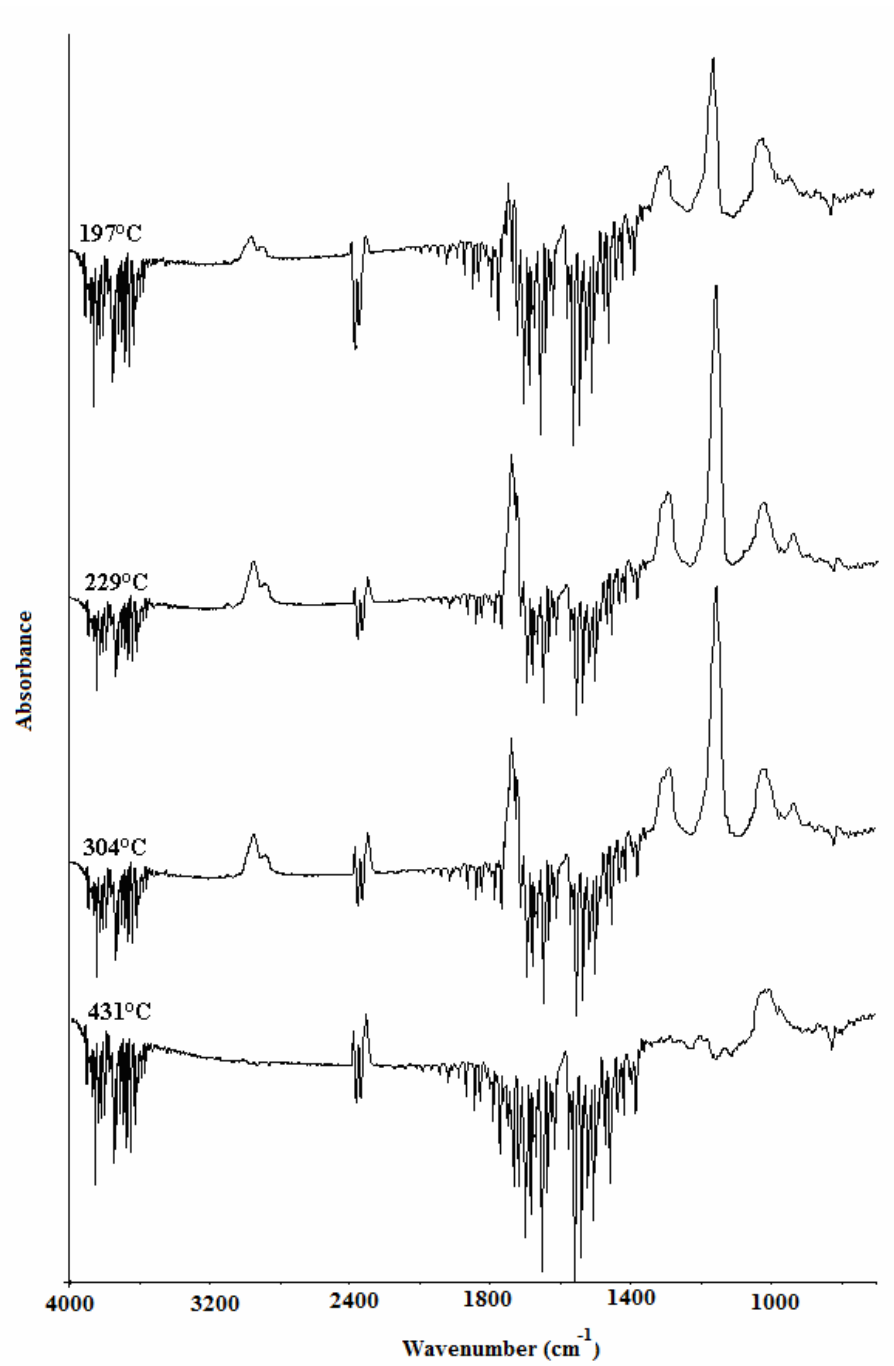


Figure 3.7 FTIR spectrum of decomposition gases from TGA analysis

In order to understand the thermal degradation better, the pyrolysis of the polymer sample under vacuum at different temperature were also carried out. The FT-IR spectra of samples after pyrolysis were recorded and shown in Figure 3.8. The spectra at different temperatures are identical to that of the polymer (Figure 3.2b), therefore, there is no side group cyclization (lactons and/or anhydrides) during the thermal degradation. The degradation is linkage and depolymerization with a combination of monomer fragmentation. The FT-IR spectra at 400(b)°C is that of condensed fragments of degraded polymer. It corresponds to polymer with a cleavage of $-\text{CH}_2\text{CH}_2\text{OH}$ or $-\text{CH}_2\text{OH}$ groups that leaves no $-\text{OH}$ groups as observed for fragmented product (Figure 3.7)

3.1.4 Mass Spectral Analysis

The mass thermogram of PHEMA is given in Figure 3.9 and the mass spectrum corresponding to maximum yield is shown in Figure 3.10. The fragmentation in the thermogram showed four stages at about (a) 30-50°C, (b) 250-350°C, (c) 350-470°C and (d) 470-520°C. The results are tabulated in Table 3.1. The fragments in the first two stages are corresponding to that of the monomer degradation. This is generally affected by electron impact rather than temperature. The degradation fragments in the first stage are the same as the fragments obtained from GC-MS of monomer (Figure 3.4 and 3.5). Unlike other acrylates if there is a functional group in the R group of ester OR, the monomer becomes unstable and degraded at low temperatures. In the second stage, the fragments are that of the monomer as in the first degradation stage with some changes in fragments abundances. In the last two stages the main fragments are given in Figure 3.11. The other fragments at these stages are those of monomer and polymer. However, the other polymer fragments have limited abundances. These are dimer, trimer, tetramer and their fragments. They are given in Table 3.1.

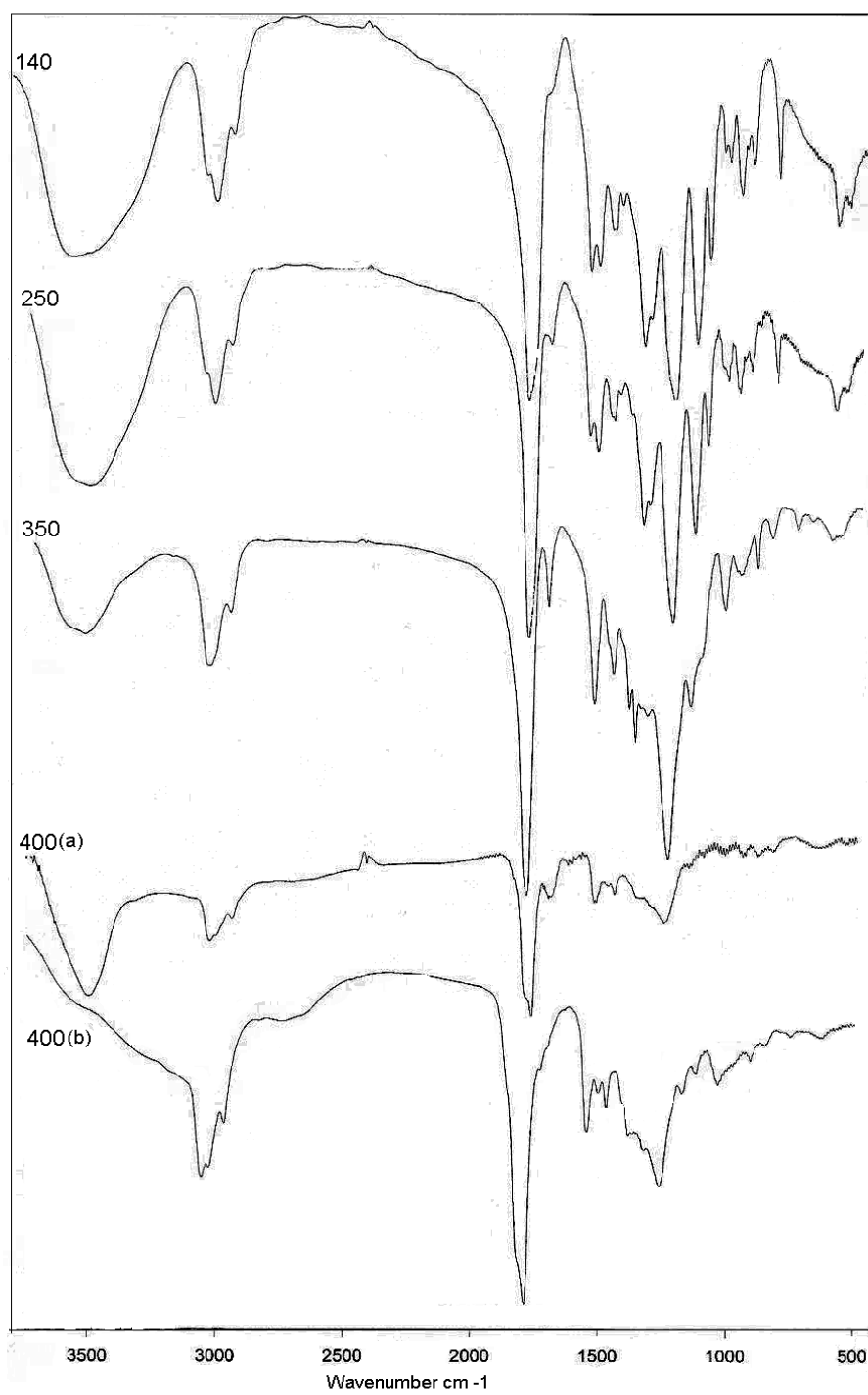


Figure 3.8 FTIR spectra of PHEMA after pyrolysis at different temperatures

Table 3.1 Mass spectral fragments at different stage of degradation

| m/z | 2.216 (48°C) | | 34.068 (365°C) | | 44.507 (470°C) | | 49.519 (520°C) | |
|-----|------------------|---|------------------|---|------------------|---|------------------|---|
| | I/I ₀ | Fragments | I/I ₀ | Fragments | I/I ₀ | Fragments | I/I ₀ | Fragments |
| 15 | 0.59 | CH ₃ | 0.69 | CH ₃ | 0.25 | CH ₃ | 1.76 | CH ₃ |
| 17 | 3.63 | OH | 0.07 | OH | 0.03 | OH | 0.58 | OH |
| 18 | 16.34 | H ₂ O | 0.25 | H ₂ O | 0.13 | H ₂ O | 2.35 | H ₂ O |
| 27 | 3.64 | C ₂ H ₃ | 3.44 | C ₂ H ₃ | 3.27 | C ₂ H ₃ | 14.96 | C ₂ H ₃ |
| 28 | 5.74 | CO,C ₂ H ₄ | 2.24 | CO,C ₂ H ₄ | 3.61 | CO,C ₂ H ₄ | 29.57 | CO,C ₂ H ₄ |
| 29 | 3.88 | C ₂ H ₅ | 6.76 | C ₂ H ₅ | 5.36 | C ₂ H ₅ | 24.98 | C ₂ H ₅ |
| 31 | 5.14 | CH ₃ O | 17.82 | CH ₃ O | 2.08 | CH ₃ O | 8.53 | CH ₃ O |
| 41 | 64.67 | C ₃ H ₅ | 62.14 | C ₃ H ₅ | 26.01 | C ₃ H ₅ | 69.87 | C ₃ H ₅ |
| 43 | 6.54 | C ₃ H ₇ ,C ₂ H ₃ O | 11.45 | C ₃ H ₇ ,C ₂ H ₃ O | 12.01 | C ₃ H ₇ ,C ₂ H ₃ O | 38.90 | C ₃ H ₇ ,C ₂ H ₃ O |
| 44 | 7.82 | C ₂ H ₄ O,CO ₂ | 12.54 | C ₂ H ₄ O,CO ₂ | 11.84 | C ₂ H ₄ O,CO ₂ | 51.21 | C ₂ H ₄ O,CO ₂ |
| 45 | 11.52 | C ₂ H ₅ O | 16.28 | C ₂ H ₅ O | 7.89 | C ₂ H ₅ O | 22.21 | C ₂ H ₅ O |
| 53 | 1.05 | C ₄ H ₅ | 1.54 | C ₄ H ₅ | 6.74 | C ₄ H ₅ | 16.17 | C ₄ H ₅ |
| 55 | 2.54 | C ₃ H ₃ O | 3.86 | C ₃ H ₃ O | 22.44 | C ₃ H ₃ O | 58.52 | C ₃ H ₃ O |
| 61 | 0.43 | C ₂ H ₅ O ₂ | 1.32 | C ₂ H ₅ O ₂ | 0.41 | C ₂ H ₅ O ₂ | 0.92 | C ₂ H ₅ O ₂ |
| 69 | 100.00 | C ₄ H ₅ O | 100.00 | C ₄ H ₅ O | 63.79 | C ₄ H ₅ O | 92.15 | C ₄ H ₅ O |
| 77 | 0.33 | C ₂ H ₅ O ₃ | 0.31 | C ₂ H ₅ O ₃ | 10.13 | C ₂ H ₅ O ₃ | 20.32 | C ₂ H ₅ O ₃ |
| 87 | 54.29 | C ₄ H ₇ O ₂ | 66.39 | C ₄ H ₇ O ₂ | 9.27 | C ₄ H ₇ O ₂ | 11.56 | C ₄ H ₇ O ₂ |
| 91 | 2.58 | C ₃ H ₇ O ₃ ,C ₄ H ₁₁ O ₂ | 2.38 | C ₃ H ₇ O ₃ ,C ₄ H ₁₁ O ₂ | 19.88 | C ₃ H ₇ O ₃ ,C ₄ H ₁₁ O ₂ | 38.10 | C ₃ H ₇ O ₃ ,C ₄ H ₁₁ O ₂ |
| 100 | 7.11 | C ₅ H ₈ O ₂ | 11.27 | C ₅ H ₈ O ₂ | 23.18 | C ₅ H ₈ O ₂ | 28.79 | C ₅ H ₈ O ₂ |

Table 3.1 Continued

| | | | | | | | | |
|------------|------|---|------|---|--------|---|--------|---|
| 113 | 1.31 | C ₆ H ₉ O ₂ | 5.84 | C ₆ H ₉ O ₂ | 100.00 | C ₆ H ₉ O ₂ | 100.00 | C ₆ H ₉ O ₂ |
| 117 | 1.35 | C ₅ H ₉ O ₃ | 1.30 | C ₅ H ₉ O ₃ | 7.64 | C ₅ H ₉ O ₃ | 13.02 | C ₅ H ₉ O ₃ |
| 129 | 0.35 | C ₇ H ₁₃ O ₂ | 0.38 | C ₇ H ₁₃ O ₂ | 12.08 | C ₇ H ₁₃ O ₂ | 15.27 | C ₇ H ₁₃ O ₂ |
| 130 | 0.09 | C ₆ H ₁₀ O ₃ ,monomer | 0.11 | C ₆ H ₁₀ O ₃ ,monomer | 3.13 | C ₆ H ₁₀ O ₃ ,monomer | 4.58 | C ₆ H ₁₀ O ₃ ,monomer |
| 141 | 0.07 | C ₇ H ₉ O ₃ | 0.10 | C ₇ H ₉ O ₃ | 11.26 | C ₇ H ₉ O ₃ | 13.62 | C ₇ H ₉ O ₃ |
| 149 | 0.13 | C ₈ H ₅ O ₃ | | C ₈ H ₅ O ₃ | 10.82 | C ₈ H ₅ O ₃ | 13.62 | C ₈ H ₅ O ₃ |
| 165 | 0.16 | C ₉ H ₉ O ₃ | 0.17 | C ₉ H ₉ O ₃ | 10.93 | C ₉ H ₉ O ₃ | 14.20 | C ₉ H ₉ O ₃ |
| 187 | - | C ₉ H ₁₅ O ₄ | 0.46 | C ₉ H ₁₅ O ₄ | 19.01 | C ₉ H ₁₅ O ₄ | 14.61 | C ₉ H ₁₅ O ₄ |
| 199 | 0.01 | C ₁₀ H ₁₅ O ₄ | 0.41 | C ₁₀ H ₁₅ O ₄ | 10.67 | C ₁₀ H ₁₅ O ₄ | 10.05 | C ₁₀ H ₁₅ O ₄ |
| 215 | 0.03 | C ₁₀ H ₁₅ O ₅ | 0.33 | C ₁₀ H ₁₅ O ₅ | 7.27 | C ₁₀ H ₁₅ O ₅ | 8.03 | C ₁₀ H ₁₅ O ₅ |
| 231 | 0.02 | C ₁₁ H ₁₉ O ₅ | 0.03 | C ₁₁ H ₁₉ O ₅ | 9.75 | C ₁₁ H ₁₉ O ₅ | 6.59 | C ₁₁ H ₁₉ O ₅ |
| 255 | - | C ₁₂ H ₁₅ O ₆ | 0.05 | C ₁₂ H ₁₅ O ₆ | 5.55 | C ₁₂ H ₁₅ O ₆ | 4.43 | C ₁₂ H ₁₅ O ₆ |
| 260 | - | C ₁₂ H ₂₀ O ₆ ,dimer | 0.01 | C ₁₂ H ₂₀ O ₆ ,dimer | 2.27 | C ₁₂ H ₂₀ O ₆ ,dimer | 2.41 | C ₁₂ H ₂₀ O ₆ ,dimer |
| 267 | - | C ₁₃ H ₁₅ O ₆ | 0.03 | C ₁₃ H ₁₅ O ₆ | 4.37 | C ₁₃ H ₁₅ O ₆ | 3.61 | C ₁₃ H ₁₅ O ₆ |
| 279 | 0.02 | C ₁₄ H ₁₅ O ₆ | 0.01 | C ₁₄ H ₁₅ O ₆ | 3.05 | C ₁₄ H ₁₅ O ₆ | 2.88 | C ₁₄ H ₁₅ O ₆ |
| 287 | - | C ₁₄ H ₂₃ O ₆ | 0.01 | C ₁₄ H ₂₃ O ₆ | 3.58 | C ₁₄ H ₂₃ O ₆ | 2.50 | C ₁₄ H ₂₃ O ₆ |
| 299 | - | C ₁₅ H ₂₃ O ₆ | 0.03 | C ₁₅ H ₂₃ O ₆ | 6.42 | C ₁₅ H ₂₃ O ₆ | 3.33 | C ₁₅ H ₂₃ O ₆ |
| 311 | 0.03 | C ₁₆ H ₂₃ O ₆ | 0.05 | C ₁₆ H ₂₃ O ₆ | 5.15 | C ₁₆ H ₂₃ O ₆ | 2.89 | C ₁₆ H ₂₃ O ₆ |
| 327 | - | C ₁₇ H ₂₇ O ₆ | 0.01 | C ₁₇ H ₂₇ O ₆ | 3.05 | C ₁₇ H ₂₇ O ₆ | 2.17 | C ₁₇ H ₂₇ O ₆ |
| 376 | - | C ₁₇ H ₂₉ O ₉ | - | C ₁₇ H ₂₉ O ₉ | 0.97 | C ₁₇ H ₂₉ O ₉ | 0.67 | C ₁₇ H ₂₉ O ₉ |
| 390 | - | C ₁₈ H ₃₀ O ₉ ,trimer | - | C ₁₈ H ₃₀ O ₉ ,trimer | 0.75 | C ₁₈ H ₃₀ O ₉ ,trimer | 0.55 | C ₁₈ H ₃₀ O ₉ ,trimer |
| 520 | - | C ₂₄ H ₄₀ O ₁₂ ,tetramer | - | C ₂₄ H ₄₀ O ₁₂ ,tetramer | 0.25 | C ₂₄ H ₄₀ O ₁₂ ,tetramer | 0.17 | C ₂₄ H ₄₀ O ₁₂ ,tetramer |

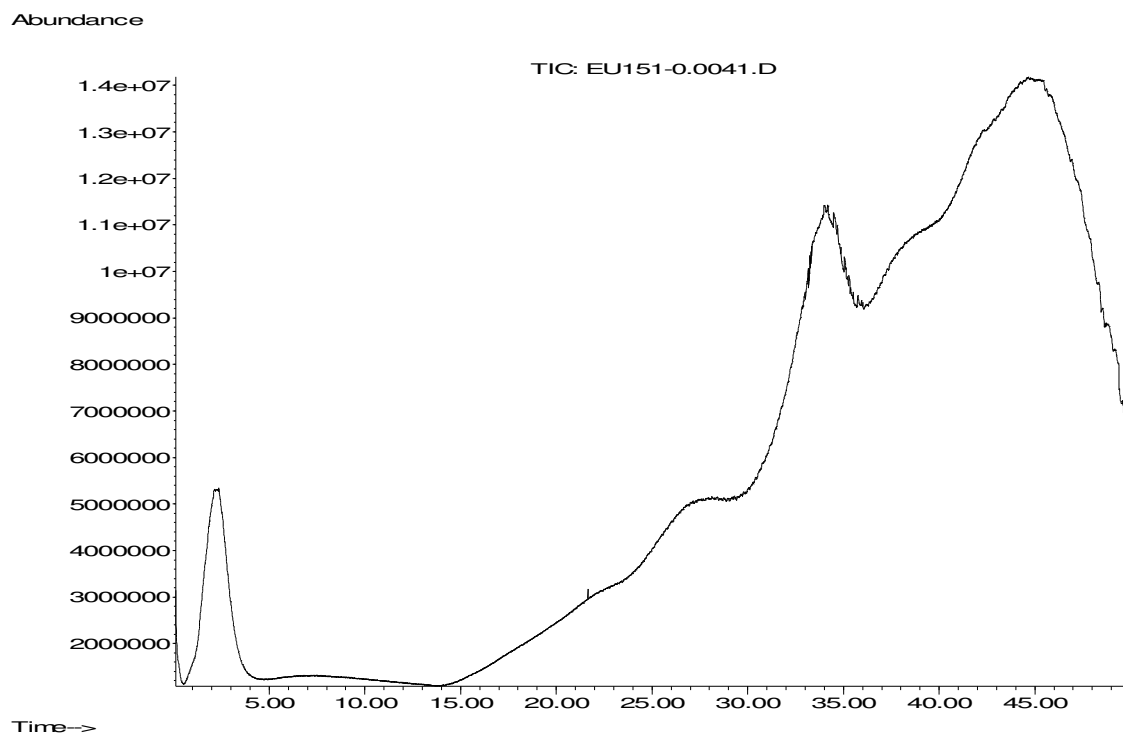


Figure 3.9 Mass thermogram of PHEMA

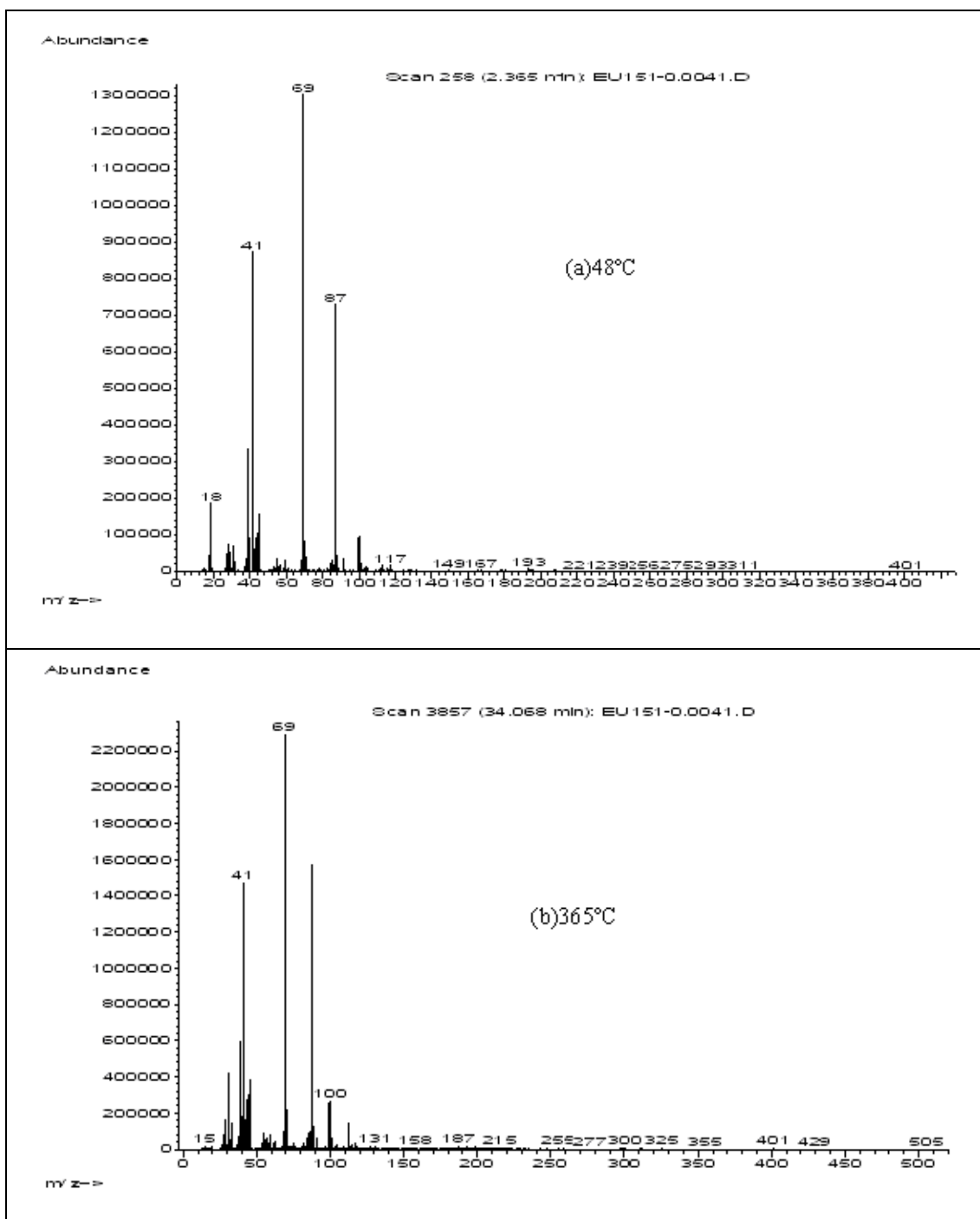


Figure 3.10 Fragments of PHEMA obtained at (a)48°C, (b)365°C

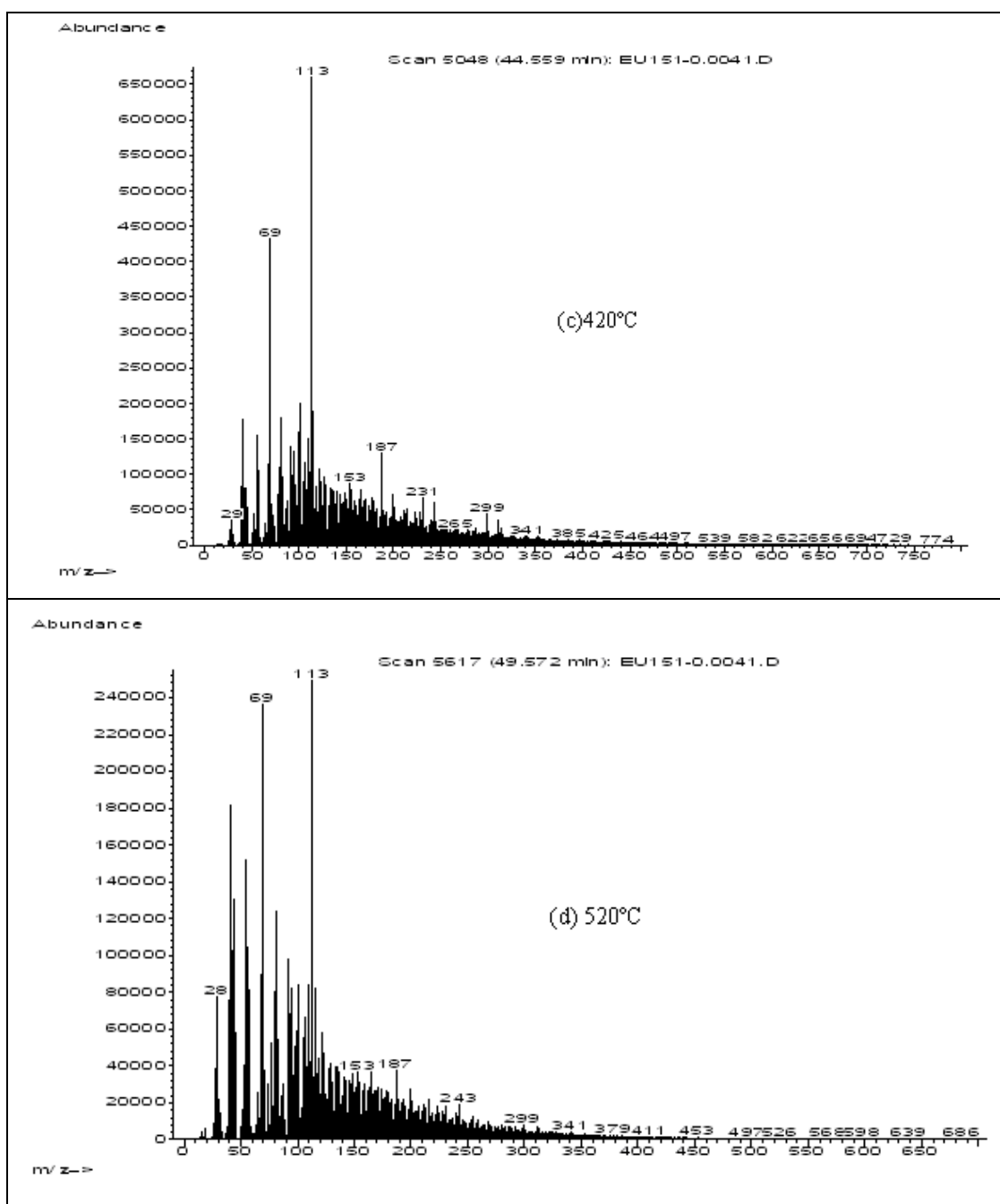


Figure 3.10 continued for (c) 420°C and (d) 520°C

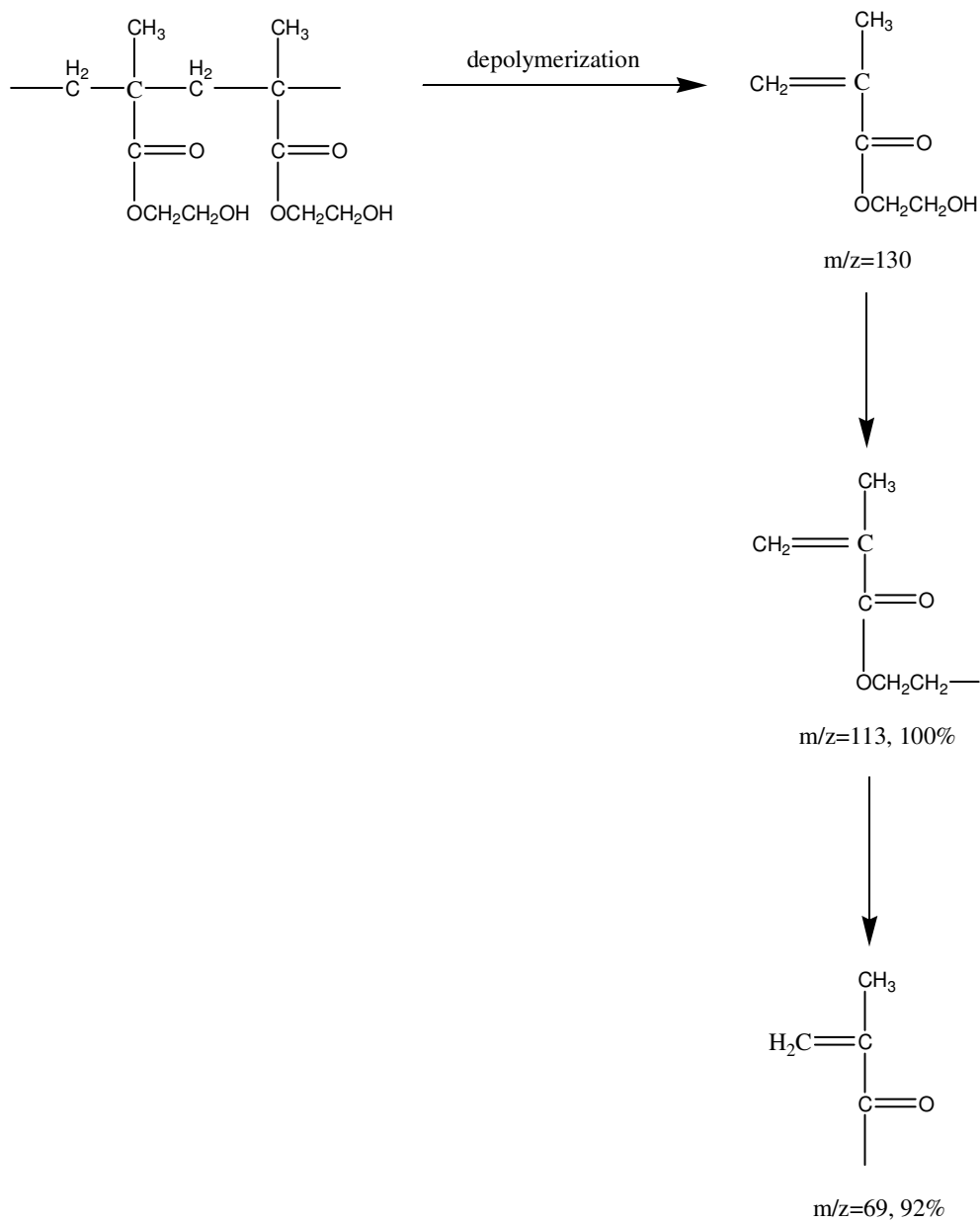


Figure 3.11 Schematic representations of main fragments in last two stages

The polymerization of HEMA was carried out in aqueous solution to saturate -CH₂CH₂OH groups and that way to prevent intra- and intermolecular hydrogen bonding. In this case, the polymer might be linear. However, the polymer obtained was

insoluble in common organic solvents and polymerization can not be proceeded in a controlled way with respect to the molecular weight. Hence, controlled living radical polymerization techniques (e.g. ATRP and RAFT polymerization) have been tried to achieve the desired molecular weights and properties of PHEMA and then, its copolymerization with PDMS.

3.2 Atom Transfer Radical Polymerization of HEMA

Copper mediated ATRP is one of the controlled living polymerization technique employed to obtain predetermined molecular weights of polymers. The details of the mechanism of ATRP were explained in Chapter 1. Briefly, the carbon-halogen bond of an initiator (RX) is reversibly cleaved by a Cu(I)X/ligand catalyst resulting in a radical (R•) and Cu(II)X₂/ligand. The radical can reversibly deactivate (mainly), add to the monomer or irreversibly terminate (Figure 3.12).

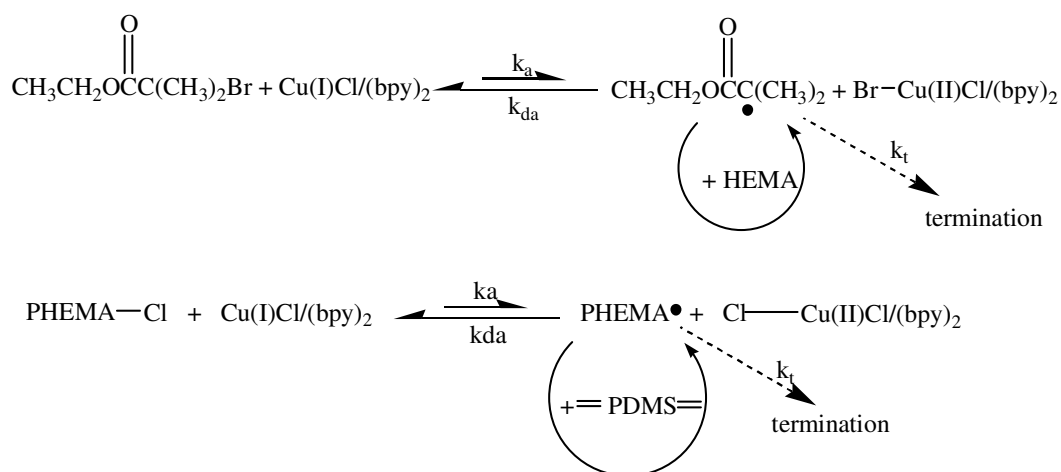


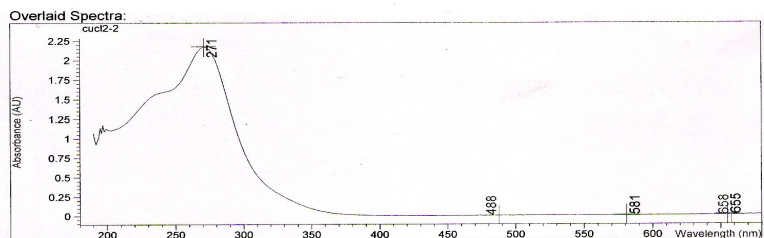
Figure 3.12 Simplified ATRP mechanism for PHEMA macroinitiator and P(HEMA-b-DMS) copolymer.

The scope of the synthesis of block copolymer via ATRP is the preparation of the first block of PHEMA and then, isolates the polymer as a macroinitiator for second block of vinyl terminated PDMS. Before the copolymerization, a best condition for the controlled radical polymerization of HEMA was aimed. The ATRP process is multicomponent system; therefore a selection of suitable catalyst and initiator for the monomer is critical. Therefore, different complexes (metals/ligands) were synthesized in different solvents and then, characterized by UV-Vis and FTIR spectroscopy techniques before the polymerization.

3.2.1 UV-Vis and FTIR results of Cu (II) complexes

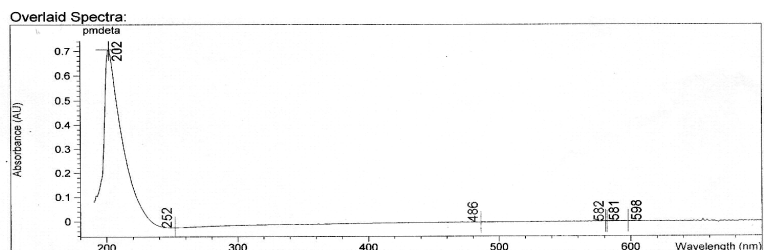
The complexation of both CuCl_2 and CuBr_2 with different nitrogen based ligand was investigated by UV-vis and FTIR spectroscopy. The absorption spectrum in visible region of Cu(II)01 complex gave a maximum intense broad peak at 290 nm which was different from both CuCl_2 (271 nm) and PMDETA (202nm) (Figure 3.13). Changing the ligand from PMDETA to 4,4-dMbpy and the solvent, the Cu(II)02 complex gave a maximum at 206 nm and 296 nm which are also different from 4,4-dMbpy (208, 239 and 272 nm) (Figure 3.14). From the UV-vis spectra of Cu(II)03, Cu(II)04 and Cu(II)05 complexes (Figure A.1-A.3, Appendix A), it can be seen that the absorption peaks of both metal (CuBr_2) and different ligands (2,2-bpy, PMDETA, and 4,4-Dmbpy) disappeared and new absorption bands formed. This means that, the complexation reactions of both CuCl_2 and CuBr_2 with different ligands were formed and the newly formed absorption bands can be assigned as a metal to ligand charge transfer (MLCT) or reverse (LMCT). FTIR results also supported the complex forming (Figure 3.15 and 3.16).

Metal : CuCl₂



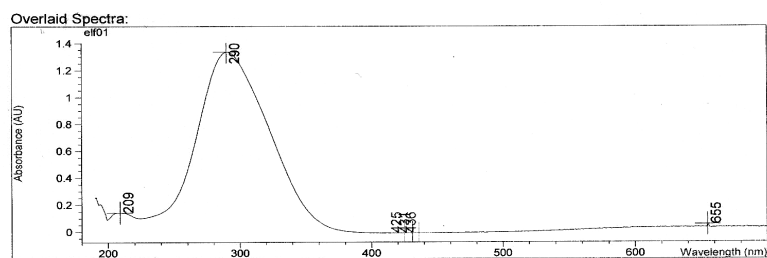
| # | Name | Peaks(nm) | Abs(AU) | Valleys(nm) | Abs(AU) |
|---|---------|-----------|-----------|-------------|-----------|
| 1 | cucl2-2 | 271.0 | 2.17500 | 488.0 | 7.3576E-4 |
| 1 | | 655.0 | 1.4065E-2 | 656.0 | 2.5845E-3 |
| 1 | | 581.0 | 4.2529E-3 | *** | *** |

Ligand : PMDETA



| # | Name | Peaks(nm) | Abs(AU) | Valleys(nm) | Abs(AU) |
|---|---------|-----------|------------|-------------|------------|
| 1 | pmdeata | 202.0 | 0.70642 | 252.0 | -2.5849E-2 |
| 1 | | 598.0 | -1.9155E-3 | 486.0 | -6.5956E-3 |
| 1 | | 581.0 | -2.3117E-3 | 582.0 | -4.5557E-3 |

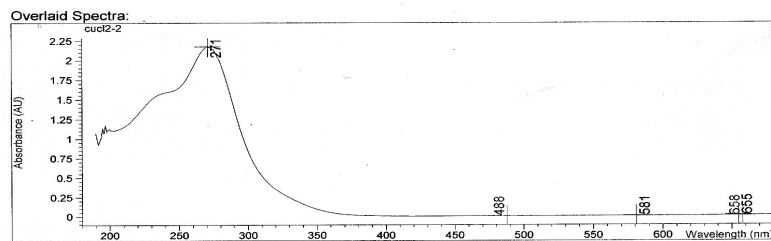
Cu(II)01 complex



| # | Name | Peaks(nm) | Abs(AU) | Valleys(nm) | Abs(AU) |
|---|-------|-----------|-----------|-------------|------------|
| 1 | elf01 | 290.0 | 1.33490 | 431.0 | -1.1728E-2 |
| 1 | | 209.0 | 0.14072 | 425.0 | -1.1651E-2 |
| 1 | | 655.0 | 4.9165E-2 | 436.0 | -1.0911E-2 |

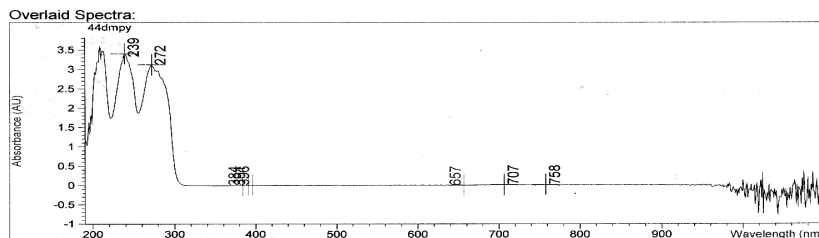
Figure 3.13 UV-Vis spectrum of Cu(II)01 complex

Metal : CuCl₂



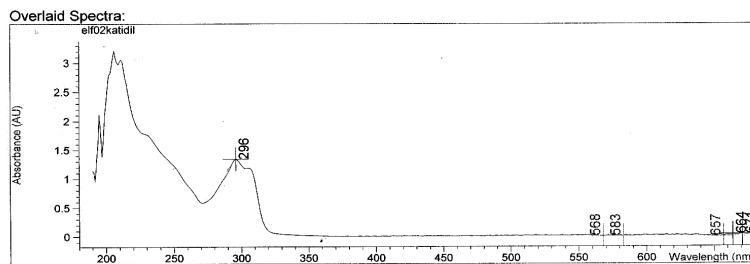
| # | Name | Peaks(nm) | Abs(AU) | Valleys(nm) | Abs(AU) |
|---|---------|-----------|-----------|-------------|-----------|
| 1 | cucl2-2 | 271.0 | 2.17500 | 488.0 | 7.3576E-4 |
| 1 | | 655.0 | 1.4085E-2 | 658.0 | 2.5845E-3 |
| 1 | | 581.0 | 4.2529E-3 | *** | *** |

Ligand : 4,4-Dmbpy



| # | Name | Peaks(nm) | Abs(AU) | Valleys(nm) | Abs(AU) |
|---|---------|-----------|-----------|-------------|------------|
| 1 | 44dmbpy | 239.0 | 3.39930 | 657.0 | -1.2693E-2 |
| 1 | | 272.0 | 3.11670 | 391.0 | -8.0533E-3 |
| 1 | | 707.0 | 7.7901E-3 | 384.0 | -7.9269E-3 |
| 1 | | 758.0 | 7.0767E-3 | 396.0 | -7.5936E-3 |

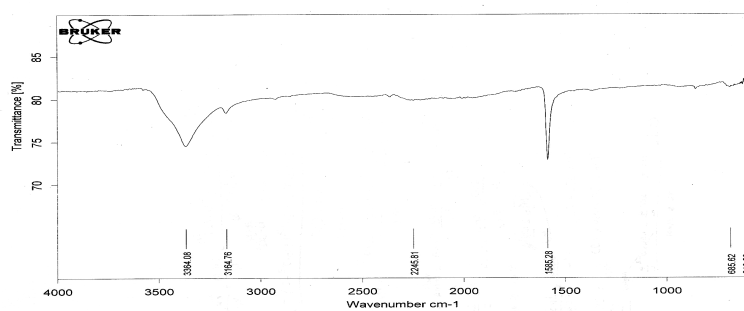
Cu(II)O2 complex



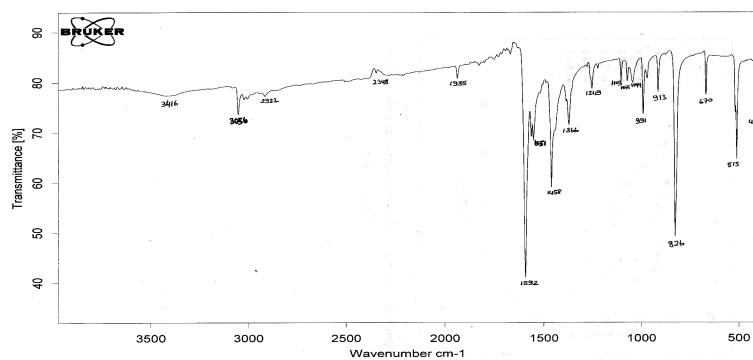
| # | Name | Peaks(nm) | Abs(AU) | Valleys(nm) | Abs(AU) |
|---|--------------|-----------|-----------|-------------|------------|
| 1 | eif02katidil | 296.0 | 1.33700 | 657.0 | -1.4187E-2 |
| 1 | | 671.0 | 2.8082E-2 | 583.0 | -1.4114E-3 |
| 1 | | 664.0 | 2.6311E-2 | 568.0 | -6.1846E-4 |

Figure 3.14 UV-Vis spectrum of Cu(II)O₂ complex

Metal : CuCl₂



Ligand : 4,4-Dmbpy



Cu(II)O2 complex

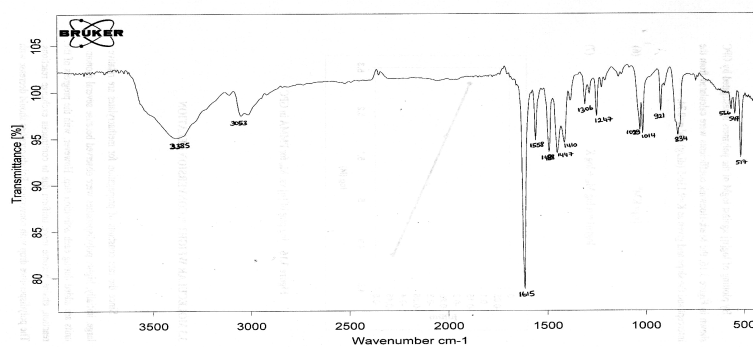


Figure 3.15 FTIR spectrum of Cu(II)O₂ complex

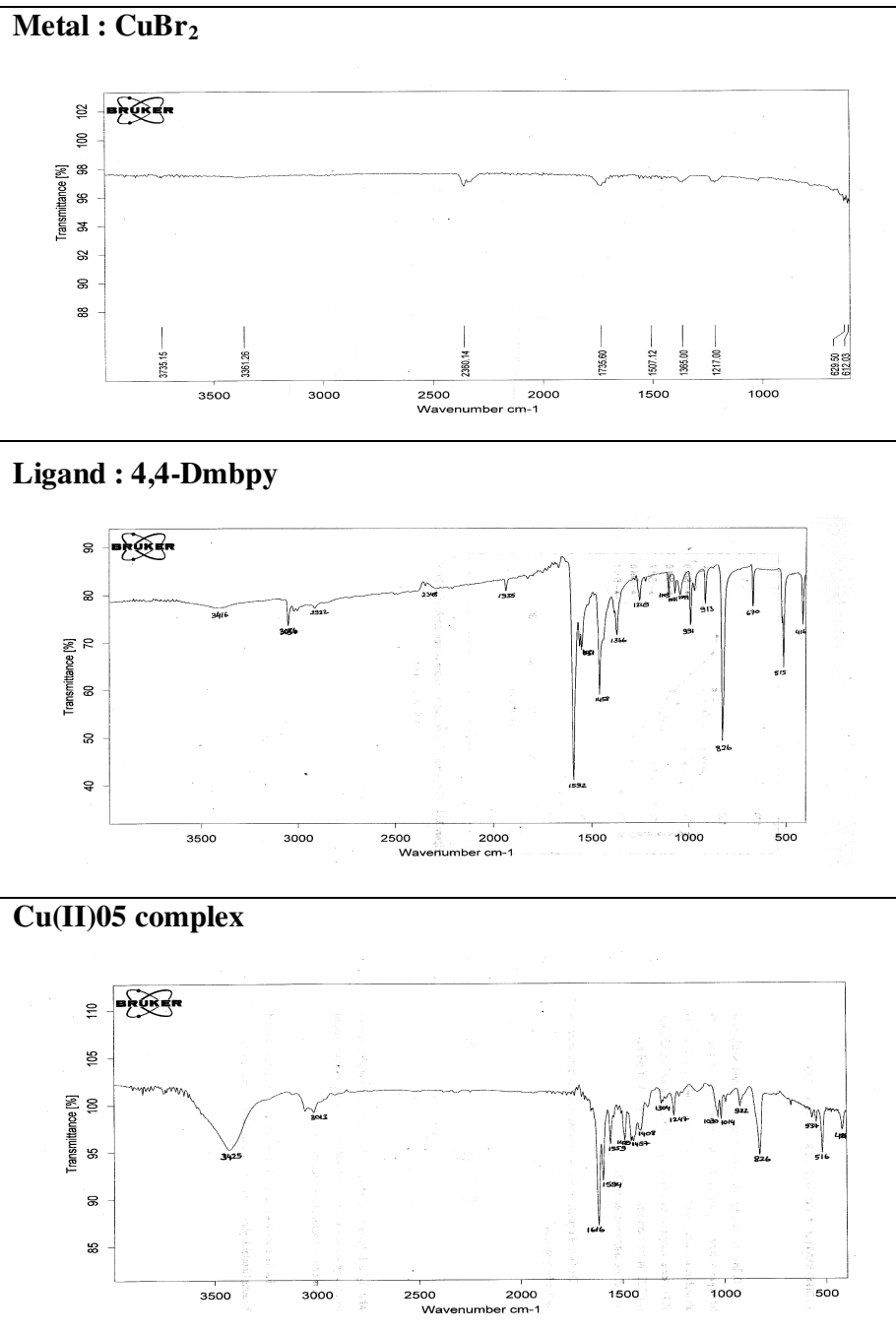


Figure 3.16 FTIR spectrum of Cu(II)05 complex

3.2.2 UV-Vis results of Cu (I) complexes

In UV-vis spectra of Cu(I)A and Cu(I)B complexes, the absorption peak at a maximum of CuCl at 199 nm disappeared and the peaks at maximum relating to both 2,2-bpy and 4,4-dM bpy ligands were disappeared. Therefore, in the polymerization medium, Cu(I) complexes formed were investigated (Figure 3.17 and 3.18).

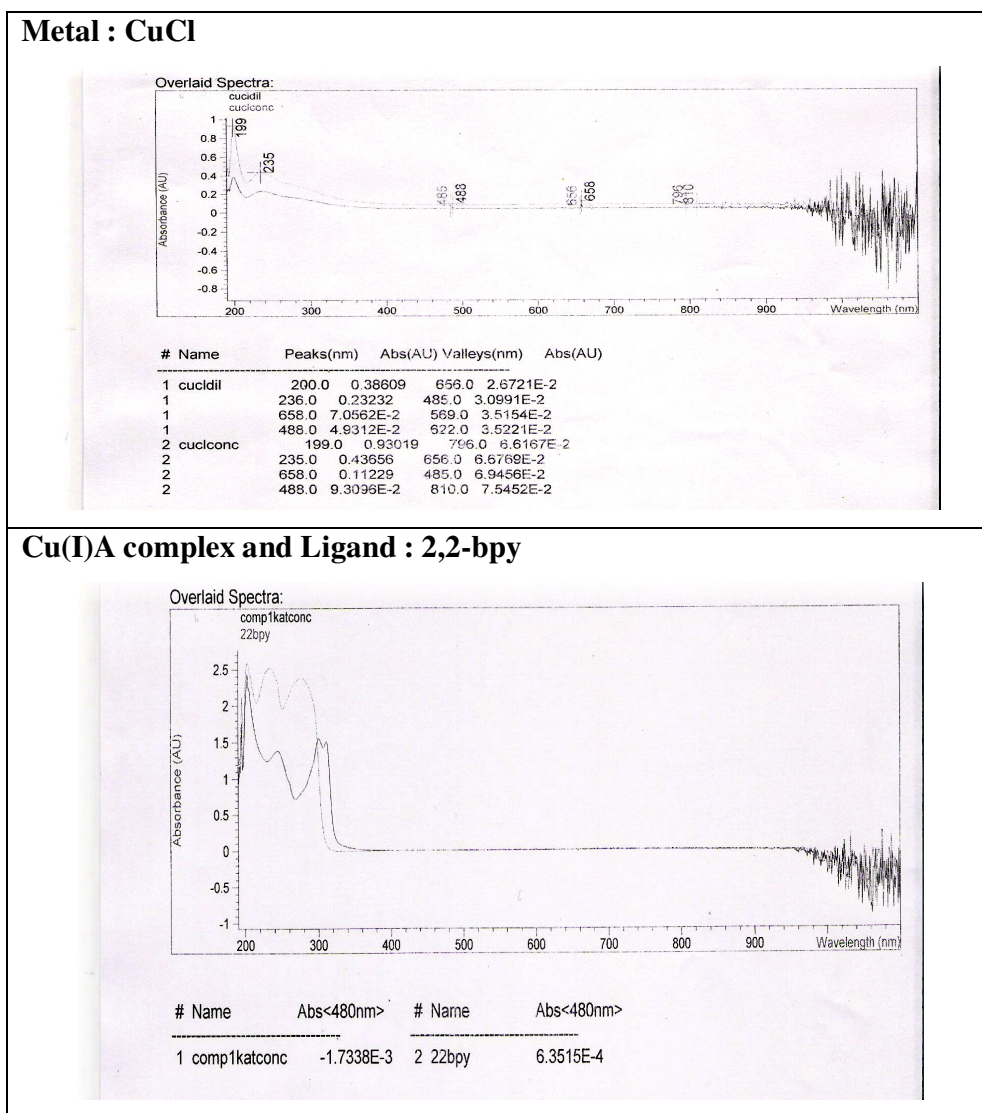
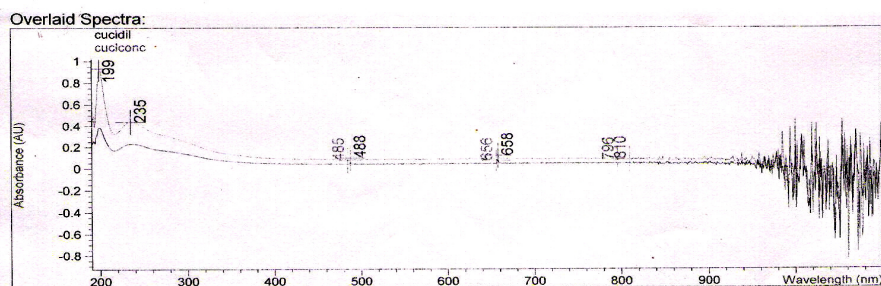


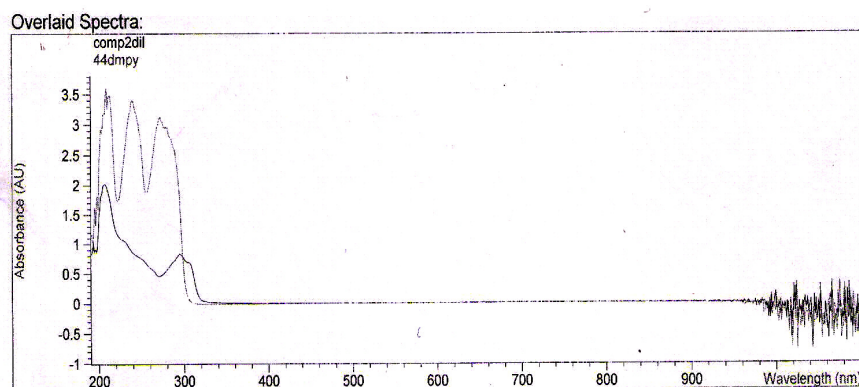
Figure 3.17 UV-Vis spectrum of Cu(I)A complex

Metal : CuCl



| # | Name | Peaks(nm) | Abs(AU) | Valleys(nm) | Abs(AU) |
|---|----------|-----------|-----------|-------------|-----------|
| 1 | cuclidil | 200.0 | 0.38609 | 656.0 | 2.6721E-2 |
| 1 | | 236.0 | 0.23232 | 485.0 | 3.0991E-2 |
| 1 | | 658.0 | 7.0562E-2 | 569.0 | 3.5154E-2 |
| 1 | | 488.0 | 4.9312E-2 | 622.0 | 3.5221E-2 |
| 2 | cuclconc | 199.0 | 0.93019 | 796.0 | 6.6167E-2 |
| 2 | | 235.0 | 0.43656 | 656.0 | 6.6769E-2 |
| 2 | | 658.0 | 0.11229 | 485.0 | 6.9456E-2 |
| 2 | | 488.0 | 9.3096E-2 | 810.0 | 7.5452E-2 |

Cu(I)B complex and Ligand : 4,4-Dmbpy



| # | Name | Abs<480nm> | # | Name | Abs<480nm> |
|---|----------|------------|---|--------|------------|
| 1 | comp2dil | 2.8419E-4 | 2 | 44dmpy | -4.1313E-3 |

Figure 3.18 UV-Vis spectrum of Cu(I)B complex

3.2.3 FTIR results of polymers prepared by ATRP

The monomer HEMA and the isolated PHEMA were characterized by FTIR spectroscopy and spectra are shown in Figure 3.19. Characteristic O-H stretching (3432 cm^{-1}) and C=O stretching (1719 cm^{-1}) were observed at both in monomer and polymers. The peaks in the range at around $2700\text{-}2950\text{ cm}^{-1}$ can be interpreted for C-H stretching for methyl CH_3 and methylene $-\text{CH}_2-$ groups. Also, at 1440 cm^{-1} alkene C-H scissoring gave a sharp peak. But the main differences between monomer and polymers can be observed in the peak at 1637 cm^{-1} which can be assigned to C=C stretching and also sharp peak at 816 cm^{-1} that can be assigned to alkene C-H out of plane bending type vibrations. This means that double bonds disappeared in IR spectra of polymers and polymerization was done via vinyl group opening.

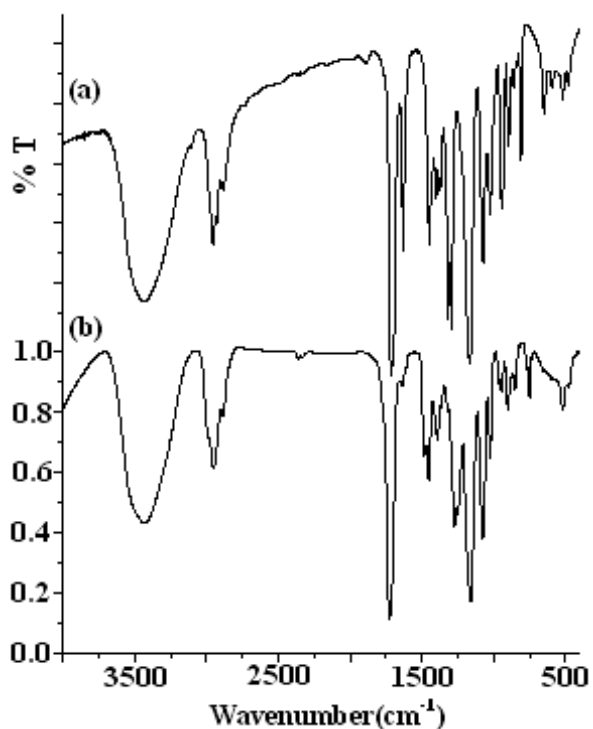


Figure 3.19 FT-IR spectra of (a)HEMA and (b)PHEMA (by ATRP method)

3.2.4 $^1\text{H-NMR}$ analysis of polymers prepared by ATRP

The chemical structure of the polymers obtained was also investigated by $^1\text{H-NMR}$ spectroscopy (Figure 3.20) and the spectrum reveals that there is no residual monomer in the polymer.

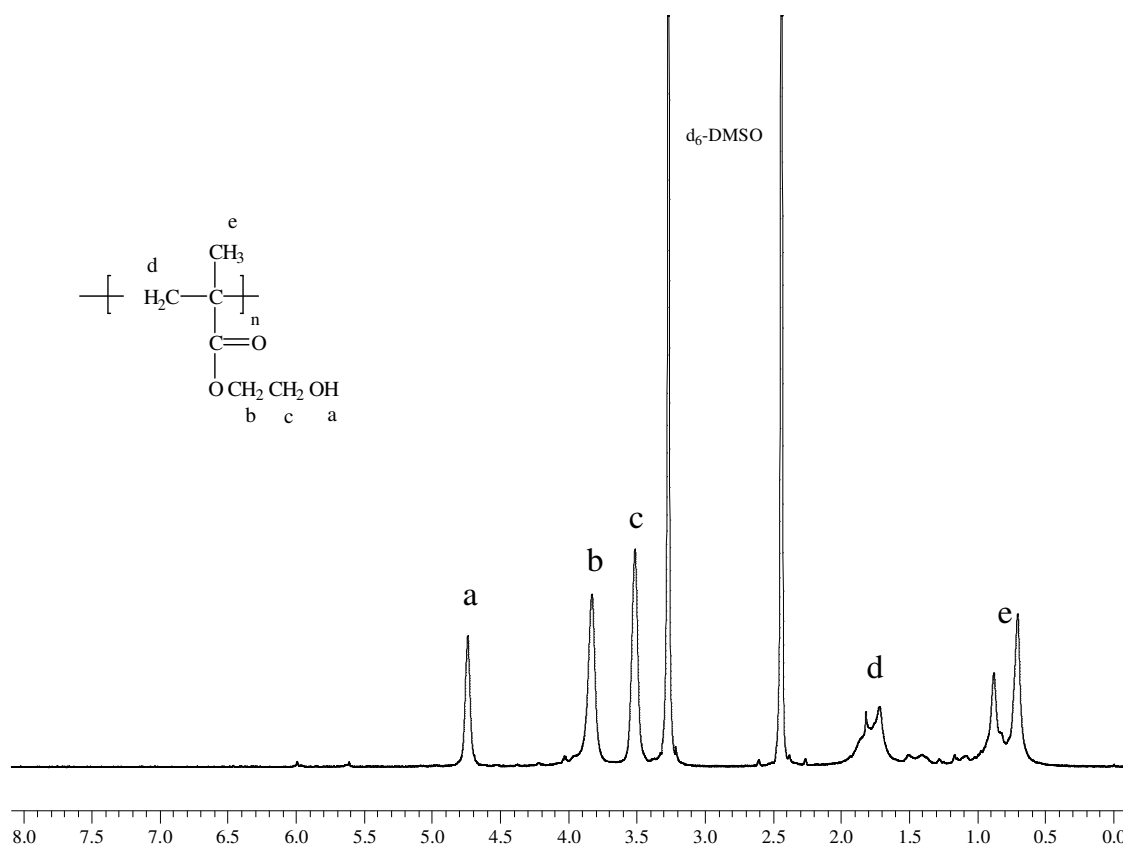


Figure 3.20 $^1\text{H-NMR}$ spectrum of PHEMA via ATRP

The recipe for the ATRP of HEMA was given in Chapter 2 (Table 2.2) and six different polymerization conditions by various components were tried to investigate the effect of addition of Cu(II)/ligand complex into the polymerization medium. Conversions data were given in Table 3.2.

Table 3.2 Conversion % data for ATRP of PHEMA

| Run No | (CuCl) (mol ratio) | (bpy) (mol ratio) | Initiator (mol ratio) | HEMA (mol ratio) | Cu(II)02 (mol ratio) | Conv % |
|--------|--------------------|-------------------|-----------------------|------------------|----------------------|--------|
| 1 | 1 | 2 | (EBriB) (1) | 200 | - | 46.4 |
| 2 | 1 | 2 | (EBriB) (1) | 200 | 0.1 | 53.4 |
| 3 | 1 | 2 | (BrMPB)(1) | 200 | - | 31.8 |
| 4 | 1 | 2 | (BrMPB)(1) | 200 | 0.1 | 37.4 |
| 5 | 1 | 2 | (BrPB) (1) | 200 | - | 47.4 |
| 6 | 1 | 2 | (BrPB) (1) | 200 | 0.1 | 51.2 |

Matyjaszewski et. al. [57,58] introduced the mixed halogen system R-Br/Cu-Cl to increase the rate of initiation due to the weaker bond of R-Br. They stated that the mixed halide initiated ATRP of MMA provided the best control of molecular weight and the lowest polydispersities. Therefore, in this study three different Br-containing initiators with CuCl/(bpy)₂ systems were used for the ATRP of HEMA. The initiators used are BriB(CH₃CH₂OC=OC(CH₃)₂Br), BrMPB((CH₃)₂CBrC=OBr) and BrPB(CH₃CHBrC=OBr). Tertiary halides (BrMPB) exchange faster than secondary halides (BrPB), thus, conversion percentages are higher in BrPB initiating system. It was also aimed to force to the equilibrium towards the dormant species by initial adding Cu(II) complexes initially (Figure 3.12), so the decrease in polymerization rate was expected. The concept of ATRP is that the polymer chains spend the majority of the time in the dormant state. If there is a very small amount of active chains in the

polymerization medium this will cause the reduction of the termination. However, with the addition of Cu(II) complexes the conversion percentages increases unexpectedly. Therefore, Cu(II) complexes were not used in copolymerization medium.

The first polymer obtained (run 1) was used as a macroinitiator for the copolymerization with PDMS via ATRP. After the addition of PDMS (vinyl terminated) some solubility problems appeared. The solvent mixture was MEK/1-propanol (70/30 v/v) and the macroinitiator (PHEMA), metal (CuCl) and ligand (bpy) were soluble in polar solvents, but PDMS is insoluble in this solvent mixture. The polarity of the solvent decreased (by adding non-polar solvents into medium) in order to increase the solubility of PDMS. In this case, the solubility of PHEMA and complexes decreased, because the Cu(II) complexes are highly soluble in polar solvents such as methanol and water. PHEMA has the hydrophilic character while the PDMS has hydrophobic. To decrease the hydrophilicity of HEMA, the -OH groups were protected by trimethyl silyl group in order to increase the solubility of HEMA in non-polar solvent. The newly formed monomer (TMSHEMA) was polymerized and copolymerized with PDMS via ATRP. The route of the copolymer synthesis was also changed as follows: after nearly complete consumption of the first monomer (TMSHEMA), the second monomer (PDMS) was added to the reaction medium. So, P(TMSHEMA) was not isolated from reaction medium and the second PDMS block was added sequentially. The P(TMSHEMA) homopolymer and P(TMSHEMA-b-DMS) copolymer were characterized by FTIR and ¹H-NMR techniques. FTIR spectra of both TMSHEMA monomer and its copolymer were given in Figure 3.21.

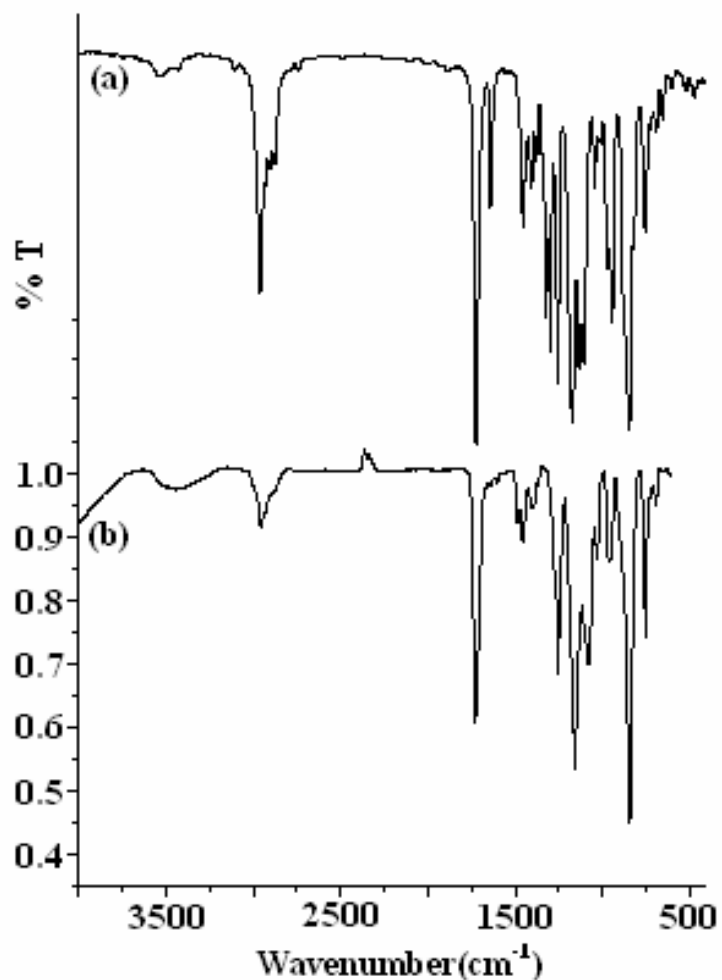


Figure 3.21 FTIR spectra of TMSHEMA (a) monomer (b) polymer via ATRP

All peaks of TMSHEMA monomer are the same as that of HEMA (Figure 3.21(a)) except the -OH stretching and the disappearing C=C stretching peak at around 1600 cm⁻¹ indicates the polymerization proceeded via opening double bonds. ¹H-NMR analysis of both monomer and polymer were also performed to characterize the chemical structures. (Figure 3.22)

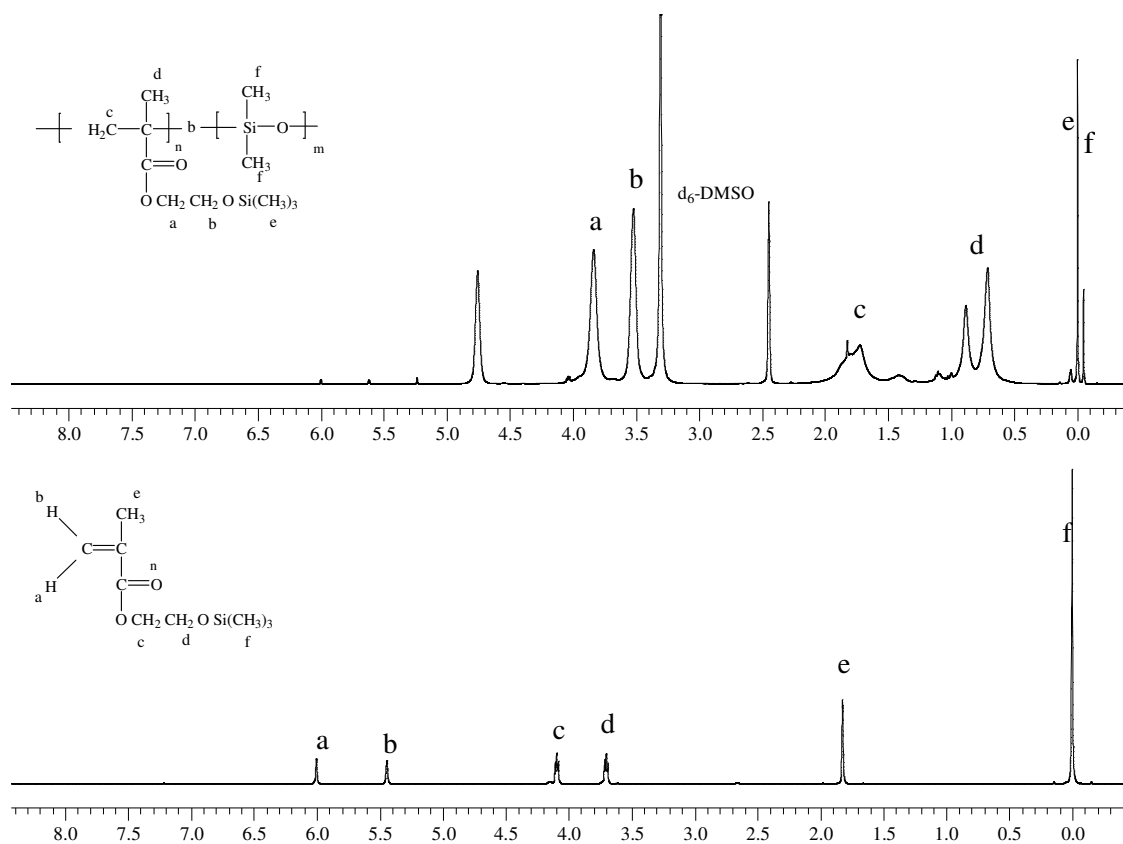


Figure 3.22 ¹H-NMR spectra of TMSHEMA and its copolymer

The -OH peak, at 4.8 ppm in ¹H-NMR spectrum of P(TMSHEMA), is due to the partial deprotection of trimethyl silyl groups (Figure 3.22). The -Si(CH₃) protons of both TMSHEMA and PDMS appeared at 0.0 ppm. The TMS groups in P(TMSHEMA) were deprotected by HCl treatment and the characterization was done by ¹H-NMR spectroscopy (Figure 3.23).

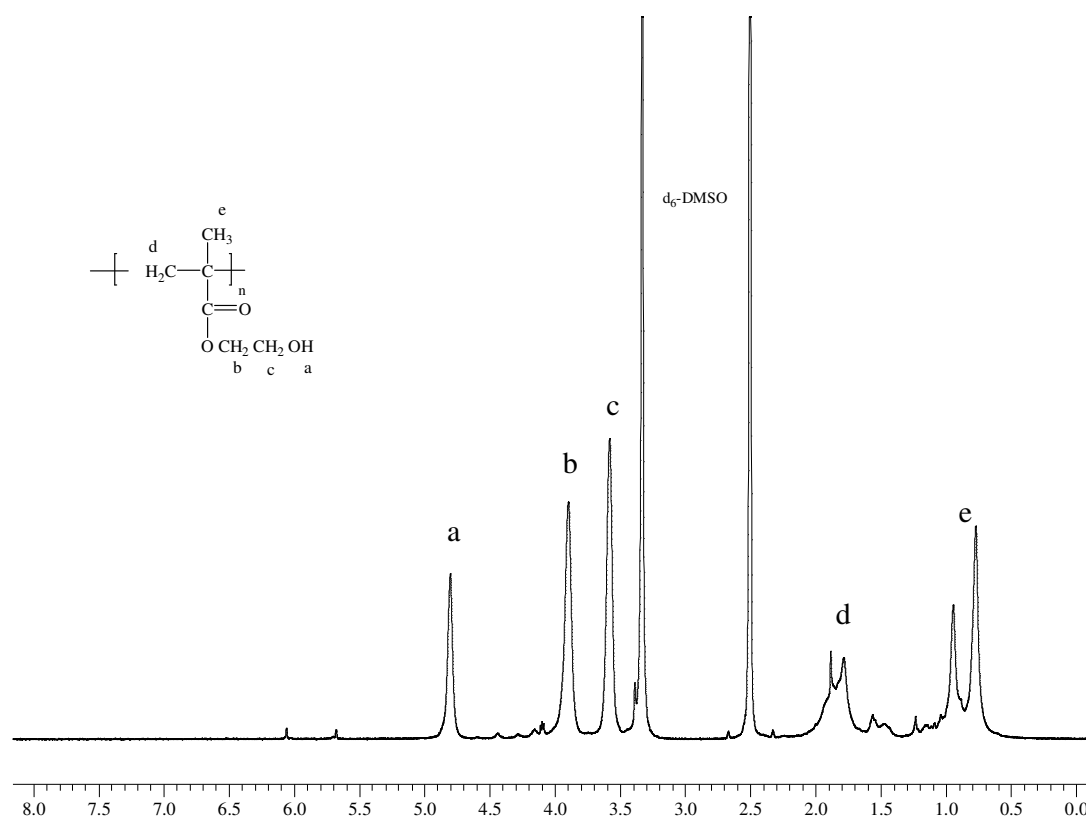


Figure 3.23 $^1\text{H-NMR}$ spectrum of P(HEMA-b-DMS)

After the deprotection of TMS groups of the copolymer, there is no peak observed at around 0.0 ppm which means that the PDMS block could not be incorporated into the copolymer (Figure 3.23). The $^1\text{H-NMR}$ spectrum of P(HEMA-b-DMS) block copolymer is identical with the $^1\text{H-NMR}$ spectrum of PHEMA (Figure 3.20). The failure in the copolymer synthesis might be caused by the different reactivities of two blocks. The reactivities of the blocks increase when the molecular weights of them are close to each other. The molecular weight of PDMS ($M_w=25000$, purchased from Aldrich) might be higher than that of P(TMSHEMA). Because the viscosity measurements revealed that the intrinsic viscosity of the P(TMSHEMA) was found as 0.1741 which could mean the low molecular weight. The big challenge lies in the synthesis of block copolymer due to the difference in reactivities of the blocks and their

molecular weights. PDMS (second block) should be added as a sequential monomer instead of a polymer for the preparation of block copolymer via ATRP. Then, the second controlled living polymerization technique (RAFT polymerization) was performed for the synthesis of P(HEMA-*b*-DMS) copolymer.

3.3 RAFT Polymerization of HEMA

The mechanism of the RAFT process is shown in Figure 1.3 and the main goal is to extend the lifetime of growing radicals like ATRP. The rate constant of chain transfer should be faster than the rate constant of propagation in RAFT polymerization. 2-phenylprop-2-yl dithiobenzoate (RAFT agent) was synthesized by reaction between the dithiobenzoic acid and α -methyl styrene, then it was characterized by ^1H and ^{13}C – NMR techniques. Spectra are shown in Figure 3.24 and 3.25. Having successfully synthesized RAFT agent, the homopolymerization of hydrophilic monomer HEMA in three different solvents was investigated. MEK and EtOAc were chosen due to the polarity. Toluene was chosen as solvent due to the copolymerization reaction of HEMA and PDMS after the synthesis of PHEMA macroinitiator, because, the PDMS is completely soluble in toluene.

Living radical polymerization characteristics are constant concentration of active centers and linear relationship between molecular weight and monomer conversion. The results for a series of thermally initiated HEMA-RAFT polymerizations performed with a range of solvents are shown in Figure 3.26-3.29 and in Table 3.3-3.5. Table 3.3 presents conversion percent-time results for RAFT polymerization of HEMA under experimental condition such as $[\text{RAFT}]/[\text{AIBN}]=18$ at $80\text{ }^\circ\text{C}$ in MEK. A linear relationship between $\ln([M]_0/[M])$ and polymerization time is shown in Figure 3.26. The first-order kinetic is observed up to the nearly 40 conversion %. Molecular weights and MWD of polymers could not be determined by GPC technique due to the insolubility of PHEMA in THF. However, intrinsic viscosity (*IV*) measurements give the relative molecular weight of copolymers and *IV* values are summarized in Table 3.3

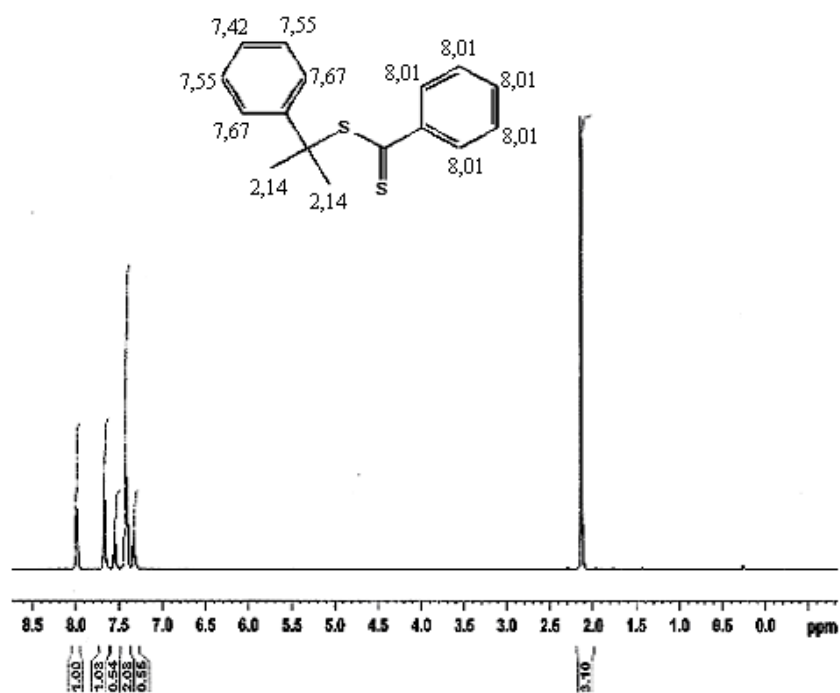


Figure 3.24 $^1\text{H-NMR}$ spectrum of RAFT Agent

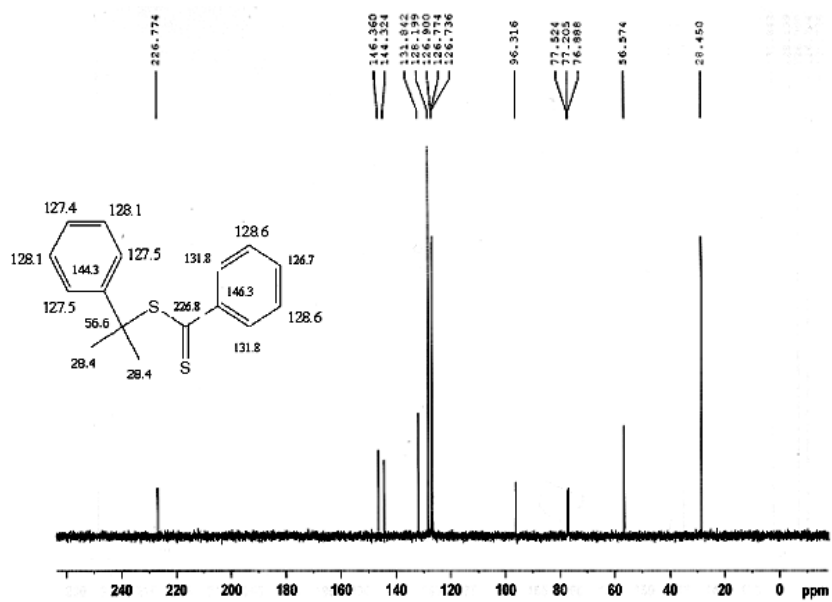


Figure 3.25 $^{13}\text{C-NMR}$ spectrum of RAFT Agent

Table 3.3 Conversion % and intrinsic viscosity results for the RAFT polymerization of HEMA in MEK, ([RAFT]= 0.018 M, [AIBN]= 0.001M at 80 °C)

| Time (h) | Conv % | IV Values |
|----------|--------|-----------|
| 0,5 | 4,1 | - |
| 1 | 13,9 | 0,0701 |
| 1,5 | 22,7 | 0,0993 |
| 2 | 37,1 | 0,1088 |
| 3 | 41,3 | 0,1107 |
| 4 | 59,6 | 0,1051 |
| 6 | 67,6 | 0,127 |
| 8 | 74,4 | 0,1363 |
| 13 | 82,0 | 0,1343 |
| 16 | 66,3 | 0,1424 |
| 20 | 68,9 | 0,1813 |
| 23 | 59,4 | 0,1412 |
| 24 | 79,4 | 0,1619 |
| 47 | 75,7 | 0,1728 |
| 50 | 70,8 | 0,2523 |
| 74 | 77,6 | 0,2223 |

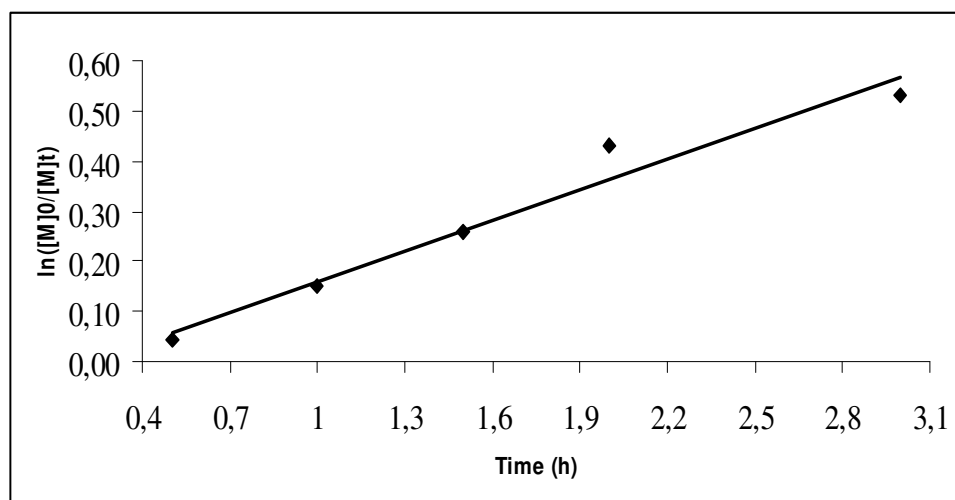


Figure 3.26 $\ln([M]_0/[M]_t)$ vs. time graph for the RAFT polymerization of HEMA in MEK, ([RAFT]= 0.018 M, [AIBN]= 0.001M at 80 °C)

Table 3.4 shows the conversion % - time results for the RAFT polymerization of HEMA in ethyl acetate under the same experimental conditions with MEK. However, the limiting conversion value is 0,35 and this value is reached at nearly 6 hours. Again, a linear relationship between $\ln([M]_0/[M])$ and polymerization time is observed up to nearly 30 % conversion (Figure 3.27) and IV values increases as conversion increases (Table 3.4).

Table 3.4 Conversion % and intrinsic viscosity results for the RAFT polymerization of HEMA in ethyl acetate, ([RAFT]= 0.018 M, [AIBN]= 0.001M at 80°C)

| Time(h) | conv % | IV Values |
|---------|--------|-----------|
| 0,5 | 2,66 | |
| 1 | 10,70 | 0,1228 |
| 1,5 | 19,36 | 0,1053 |
| 2 | 26,59 | 0,1165 |
| 3 | 26,79 | 0,3039 |
| 4 | 29,14 | 0,3083 |
| 5 | 29,83 | 0,2863 |
| 6 | 32,96 | 0,3579 |
| 8 | 32,73 | 0,3301 |
| 12 | 33,37 | 0,2271 |

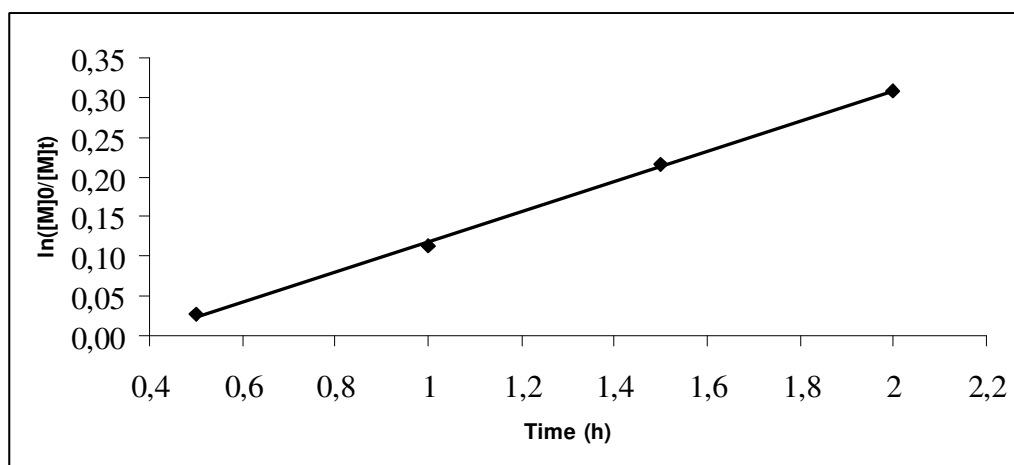


Figure 3.27 $\ln([M]_0/[M]_t)$ vs. time graph for the RAFT polymerization of HEMA in ethyl acetate, ([RAFT]= 0.018 M, [AIBN]= 0.001M at 80 °C)

Results for the RAFT polymerization of HEMA under the same experimental conditions in toluene is shown in Table 3.5. The homopolymerization of HEMA in toluene is so fast that it was completed in just a few hours. There is no linearity between $\ln([M]_0/[M])$ and polymerization time in toluene so the polymerization is not proceeded in a controlled way (Figure 3.28).

Table 3.5 Conversion % and intrinsic viscosity results for the RAFT polymerization of HEMA in toluene, ([RAFT]= 0.018 M, [AIBN]= 0.001M at 80°C)

| Time(h) | conv % | IV Values |
|---------|--------|-----------|
| 0,5 | 2,52 | |
| 1,0 | 8,85 | 0,0116 |
| 1,5 | 13,22 | 0,0646 |
| 2,0 | 29,19 | 0,0957 |
| 2,0 | 27,08 | 0,1304 |
| 2,5 | 89,02 | 0,2561 |
| 3,0 | 87,90 | 0,2131 |
| 4,0 | 10,31 | 0,1947 |
| 8,0 | 96,38 | 0,2969 |
| 11,5 | 91,43 | 0,5091 |
| 14,0 | 90,85 | 0,5651 |
| 16,0 | 82,47 | 0,4072 |
| 24,0 | 98,78 | 0,3217 |

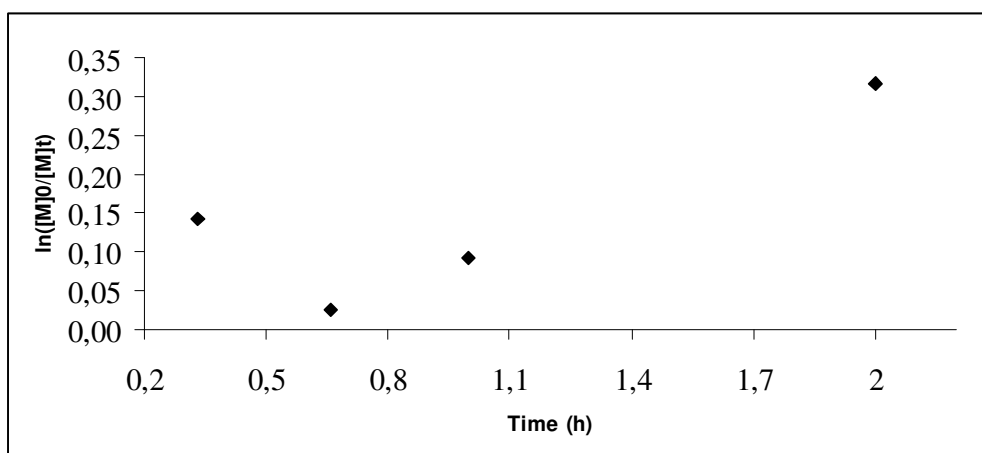


Figure 3.28 $\ln([M]_0/[M]_t)$ vs. time graph for the RAFT polymerization of HEMA in toluene, ($[RAFT]=0.018\text{ M}$, $[AIBN]=0.001\text{ M}$ at $80\text{ }^\circ\text{C}$)

Highest conversions were achieved in toluene and the lowest ones were obtained in ethyl acetate. This is caused by the polarity of the solvents used and the activity of the RAFT agent in different solvents. Polymerizations resulted in higher conversions in toluene due to the low solubility of CDB and HEMA. The conversions reached the limiting value (at around %35) in ethyl acetate and as the time increases the conversion did not change much. This can be explained by the higher transfer activity of RAFT agent in ethyl acetate. Polymerizations in both MEK and ethyl acetate, CDB has a rapid rate of exchange between dormant and living chains so the rate of polymerization was decreased when comparing with toluene. It means that the effectiveness of CDB in MEK and ethyl acetate is much better than that in toluene.

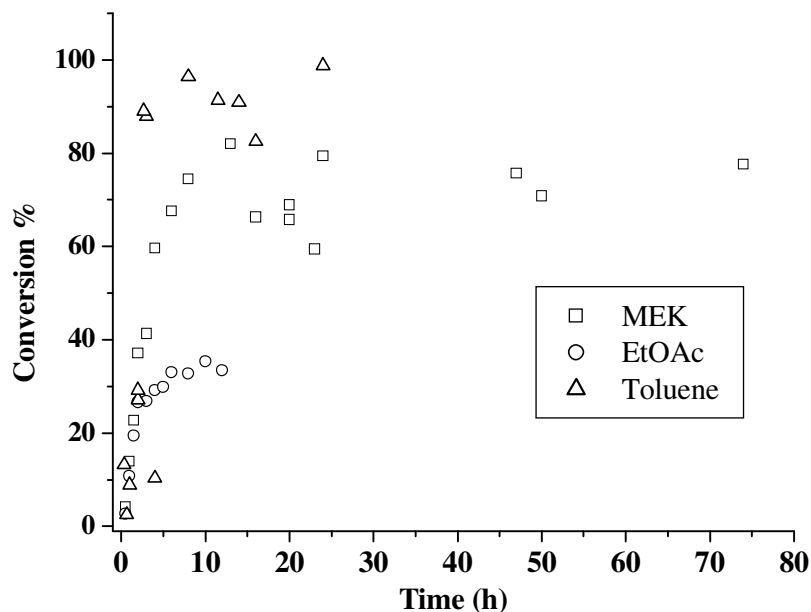


Figure 3.29 Comparison of three conversion – time graphs for the RAFT polymerization of HEMA, [RAFT]= 0.018 M, [AIBN]= 0.001M at 80 °C

The effect of different [CTA]/[AIBN] ratios were also investigated in three solvents in order to optimum control of the polymerization of HEMA. The polymerizations were performed at different [CTA]/[AIBN] ratios, as 9, 18, 27 while other reaction conditions remained the same. The results are tabulated in Table 3.6. In all solvents, % conversions decreased when the [CTA]/[AIBN] ratios are increased from 9 to 18 and 27. In the case of the lower [CTA]/[AIBN] , the reduction of the chain transfer reaction of the CDB lead to the higher % conversions.

Table 3.6 %Conversion-time and IV results for the HEMA polymerization with different [CTA]/[AIBN] ratios in three different solvents

| Solvents | | MEK | | Ethyl Acetate | | Toluene | |
|----------|------------|---------|-----------|---------------|-----------|---------|-----------|
| Time (h) | [RAFT] (M) | conv. % | IV Values | conv. % | IV Values | conv. % | IV Values |
| 1 | 0 | 63.9 | - | 100.0 | - | 99.8 | - |
| 2 | 0 | 95.7 | - | 98.8 | - | 100.0 | - |
| 1 | 0.009 | 23.5 | 0.1454 | 15.5 | 0.1376 | 28.5 | 0.2236 |
| 2 | 0.009 | 51.7 | 0.2522 | 59.4 | 0.3104 | 88.7 | 0.2604 |
| 3 | 0.009 | 62.2 | 0.1931 | 58.8 | 0.3026 | 91.4 | 0.2880 |
| 4 | 0.009 | 70.6 | 0.2199 | 67.5 | 1.2194 | 98.1 | 0.2808 |
| 1 | 0.018 | 13.9 | 0.0701 | 10.7 | 0.1228 | 8.9 | 0.0116 |
| 2 | 0.018 | 37.1 | 0.1051 | 26.6 | 0.1165 | 27.1 | 0.1304 |
| 3 | 0.018 | 41.3 | 0.1088 | 26.8 | 0.3039 | 87.9 | 0.2131 |
| 4 | 0.018 | 59.6 | 0.1107 | 29.1 | 0.3083 | 10.3 | 0.1947 |
| 1 | 0.027 | 8.6 | 0.1003 | 0.5 | - | 9.2 | - |
| 2 | 0.027 | 26.7 | 0.1049 | 3.0 | - | 12.0 | 0.1066 |
| 3 | 0.027 | 40.0 | 0.1119 | 10.6 | 0.0711 | 23.6 | 0.1281 |
| 4 | 0.027 | 47.0 | 0.1619 | 75.8 | 0.1078 | 31.1 | 0.1087 |

Generally, increasing the concentration CTA caused an improvement of the control of the polymerization. But the effects of solvent and different [CTA]/[AIBN] ratios on the chain length and molecular weight distribution could not be examined. However, intrinsic viscosity (IV) measurements were utilized to relatively measure the molecular weight of PHEMA homopolymers obtained by different conditions. Results are also tabulated in Table 3.6. IV values increases with reaction time and it decreases with increasing [CTA]/[AIBN] ratios as expected. After the comparison of three different solvents and [CTA]/[AIBN] ratios it was concluded that the methyl ethyl ketone (MEK) is a suitable solvent and [CTA]/[AIBN] = 18 is a proper ratio for the copolymerization of HEMA and PDMS. After the optimization of the RAFT polymerization of HEMA, the copolymerization with the PDMS was studied. The firstly prepared PHEMA block was not isolated from the medium. After the completion

of the polymerization of HEMA , the second block of PDMS was added sequentially. The product was analyzed by $^1\text{H-NMR}$ spectroscopy (Figure 3.30).

The cyclic protons of RAFT agents can be seen in $^1\text{H-NMR}$ spectrum of polymer, which means the end groups of polymer have living character. RAFT process yields thiocarbonyl thio-terminated P(HEMA-b-DMS) that can be chain extended with vinyl terminated PDMS to obtain block copolymer. However, the silyl protons correspond to the PDMS segment does not exist in the spectrum indicating no copolymer formation. The reasons of the failure might be either the different hydrophilic/hydrophobic characters of the blocks or the difference in molecular weights of two blocks like in ATRP case. Another reason of no copolymerization might be the low ability of the PHEMA as a leaving group in the copolymerization reaction. Firstly prepared PHEMA block was used as a macroRAFT agent and it should have a better leaving property for the copolymerization. It was concluded that the main reason of the failure is the PDMS block. The second block should be added as a monomer (DMS) not in a polymer (PDMS) form, because, the possibility of the reaction between the active sites of macroRAFT and vinyl groups of monomers is much more than that of the polymer. Therefore, the aim of the project was the synthesis of silicone-methacrylate based copolymers and the route of the synthesis was changed to the modification of the end groups of hydroxyl-terminated PDMS as a macroazoinitiator. The molecular weight of vinyl terminated PDMS ($M_w=25000$) was lowered to hydroxyl-terminated PDMS ($M_n=6000$) for the macroazoinitiator synthesis.

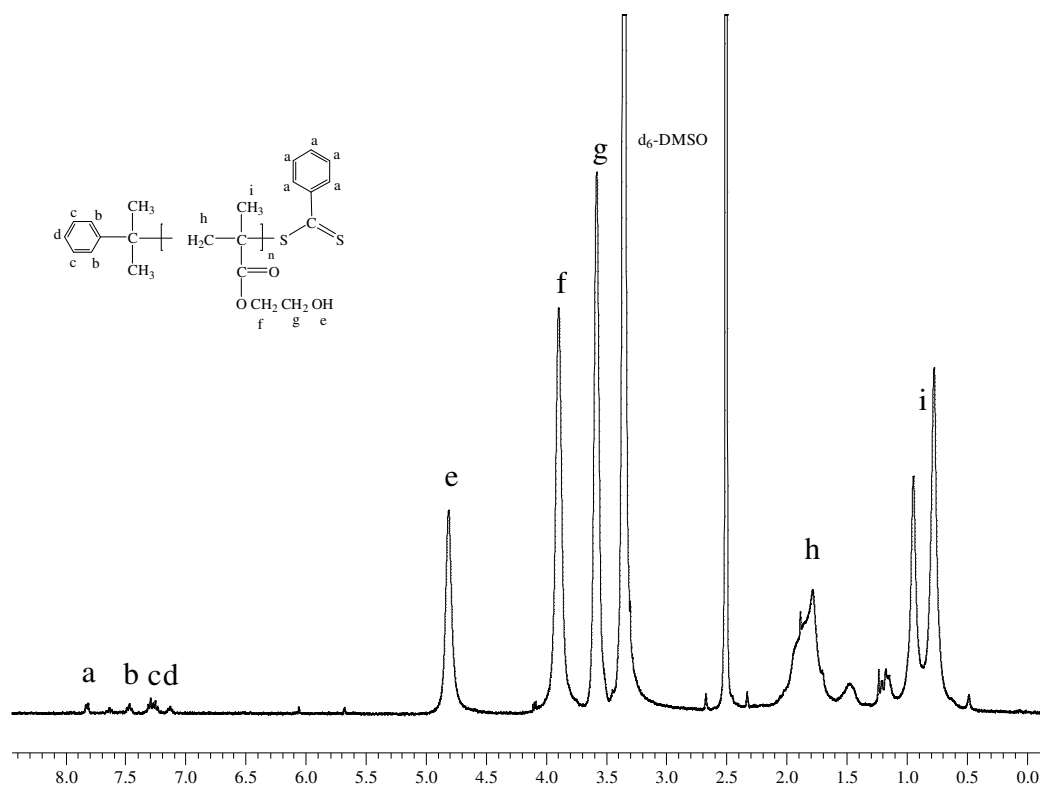


Figure 3.30 $^1\text{H-NMR}$ spectrum of P(HEMA-*b*-DMS) copolymer via RAFT polymerization

3.4 Block Copolymer Synthesis by PDMS Macroazoinitiator

PDMS macroazoinitiator (MAI) was prepared from bishydroxy-terminated polydimethylsiloxane (HO-PDMS-OH) and 4,4'-azobis-4-cyanopentanoic acid (ACPA) by direct polycondensation reaction and then it was used as a macroazoinitiator in block copolymerization with MMA, EMA, HEMA and TMSHEMA monomers. General steps are represented in Figure 3.31 and the details about the experimental conditions are given in Chapter 2. Products are purified by dissolution-precipitation cycles and dried before the characterization. The chemical and

physical properties of both homopolymers and copolymers were determined by different techniques. Surface properties of copolymer films were also examined. The following sections are dedicated to characterize the PDMS-MAI, P(DMS-b-MMA), P(DMS-b-EMA) and P(DMS-b-TMSHEMA) polymers.

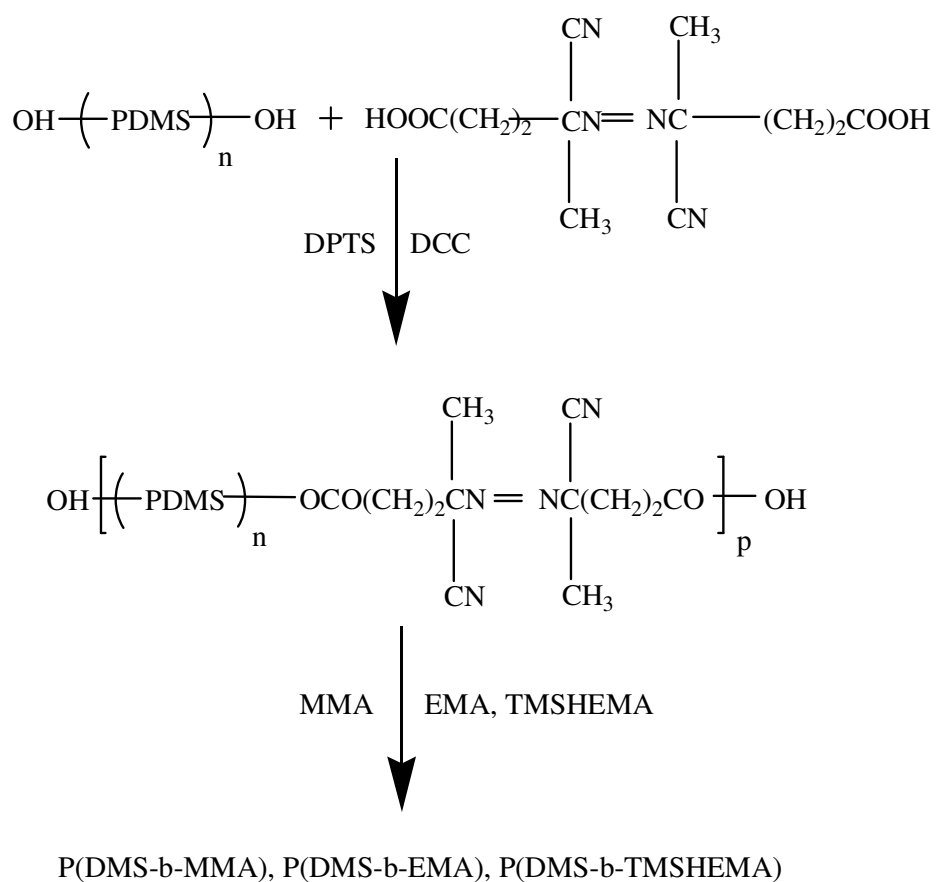


Figure 3.31 Schematic representation of copolymer synthesis

3.4.1 FTIR Analysis of Block Copolymers

3.4.1.1 P(DMS-b-MMA)

P(DMS-b-MMA) block copolymer synthesis was confirmed by FT-IR spectroscopy and shown in Fig 3.32. The strong absorption at 1261 cm^{-1} of PDMS attributed to Si-CH₃ deformation. A very broad peak at $1096\text{--}1020\text{ cm}^{-1}$ for Si-O-Si asymmetric stretching vibrations can be seen as a doublet. Strong Si-O bands appeared at 798 cm^{-1} , also, C-H stretching and C-H bending in CH₃ groups was observed at 2963 and 1446 cm^{-1} , respectively. The appearance of intense absorptions near 1259 , $1087\text{--}1015$ and 795 cm^{-1} of block copolymer clearly show the presence of siloxane segments. The strong absorption at 1723 cm^{-1} showed C=O and -CH₃ stretching vibrations appeared around 2962 cm^{-1} for PMMA segments. For both PDMS and PMMA segments, C-H bending in CH₃ groups appeared at 1435 cm^{-1} . The characteristic C-O stretching for ester (*C-C(=O)-O and O-*C-C) were observed at 1140 cm^{-1} and at around 900 cm^{-1} . The presence of both PDMS and PMMA segments (blocks) in copolymer were also evidenced by ¹H-NMR studies.

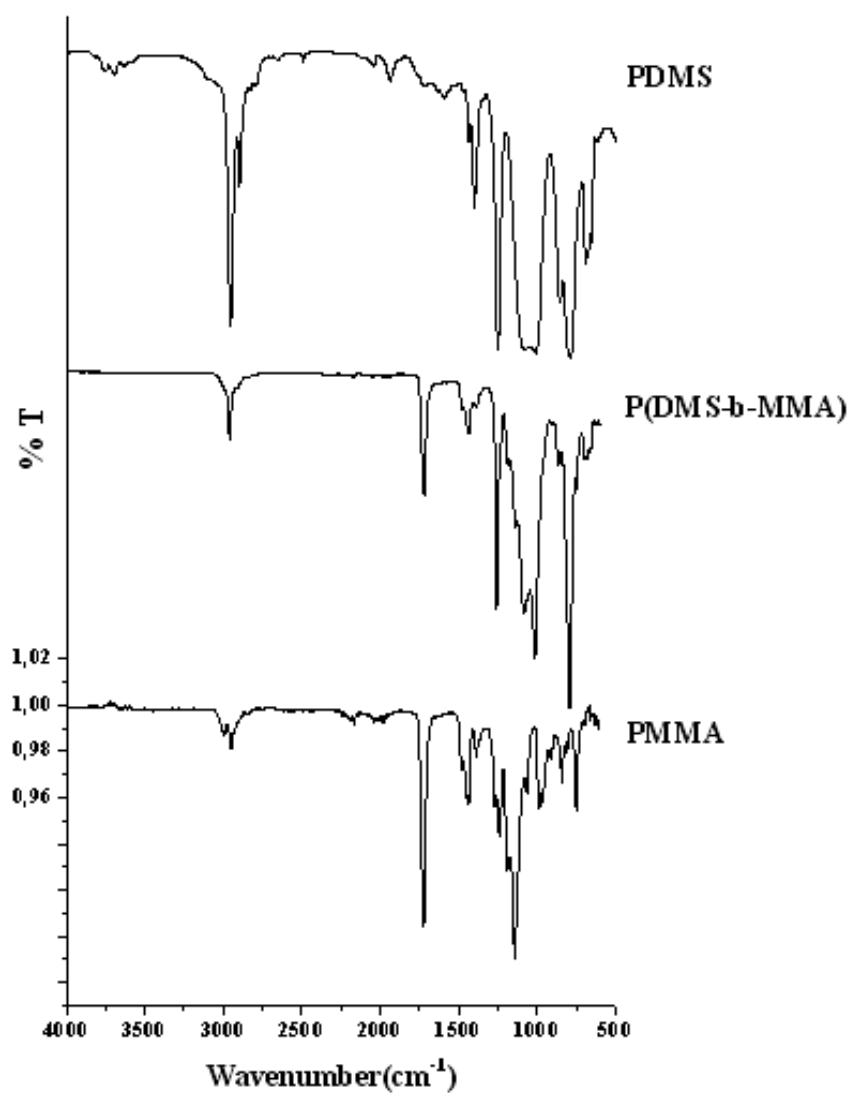


Figure 3.32 FTIR Spectra of PDMS , P(DMS-b-MMA) and PMMA

3.4.1.2 P(DMS-b-EMA)

Similar FTIR spectrum was obtained for the PDMS-b-PEMA (Fig 3.33). C=O stretching vibration was seen at around 1722 cm^{-1} and the peaks in the range at around 2963 cm^{-1} can be interpreted for C-H stretching for methyl CH_3 and for methylene –

CH₂- groups. Also, at 1479cm⁻¹ methylene CH₂ scissoring gave a sharp peak (generally overlaps the C-H bending vibration of CH₂ and CH₃ groups at 1447 cm⁻¹). The broad absorption bands around 1173-1143 cm⁻¹ were caused by C-O-C- ester group stretchings. Also, PDMS segments can be seen at 1260, 1092-1019 and 797 cm⁻¹.

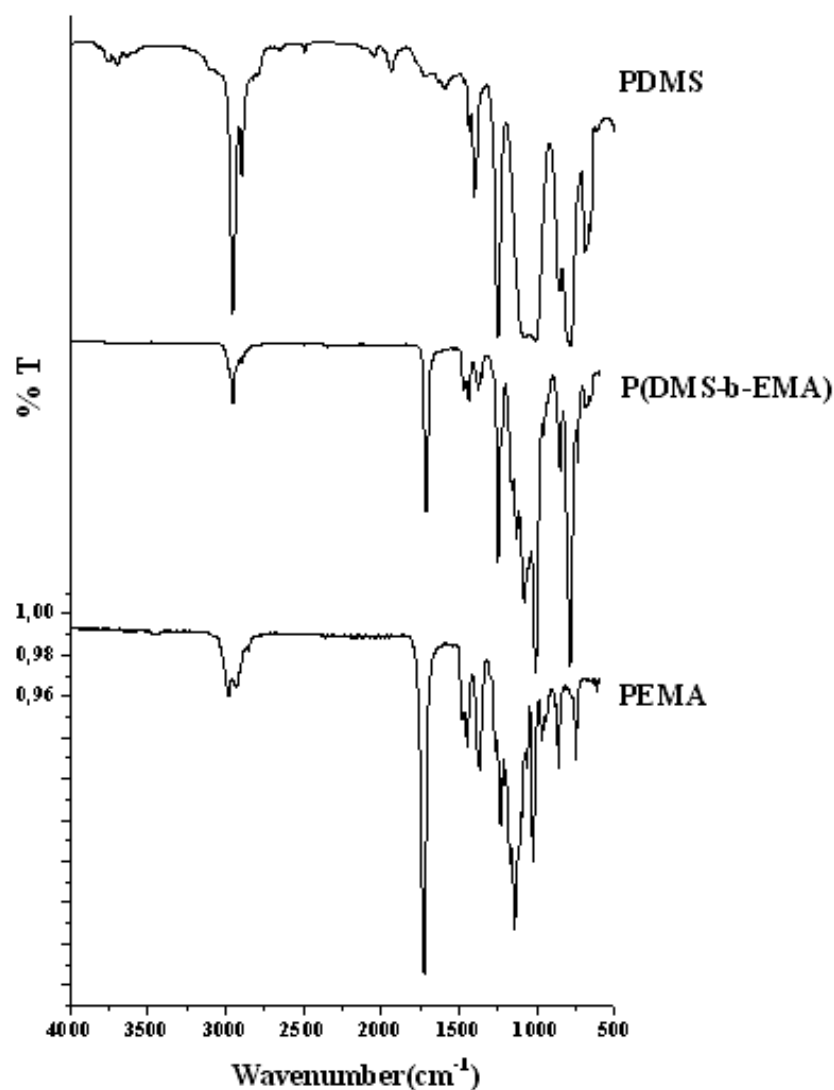


Figure 3.33 FTIR Spectra of PDMS, P(DMS-b-EMA) and PEMA

3.4.1.3 P(DMS-b-TMSHEMA)

In Figure 3.34, characteristic O-H stretching was observed at around 3386 cm^{-1} . Also, peaks in the range at around 2962 cm^{-1} were attributed to C-H stretching for $-\text{CH}_3$ and $-\text{CH}_2$ groups. Other peaks corresponding to $-\text{C}=\text{O}$ (1715 cm^{-1}), $-\text{C}-\text{O}-\text{C}-$ ($1259-1019\text{ cm}^{-1}$), $-\text{CH}_2$ scissoring and C-H bending ($1450-1417\text{ cm}^{-1}$) are present in P(DMS-b-TMSHEMA) FTIR spectrum. These characteristic peaks confirmed that the TMSHEMA was incorporated into the PDMS. The strong peak at 1259 cm^{-1} (Si-CH₃), a broad band at $1072-1019\text{ cm}^{-1}$ (Si-O-Si) and a sharp peak at 797 cm^{-1} (Si-O) corresponds to the PDMS segments. Both PDMS and PHEMA segments were identified in the FTIR spectrum of block copolymer. For further chemical composition confirmation of block copolymer ¹H-NMR analysis was done.

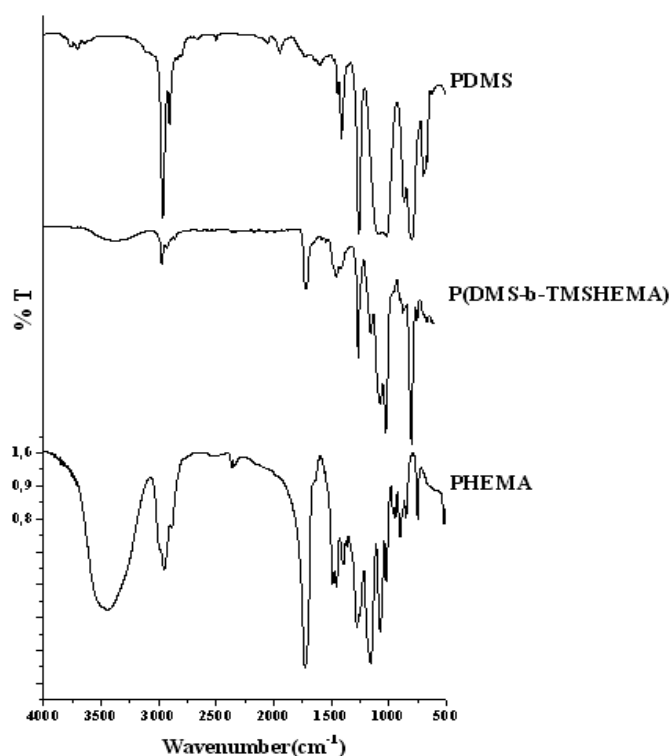


Figure 3.34 FTIR Spectra of PDMS, P(DMS-b-TMSHEMA) and PHEMA

3.4.2 ¹H-NMR Analysis of Block Copolymers

3.4.2.1 P(DMS-b-MMA)

¹H-NMR spectra of PDMS, PDMS-MAI and P(DMS-b-MMA) copolymer are shown in Fig.3.35.a, Fig.3.35.b, and Fig.3.35.c respectively. In the ¹H-NMR spectrum of PDMS (starting polymer) only methylsiloxane protons are observed. For the PDMS-MAI, new peaks appeared in addition to strong methylsiloxane protons, which are –CH₃ and –CH₂ groups originating from ACPA. In the ¹H-NMR spectrum of P(DMS-b-MMA) copolymer -OCH₃, –CH₂ and –CH₃ groups protons at 3.5, 2.0-1.6 and 1.5-0.8 ppm due to the PMMA chain and –CH₃ protons of PDMS segments at 0.0 ppm are assigned. Hence, the ¹H-NMR spectrum of P(DMS-b-MMA) confirms the chemical structure of copolymer.

3.4.2.2 P(DMS-b-EMA)

Both the ¹H-NMR spectra of the starting polymer (PDMS) and macroazoinitiator (PDMS-MAI) are shown in Fig 3.36.a and Fig 3.36.b with the same structure confirmations as P(DMS-b-MMA) copolymer. The ¹H-NMR spectrum of P(DMS-b-EMA) reveals the characteristic -OCH₂, –CH₂ and –CH₃ peaks at 3.9, 2.0-1.6 and 1.5-0.8 ppm, respectively (Fig3.36.c). Also, PDMS segments are observed in the spectrum.

3.4.2.3 P(DMS-b-TMSHEMA)

The ¹H-NMR spectra of PDMS, PDMS-MAI, P(DMS-b-TMSHEMA) and P(DMS-b-HEMA) copolymers are shown in Fig.3.37.a, Fig.3.37.b, Fig.3.37.c and Fig.3.37.d, respectively. All protons are labeled in figures and both segments can be seen clearly. The only difference is that the methylsiloxane protons peak was disappeared due the deprotection of trimethylsilyl groups of P(TMSHEMA) at 0.11 ppm (Fig.3.37.d). The ¹H-NMR analysis indicates that PDMS-MAI initiates the copolymerization of TMSHEMA and then the copolymer is obtained successfully.

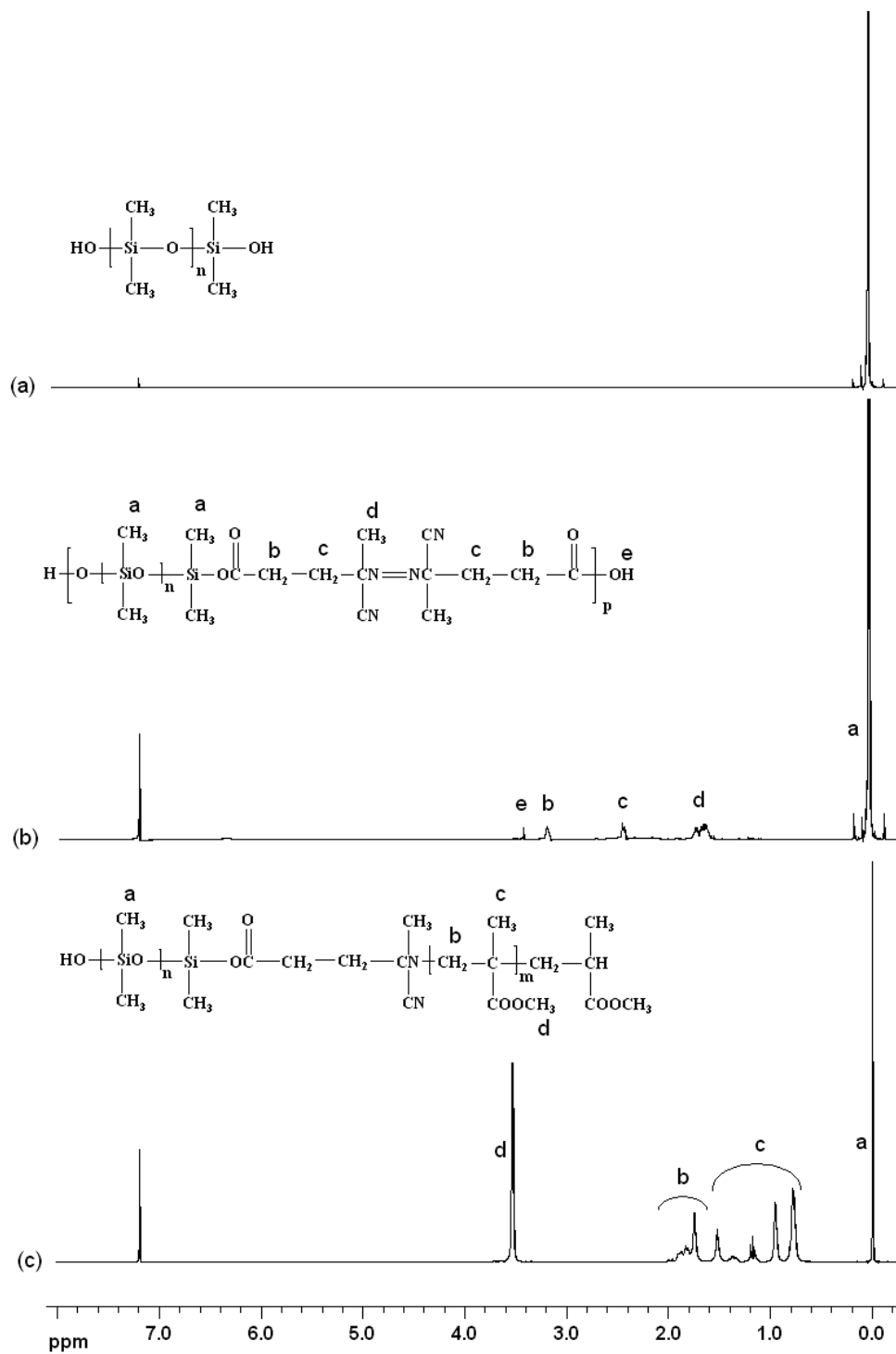


Figure 3.35 ^1H -NMR spectra of PDMS, PDMS-MAI and P(DMS-b-MMA) copolymer

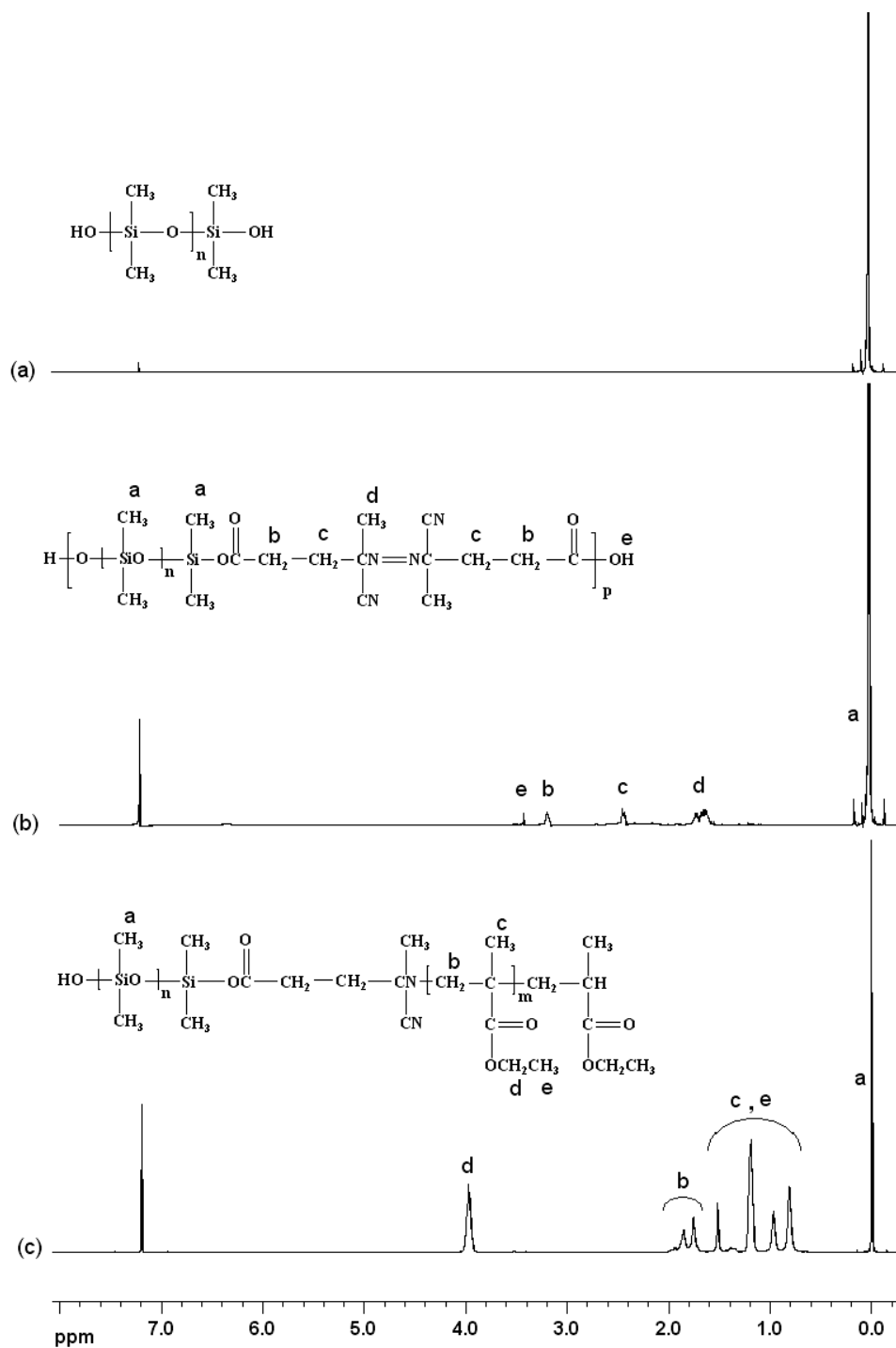


Figure 3.36 ^1H -NMR spectra of PDMS, PDMS-MAI and P(DMS-b-EMA) copolymer

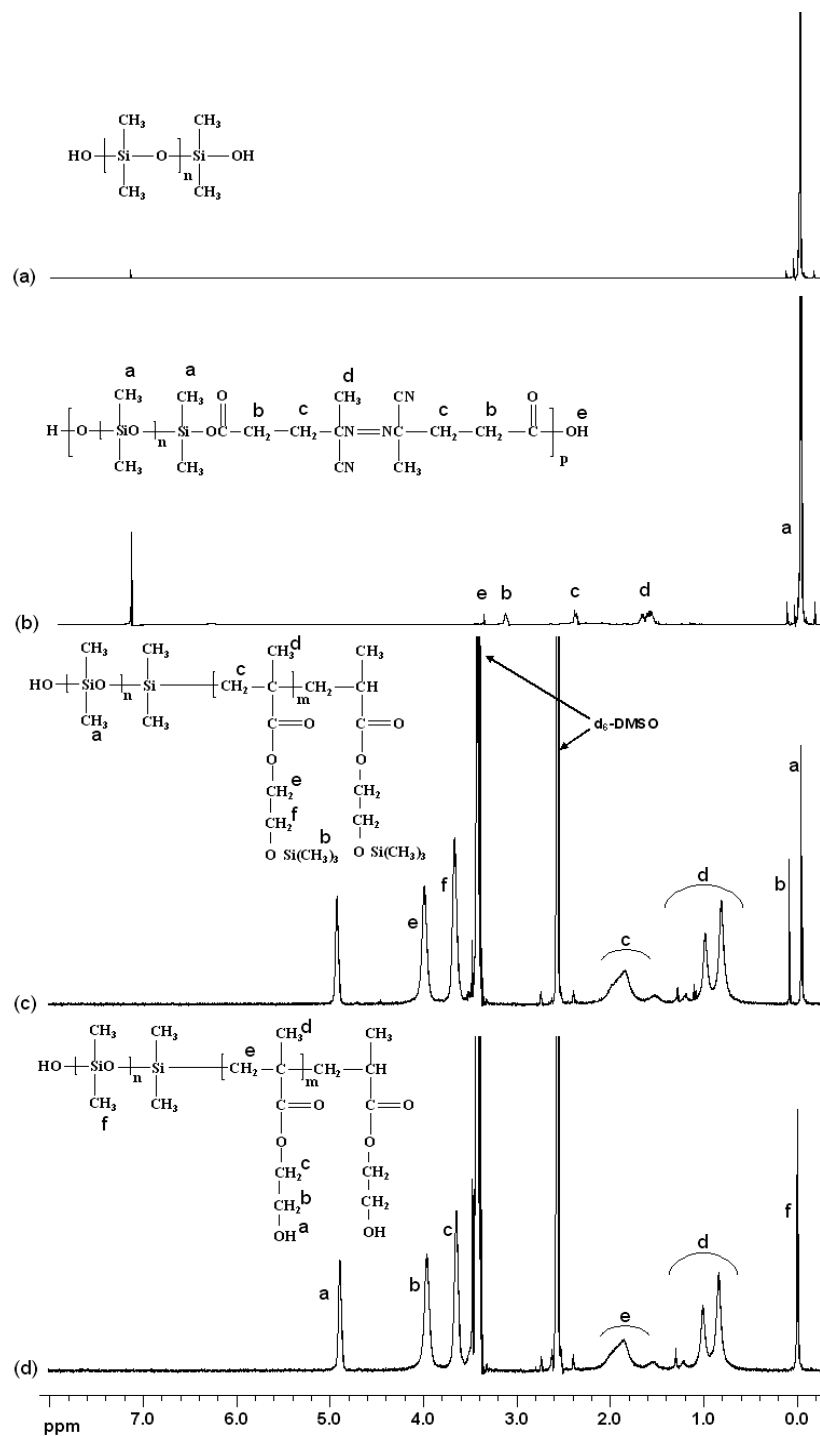


Figure 3.37 $^1\text{H-NMR}$ spectra of PDMS, PDMS-MAI, P(DMS-b-TMSHEMA) and P(DMS-b-HEMA)

3.4.3 Solid State NMR Studies

3.4.3.1 P(DMS-b-MMA)

^{29}Si MAS and ^{13}C CPMAS NMR analysis of P(DMS-b-MMA) were performed at room temperature where PMMA (glassy) and PDMS (rubbery) are in different states and mobility. ^{13}C CPMAS NMR spectrum of P(DMS-b-MMA) shows carbon atoms have different chemical environments (Fig.3.38).

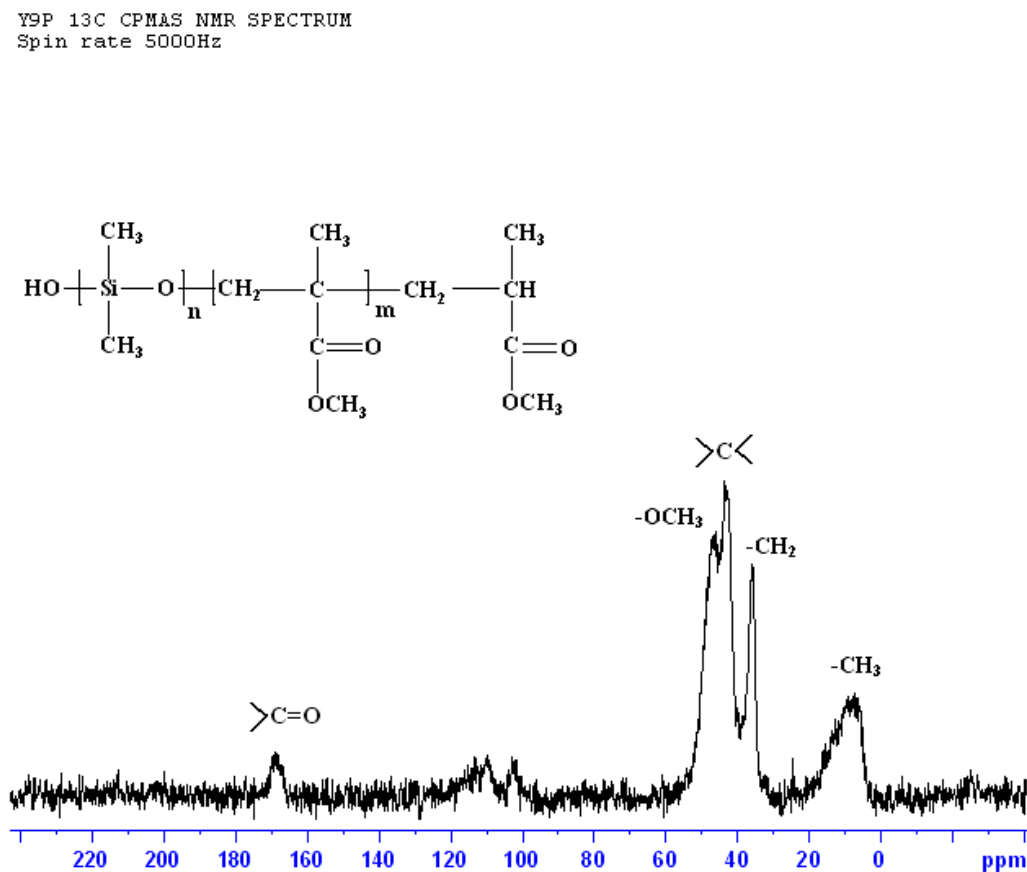


Fig. 3.38 ^{13}C CPMAS NMR spectrum of P(DMS-b-MMA)

Solid-state ^{29}Si MAS NMR spectrum of the same sample, resonance at chemical shift -33,57 ppm can only be assigned to Si atoms from DMS units in the copolymer (Fig. 3.39).

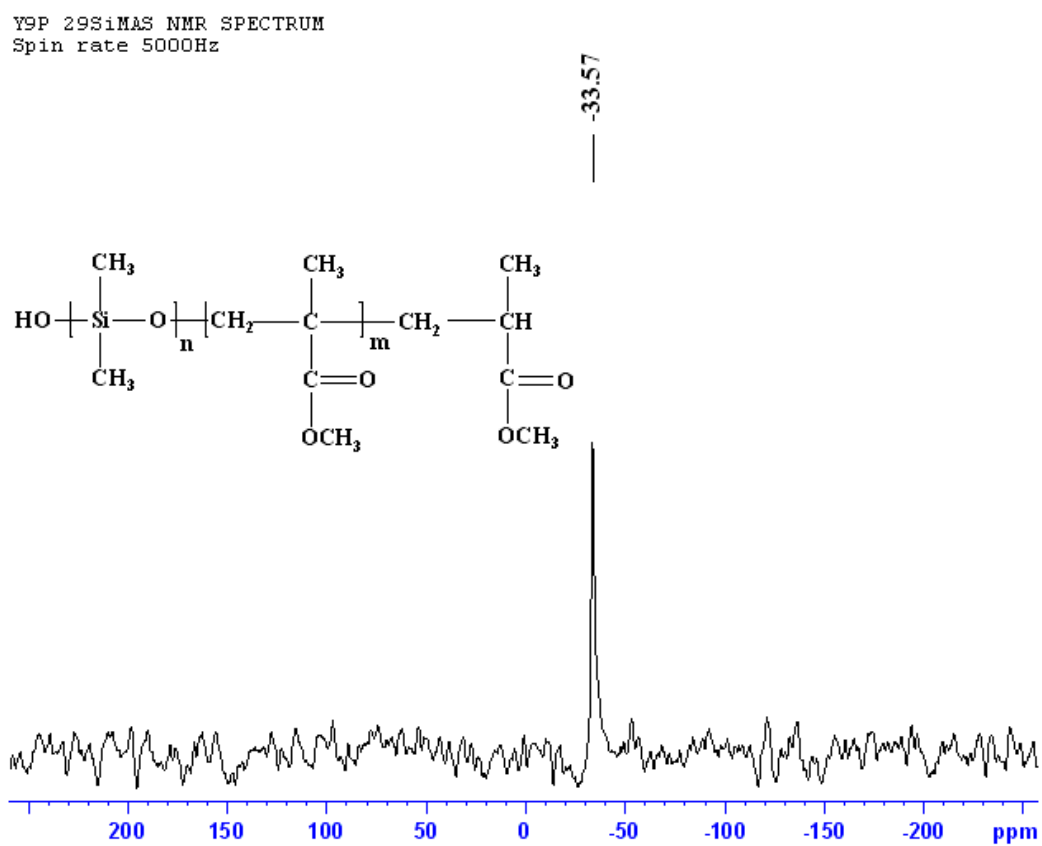


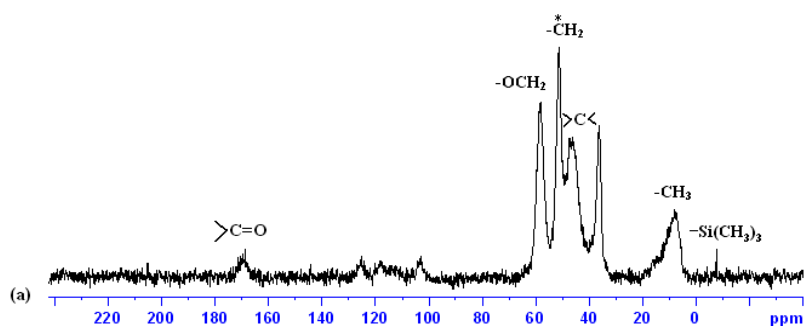
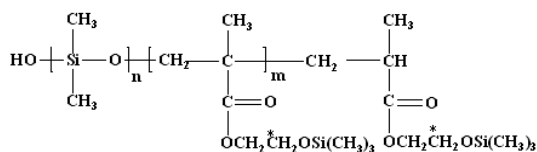
Figure 3.39 Solid-state ^{29}Si MAS NMR spectrum of P(DMS-b-MMA)

3.4.3.2 P(DMS-b-TMSHEMA) and P(DMS-b-HEMA) Block Copolymers

The chemical structures of P(DMS-b-TMSHEMA) and P(DMS-b-HEMA) copolymers were also verified using ^{13}C CPMAS NMR analysis (Fig. 3.40.a and 3.40.b). The assignment of the observed peaks of P(TMS-HEMA) and PHEMA carbons is shown in the same figures. $-\text{CH}_3$ groups' carbons are observed at 2-20 ppm with a very broad band, so $-\text{CH}_3$ carbons corresponding to the PDMS segments can not be identified clearly. Then ^{29}Si MAS NMR experiments were performed on P(DMS-b-TMSHEMA) and P(DMS-b-HEMA) copolymers.

The ^{29}Si MAS NMR spectrum of P(DMS-b-TMSHEMA) shows that two kinds of silicons with different environments (Fig. 3.41.a). Resonances at -4,21 and -33,37 ppm can be attributed to the silicones directly connected to the TMSHEMA and the DMS segments, respectively. After the deprotection of trimethyl silyl groups ($-\text{Si}(\text{CH}_3)_3$) of the P(DMS-b-TMSHEMA) copolymer, peak at -4,21 ppm disappeared and the main peak at -33,49 ppm was only observed due to DMS sequences (Fig. 3.41.b). The ^{29}Si MAS NMR spectrum of P(DMS-b-HEMA) confirmed complete deprotection of ($-\text{Si}(\text{CH}_3)_3$) groups.

Y33P 13C CPMAS SPECTRUM
Spin rate 5000Hz



de-Y33P 13C CPMAS SPECTRUM
Spin rate 5000Hz

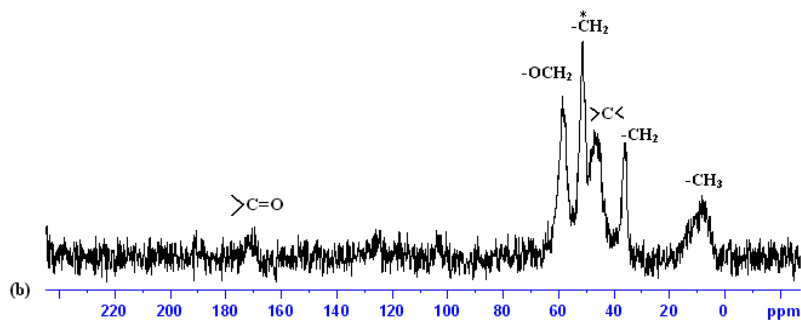
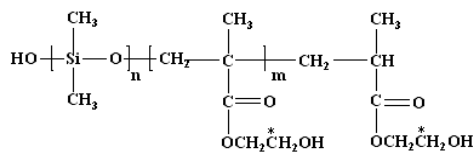


Fig. 3.40 ^{13}C CPMAS NMR spectra of P(DMS-b-TMSHEMA) & P(DMS-b-HEMA)

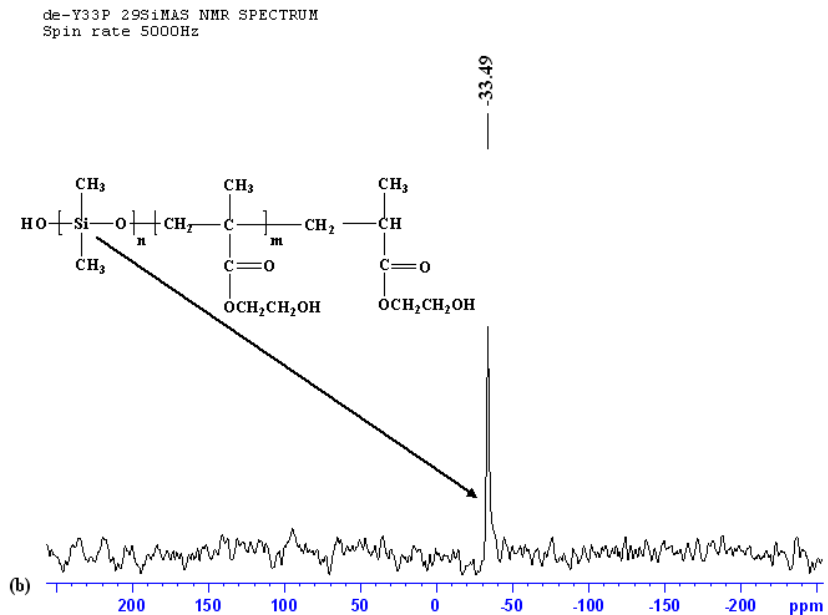
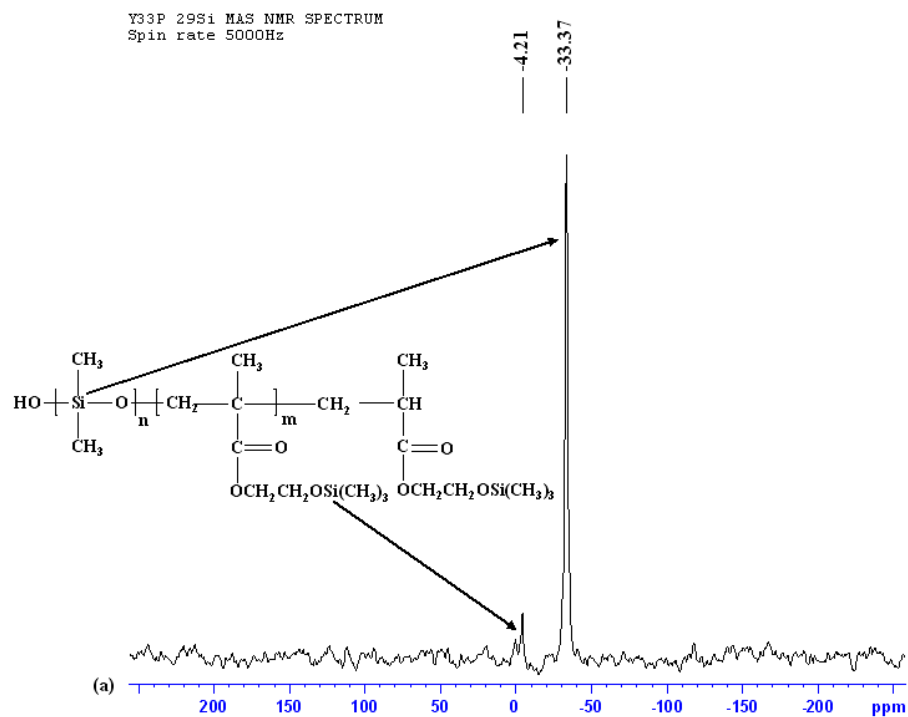


Figure 3.41 ^{29}Si MAS NMR spectra of P(DMS-b-TMSHEMA)& P(DMS-b-HEMA)

3.4.4 GPC Analysis of P(DMS-b-MMA) and P(DMS-b-EMA) Block Copolymers

PDMS ($M_n=6000 \text{ g}\cdot\text{mol}^{-1}$) was converted to the PDMS-MAI ($M_{n\text{GPC}}=39127$ and $M_w/M_n=7.29$) to prepare block copolymers of P(DMS-b-MMA), P(DMS-b-EMA) and P(DMS-b-TMSHEMA). Therefore, the number average degree of condensation, i.e. p value, was found to be about 6. Table 2.3 shows GPC results of P(DMS-b-MMA) copolymers with different PDMS-MAI and MMA feed ratios and different copolymerization times. M_w of copolymers decreases with increase of the initiator concentration, which is reasonable from the radicalic mechanism of initiation. (Run 2, 5 and 8) The effect of polymerization time can be seen as a slight change in molecular weight and impressive increase in polymer yield.

Table 2.4 summarizes the results of GPC measurements for P(DMS-b-EMA) and again the increase in the amount of the PDMS-MAI macroinitiator resulted in the decrease of molecular weights (Run 1, 4 and 7). GPC traces of PDMS-MAI macroazoinitiator and block copolymers were shown in Figure B.1-B.3 in Appendix B. A symmetrical single peak could be observed and the molecular weights shifted to the higher values from macroazoinitiator to copolymers. Also, it is proven by the GPC patterns, block copolymers do not contain low molecular weight impurities.

The recipe of copolymerization and the yields of the P(DMS-b-TMSHEMA) block copolymers are given in Table 2.5. Yields of resulting block copolymers increases with increasing PDMS-MAI weight percent and polymerization times, which verify the initiation efficiency of PDMS-MAI. However, molecular weights and its distribution can not be determined due to the insolubility of P(DMS-b-TMSHEMA) copolymers in THF. Solubility behaviors of block copolymers are also different (Table 3.7).

Table 3.7 Solubility test for copolymers at room temperature

| POLYMERS SOLVENTS | DMF | THF | DMSO | Toluene | Acetone | Ethanol | Methanol | Chloroform | Hexane |
|----------------------|-----|-----|------|---------|---------|---------|----------|------------|--------|
| P(DMS-b-MMA) | s | s | is | s | s | is | is | s | is |
| P(DMS-b-EMA) | ss | s | ss | s | s | is | is | s | is |
| P(DMS-b-TMSHEMA) | s | is | s | is | ss | s | s | is | is |

96

*s: soluble, ss: slightly soluble, is: insoluble

P(DMS-b-EMA) copolymer is insoluble in polar solvents such as DMF, DMSO, methanol, and soluble in toluene, whereas P(DMS-b-TMSHEMA) copolymer is completely soluble in polar solvents and insoluble in aromatic solvents. Methanol is a poor solvent for PDMS, but a good solvent for PHEMA. Also, toluene is a good solvent for PDMS and a poor solvent for PHEMA. Thus, the solution of P(DMS-b-TMSHEMA) copolymer in DMF appeared as a turbid solution.

3.4.5 XPS Results of Copolymers

XPS technique was utilized the qualitative and quantitative determination of block copolymer film surfaces. Especially for the amphiphilic block copolymers, the surface rearrangements are very important for the certain application area.

3.4.5.1 P(DMS-b-MMA)

The XPS spectrum of P₄M(12) P(DMS-b-MMA) copolymer (glass side) is given in Figure 3.42 and the elements found were C, O and Si on both the glass and the air sides of films. From this point to prevent the confusion about types of copolymers, they are coded as P₄M(12), where the number written as subscript represents the weight fraction of PDMS and the number in parenthesis represents the polymerization time. (Table 2.3) Other XPS spectra of P(DMS-b-MMA) copolymers are shown in Appendix C.

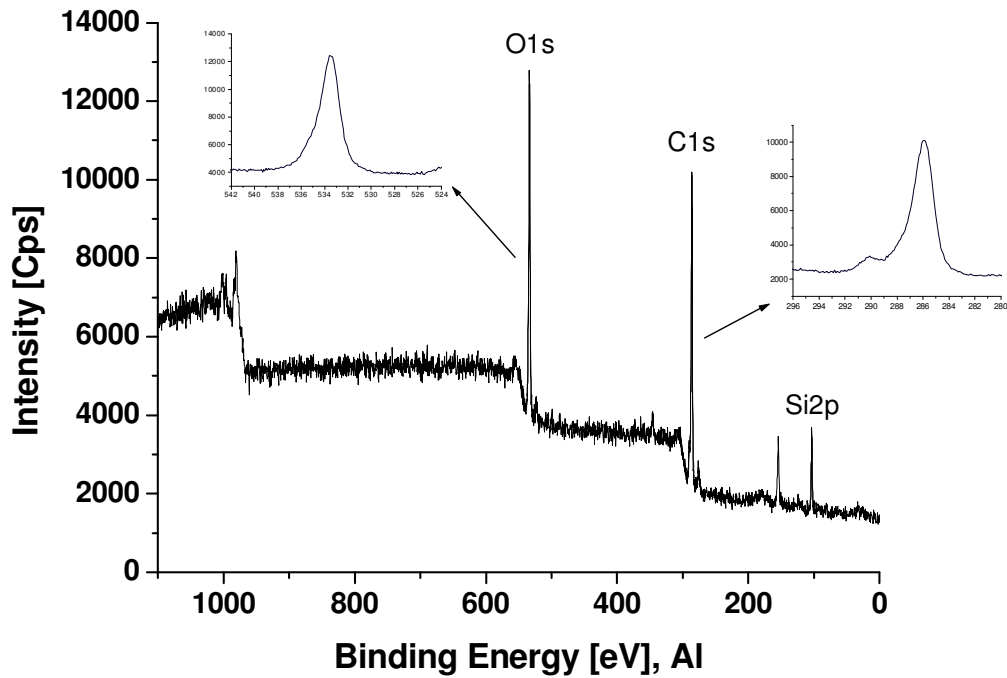
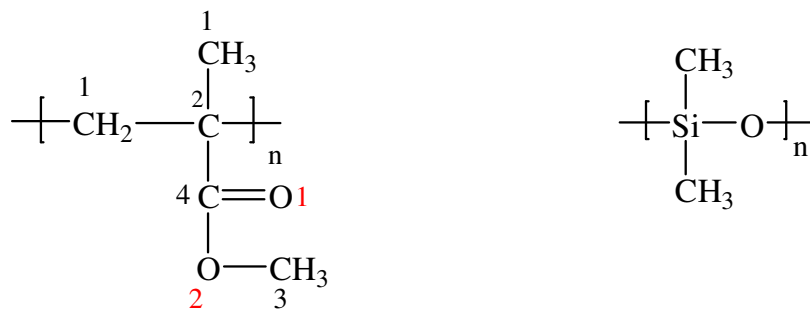


Figure 3.42 Full scan XPS of P_{14,3}M(12) copolymer on glass side

Curve fitting is employed to identify and to quantify C atoms (mixing ratio was 80 % Lorentzian). Based on the curve fit results four different C atoms corresponding to PMMA and one C atom from PDMS chain were labeled below:



Also, binding energies of these C atoms (C1 ~285.10, C2 ~285.93, C3 ~287.02, C4~289.21 and C_{PDMS} ~284.48 eV) are in agreement with the literature [59, 60]. As previously reported, polysiloxanes have the tendency for surface segregation in copolymers, which was derived from its lower surface free energy [61, 62].

Figure 3.43 illustrates C1s XPS spectra of P(DMS-b-MMA) copolymers with mole percentages of each carbons and their binding energies. The surface atomic compositions of different PDMS containing P(DMS-b-MMA) copolymers are tabulated in Table 3.8 on both sides. When the mole percent of each carbon is compared with theoretical values in the molecule, it is observed that the configuration of molecules on glass side and air sides are quite different. Since XPS gives very thin surfacelayer, the observed values and theoretical values of mole percent of each carbons are close on the glass side but much different on air side. The glass surface is more compatible with O and Si in the copolymer, therefore does not change the planar configuration of methacrylate molecule. However, on the air side, C2 carbon is more close to the surface and the methacrylate molecule is not completely planar.

Table 3.8 Surface atomic ratio of Si/C, wt % of PDMS and PMMA in different samples

| Sample | Atomic Composition (%) | | | | | |
|--|------------------------|------|------|--------|-------------|-------------|
| | C1s | O1s | Si2p | Si/C | wt % (PDMS) | wt % (PMMA) |
| P ₄ M(12) _{air} | 61,2 | 28,1 | 10,7 | 0,1748 | 49,86 | 50,14 |
| P ₄ M(12) _{glass} | 57,9 | 29,8 | 12,3 | 0,2124 | 57,74 | 42,26 |
| P _{14.3} M(12) _{air} | 53,1 | 28,5 | 18,4 | 0,4365 | 80,68 | 19,32 |
| P _{14.3} M(12) _{glass} | 60,4 | 27,5 | 12,1 | 0,2003 | 55,29 | 44,71 |

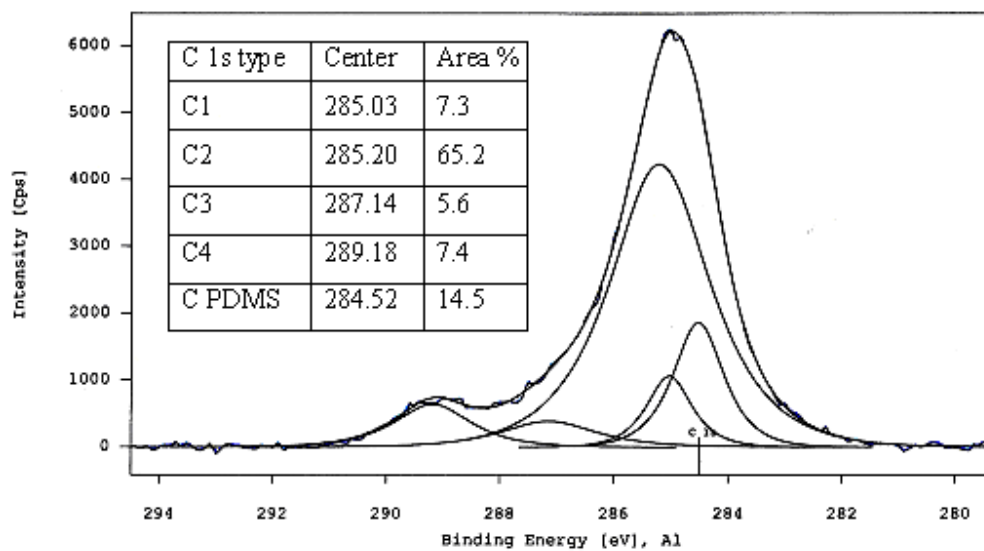
PDMS concentration (wt %) and PMMA concentration (wt %) on both air and glass surfaces of films were calculated by using the equations given below (Eq.3.1 and 3.2), where the Si/C ratio was obtained by XPS data. [63]

$$\text{Si/C} = \frac{\text{wt \% (PDMS) /74}}{2 \text{ wt\% (PDMS) /74} + 5 \text{ wt\% (PMMA) /100}} \quad \text{Eq.3.1}$$

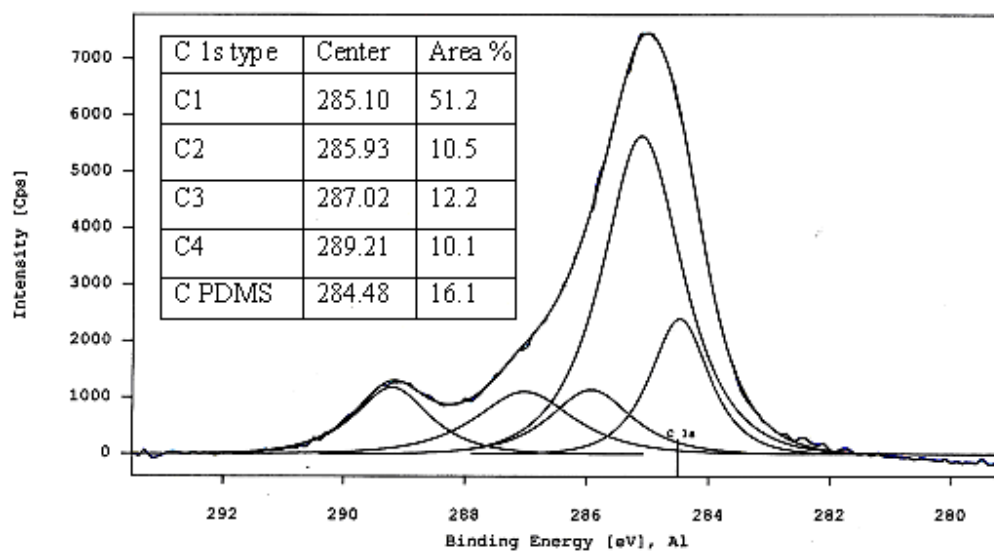
$$\text{wt \% (PMMA)} = 100 - \text{wt\% (PDMS)} \quad \text{Eq.3.2}$$

Then, surface PDMS and PMMA concentrations were also tabulated in Table 3.8 and show the effect of the PDMS content on the surface compositions of both air and glass sides.

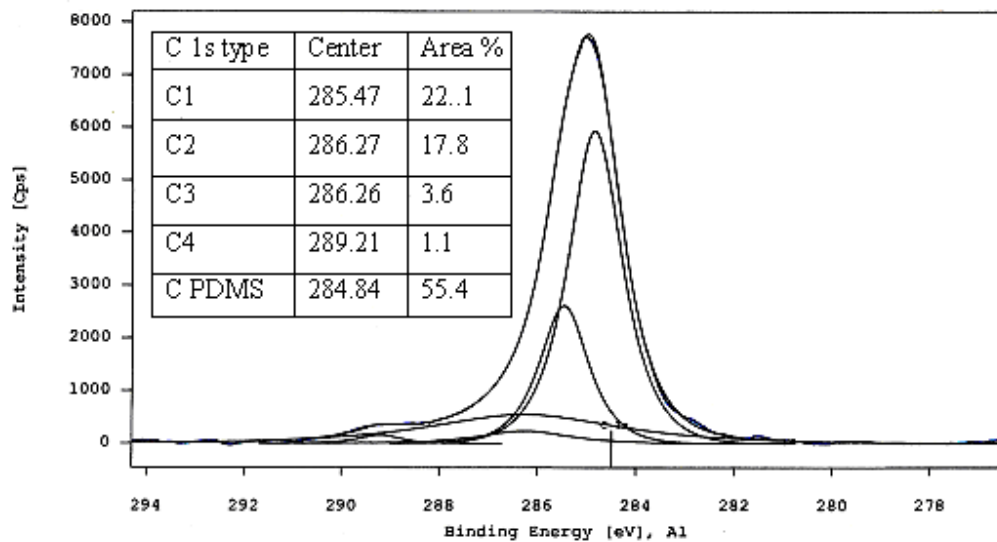
a)



b)



c)



d)

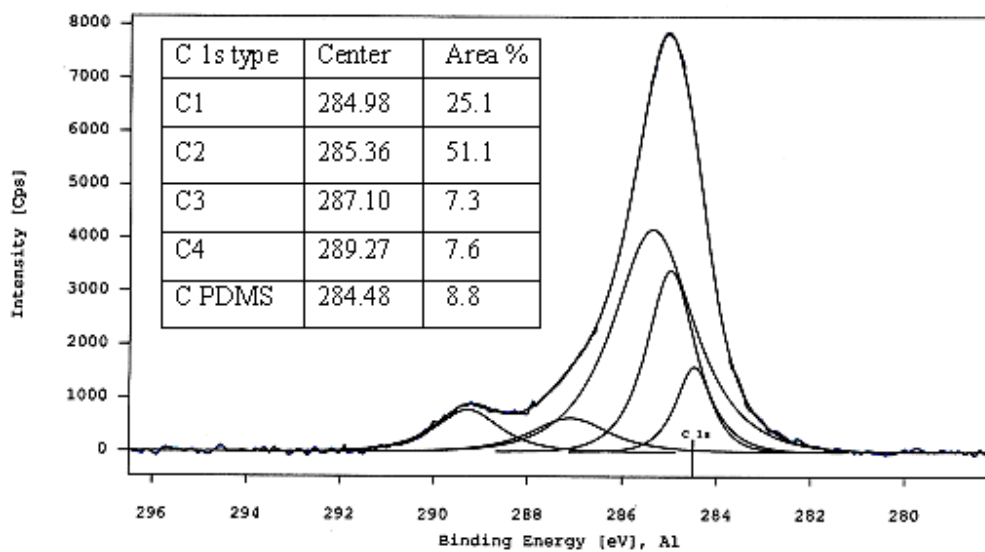


Figure 3.43 C1s XPS spectra of P4M(12) (a air side, b glass side) and P14.3M(12) (c air side, d glass side) copolymers

In the P(DMS-b-MMA) film, as the siloxane content increases, PDMS concentrations increases on the air side. This can be attributed to the accumulation of PDMS segments on the surface of the film with increasing DMS content.

3.4.5.2 P(DMS-b-EMA)

Surface reorganization of P(DMS-b-EMA) copolymer films with varying PDMS content was also studied by the XPS technique and Figure 3.44 shows the XPS survey spectrum of P_{1.8}E(12) copolymer (glass side). Other XPS spectra of P(DMS-b-EMA) copolymers are given in Appendix C.

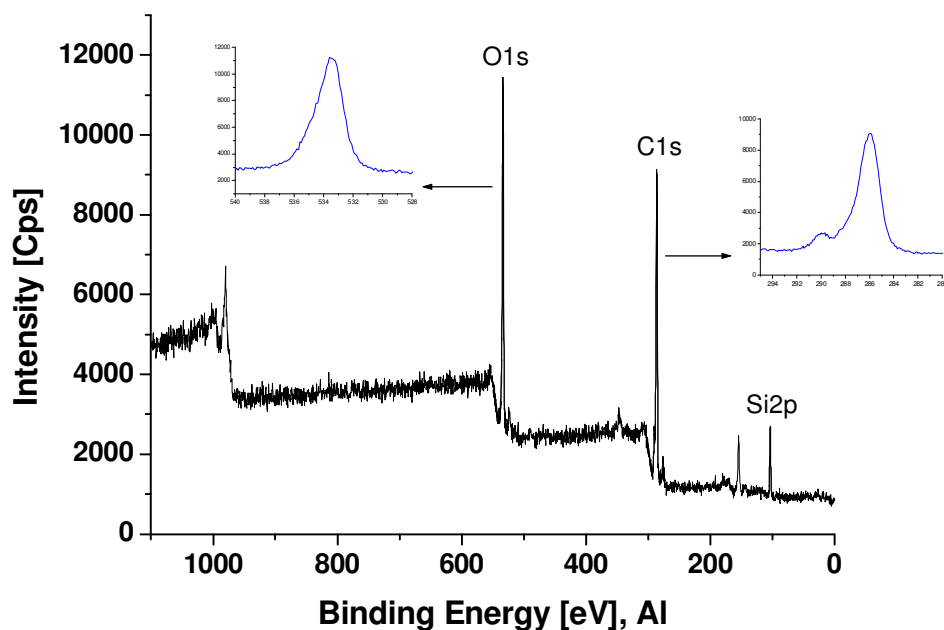


Figure 3.44 Full scan XPS of P_{1.8}E(12) copolymer on glass side

Curve fitting of C1s XPS spectra of P(DMS-b-EMA) copolymers was illustrated in Figure C.5 (Appendix C) and their atomic compositions on air and glass sides were tabulated in Table 3.9 Then PDMS and PEMA surface (air and glass) concentrations were calculated using the following equations (Eq. 3.3 and 3.4). Results are shown in Table 3.9.

$$\text{Si/C} = \frac{\text{wt \% (PDMS) /74}}{2 \text{ wt\% (PDMS) /74} + 6 \text{ wt\% (PEMA) /114}} \quad \text{Eq.3.3}$$

$$\text{wt \% (PEMA)} = 100 - \text{wt\% (PDMS)} \quad \text{Eq.3.4}$$

Table 3.9 Surface atomic ratio of Si/C, wt % of PDMS and PEMA in different samples

| Sample | Atomic Composition (%) | | | | | |
|---|------------------------|------|------|--------|-------------|-------------|
| | C1s | O1s | Si2p | Si/C | wt % (PDMS) | wt % (PEMA) |
| P _{1.8} E(12) _{air} | 71.8 | 28.0 | 0.2 | 0.0028 | 1.09 | 98.91 |
| P _{1.8} E(12) _{glass} | 61.3 | 28.3 | 10.4 | 0,1697 | 50,01 | 49.99 |
| P _{6.8} E(12) _{air} | 56.6 | 28.3 | 15.2 | 0,2685 | 69.31 | 30.69 |
| P _{6.8} E(12) _{glass} | 52.2 | 28.3 | 20.1 | 0.3851 | 86.71 | 13.29 |

Similar to the P(DMS-b-MMA) copolymer, in the P(DMS-b-EMA) copolymer the PDMS concentration increases, as the DMS content increases on both sides (air and glass). On the contrary, the PDMS concentration on the glass side is more than that on air sides. It was noticed that PDMS segments inclined and moved to the glass surface. So, the DMS content is a critical factor for the reorganization and the modification of

block copolymer surfaces, besides casting parameters e.g. solvent, temperature, etc. C1s peak patterns are also similar with increasing siloxane content.

3.4.5.3 P(DMS-b-TMSHEMA)

Wide scan of XPS spectrum of P_{8.7}TH(12)_{glass} film was shown in Figure 3.45 and others were given in Appendix C.

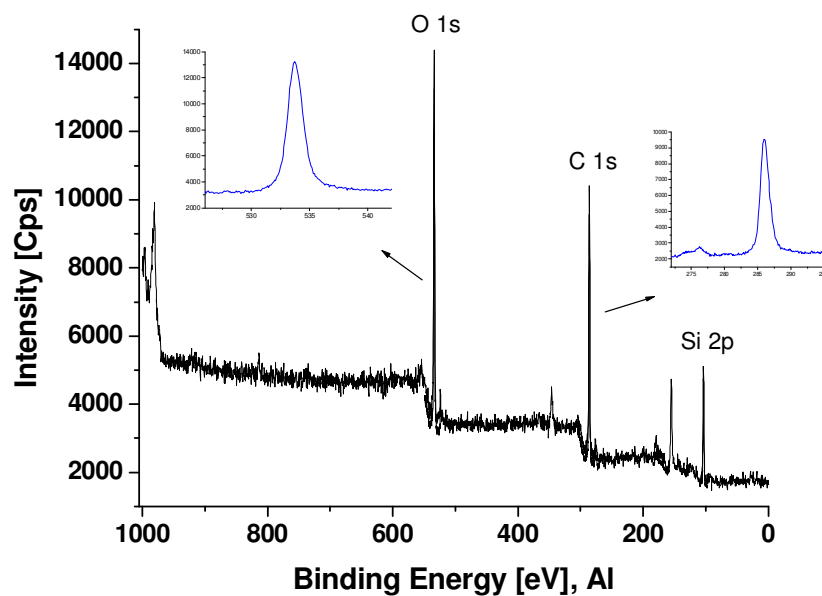
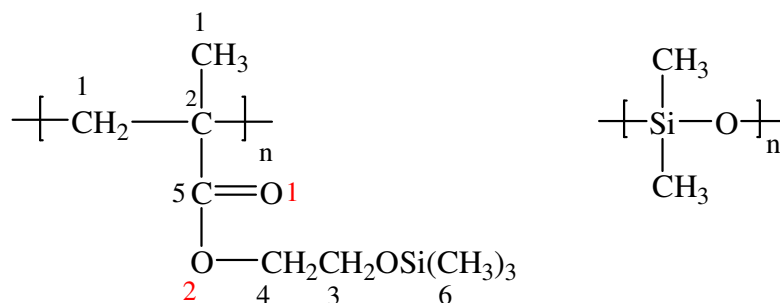


Figure 3.45 Full scan XPS of P_{8.7}TH(12) copolymer on glass side

Different surface C atoms in P(DMS-b-TMSHEMA) copolymers were identified and results are shown in Figure C.8 (Appendix C).



Surface chemical compositions on both sides (air and glass) were calculated by using Eq. 3.5 and 3.6 and results were tabulated in Table 3.10

$$\text{Si/C} = \frac{\text{wt \% (PDMS)} / 74 + \text{wt \% (PTMSHEMA)}}{2 \text{ wt \% (PDMS)} / 74 + 9 \text{ wt \% (PTMSHEMA)} / 202} \quad \text{Eq.3.5}$$

$$\text{wt \% (PTMSHEMA)} = 100 - \text{wt \% (PDMS)} \quad \text{Eq.3.6}$$

Table 3.10 Surface atomic ratio of Si/C, wt % of PDMS and PTMSHEMA in different samples

| Sample | Atomic Composition (%) | | | | | |
|--|------------------------|------|------|--------|-------------|-----------------|
| | C1s | O1s | Si2p | Si/C | wt % (PDMS) | wt % (PTMSHEMA) |
| P _{4.6} TH(12) _{air} | 57.4 | 26.2 | 16.4 | 0.2857 | 57.32 | 42.68 |
| P _{4.6} TH(12) _{glass} | 55.5 | 27.3 | 17.1 | 0.3081 | 62.86 | 37.14 |
| P _{8.7} TH(12) _{air} | 48.9 | 29.4 | 21.6 | 0.4417 | 90.34 | 9.64 |
| P _{8.7} TH(12) _{glass} | 50.1 | 29.6 | 20.3 | 0.4052 | 83.65 | 16.35 |

As can be seen from Figure C.8 (Appendix C) and Table 3.10 there is no great change in surface composition with increasing PDMS content and C1s peak patterns are similar. This can be explained by the chemical structures of both segments. By changing the hydroxyl group of HEMA to trimethyl silyl group, the difference in the chemical structure of PDMS and the PHEMA was diminished and compatibility of two segments was improved.

3.4.5.4 P(DMS-b-HEMA)

After the acid treatment of P(DMS-b-TMSHEMA) copolymer to remove the TMS group XPS analysis was performed and the XPS survey spectrum of the $P_{4.6}H(8)_{air}$ copolymer was given in Figure 3.46

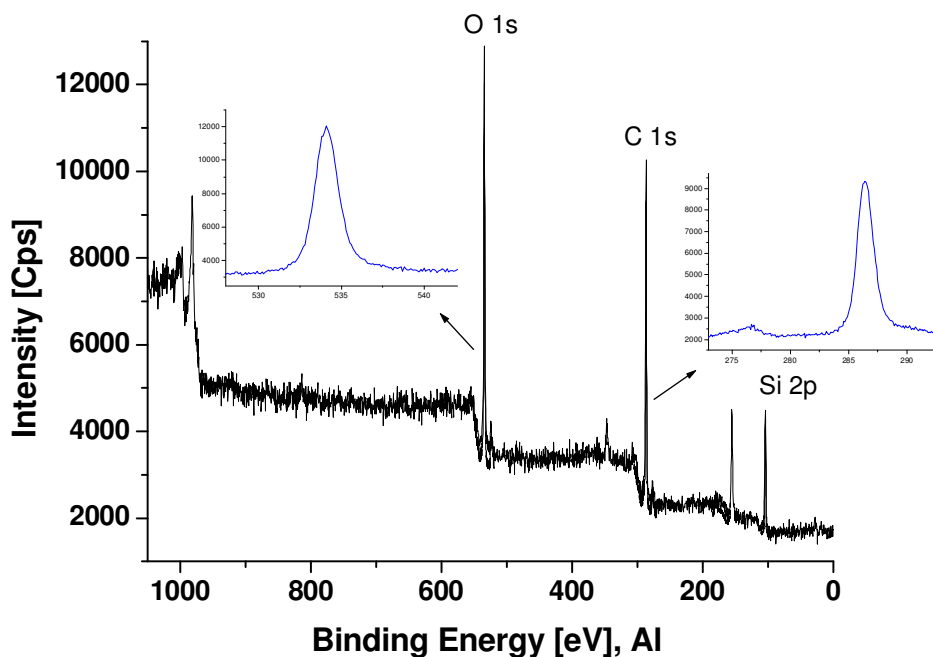


Figure 3.46 Full scan XPS of $P_{4.6}H(8)$ copolymer on air side

Curve fitting of C1s peaks was carried out to identify different C atoms and shown in Figure C.11.

PDMS and PHEMA surface (air and glass) concentrations were calculated using following equations (Eq. 3.7 and 3.8). Results are shown in Table 3.11

$$\text{Si/C} = \frac{\text{wt \% (PDMS) /74}}{2 \text{ wt\% (PDMS) /74} + 6 \text{ wt\% (PHEMA) /130}} \quad \text{Eq.3.7}$$

$$\text{wt \% (PHEMA)} = 100 - \text{wt\% (PDMS)} \quad \text{Eq.3.8}$$

Table 3.11 Surface atomic ratio of Si/C, wt % of PDMS and PHEMA in different samples

| Sample | Atomic Composition (%) | | | | | |
|---|------------------------|------|------|--------|-------------|--------------|
| | C1s | O1s | Si2p | Si/C | wt % (PDMS) | wt % (PHEMA) |
| P _{4.6} H(8) _{air} | 53.2 | 28.2 | 18.6 | 0.4396 | 79.88 | 20.12 |
| P _{4.6} H(8) _{glass} | 55.4 | 29.3 | 15.3 | 0.2762 | 67.82 | 32.18 |
| P _{16.1} H(8) _{air} | 48.8 | 29.5 | 21.7 | 0.4447 | 93.21 | 6.79 |
| P _{16.1} H(8) _{glass} | 52.9 | 28.9 | 18.2 | 0.3441 | 79.03 | 20.97 |

After the deprotection process of P(DMS-b-TMSHEMA) it can be concluded that PDMS segments tend to the air side of the film and this orientation to the air side becomes evident while increasing the DMS content.

3.4.6 SEM Analysis of Block Copolymers

3.4.6.1 P(DMS-b-MMA)

SEM images of different PDMS containing P(DMS-b-MMA) copolymer films of air sides can be seen in Figure 3.47. As depicted from SEM micrographs, PMMA has appeared as a continuous phase and PDMS is dispersed (white dots) in PMMA phase. Morphologies of the three different PDMS content of copolymers ($P_4M(12)_{air}$, $P_{7.7}M(12)_{air}$ and $P_{14.3}M(12)_{air}$) are different (Figure 3.47 (a), (b) and (c), respectively). Overview of SEM images shows that PDMS particles were enlarged with increasing DMS content in continuous PMMA matrix. Up to the 14 weight percent, there is no phase separation occurs between PMMA and PDMS segments.

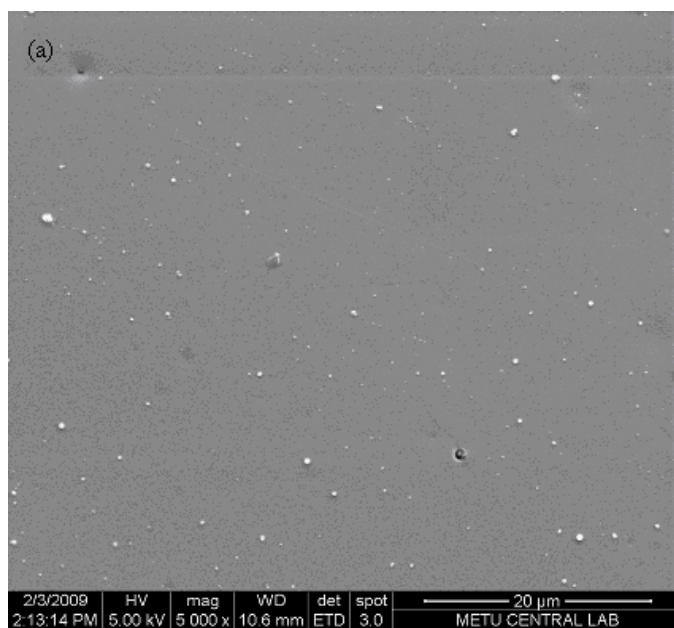


Figure 3.47 SEM micrographs of (a) $P_4M(12)_{air}$, (b) $P_{7.7}M(12)_{air}$ and (c) $P_{14.3}M(12)_{air}$

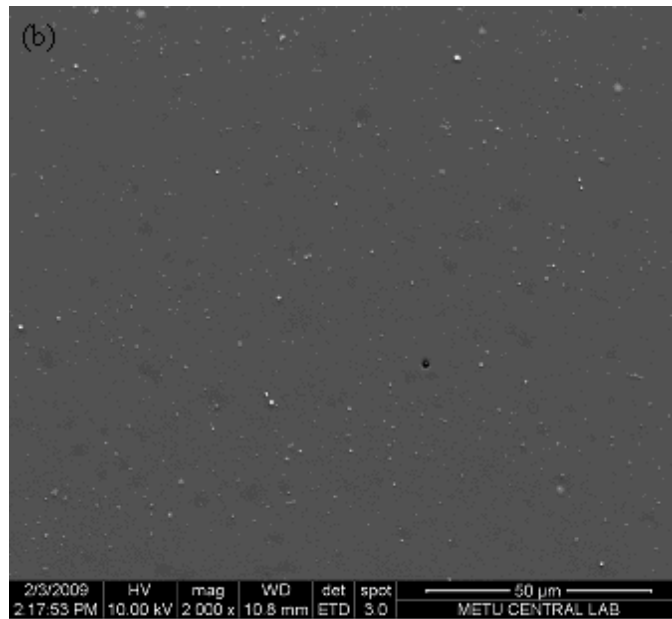


Figure 3.47 (cont'n)

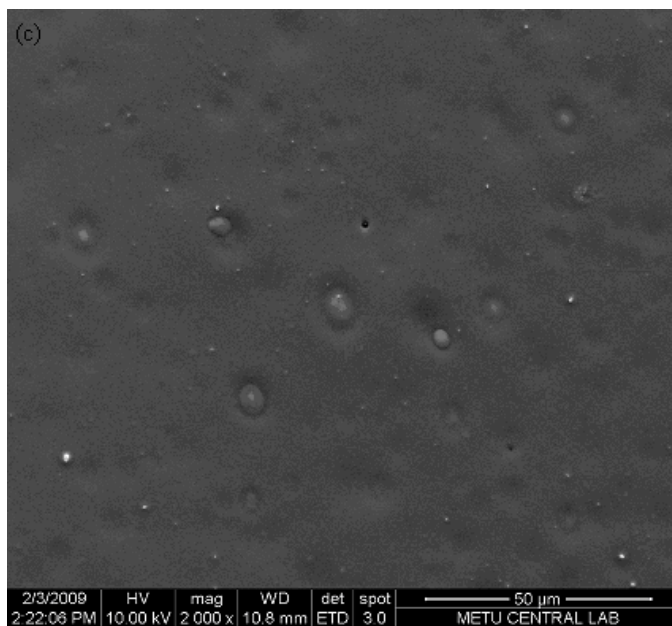


Figure 3.47 (cont'n)

3.4.6.2 P(DMS-b-EMA)

Figure 3.48 illustrates SEM images of different PDMS containing P(DMS-b-EMA) copolymers films of glass sides. It can be noticed that the microphase separation occurs between PEMA and PDMS domains and the segregation become clear with increasing DMS content ($P_{1.8}E(12)_{\text{glass}}$ and $P_{3.5}E(12)_{\text{glass}}$, Figure 3.48 (a) and (b), respectively). PDMS blocks can be seen as discrete particles in low weight percent, while these particles aggregate at high weight percent. Results obtained from XPS data are consistent with SEM analysis.

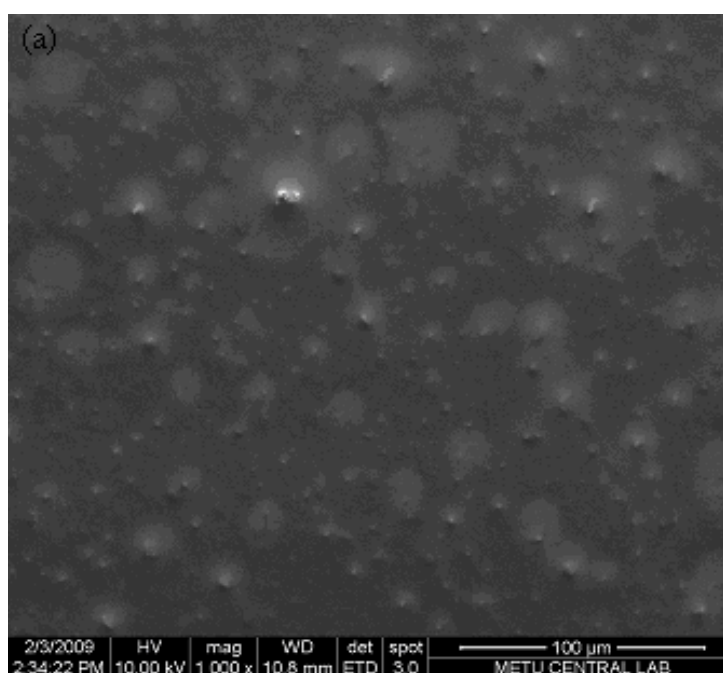


Figure 3.48 SEM micrographs of (a) $P_{1.8}E(12)_{\text{glass}}$ and (b) $P_{3.5}E(12)_{\text{glass}}$,

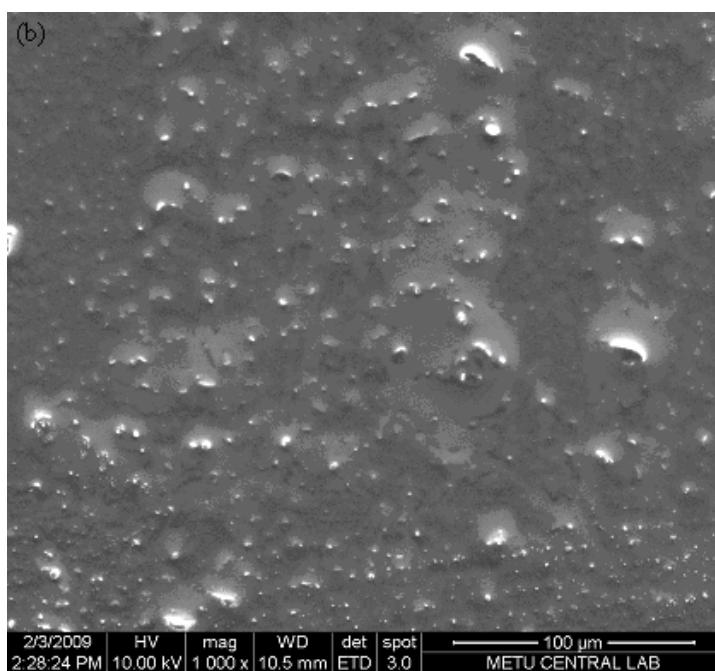


Figure 3.48 (cont'n)

3.4.6.3 P(DMS-b-TMSHEMA) and P(DMS-b-HEMA)

SEM images of P(DMS-b-TMSHEMA) and P(DMS-b-HEMA) copolymers indicates the increase in surface roughness, different from MMA and EMA cases (Figure 3.49). After deprotection of P(DMS-b-TMSHEMA) copolymer white PDMS particles appeared at the surface and this trend can be displayed prominently by increasing the DMS content of copolymer (Figure 3.50). It agrees with XPS results which pointed out air side surface accumulation of PDMS segments.

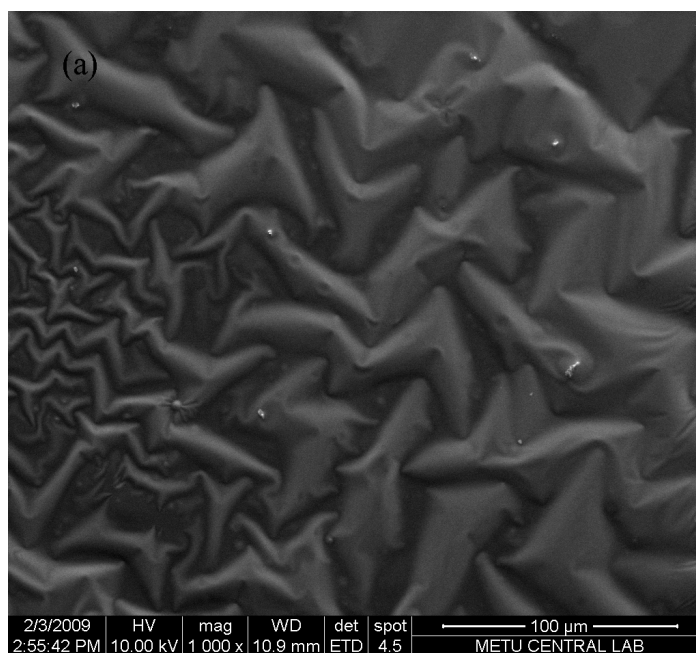


Figure 3.49 SEM micrographs of (a) $P_{4.6}TH(12)_{air}$ and (b) $P_{8.7}TH(12)_{air}$

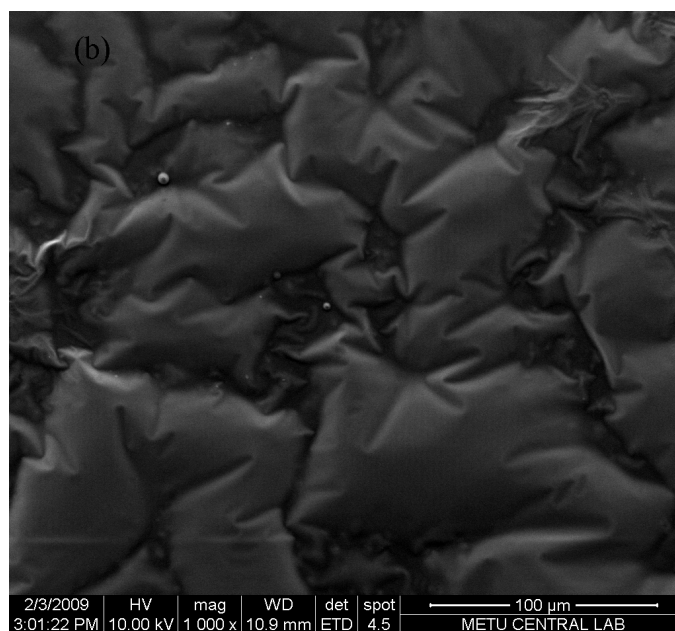


Figure 3.49 (cont'd)

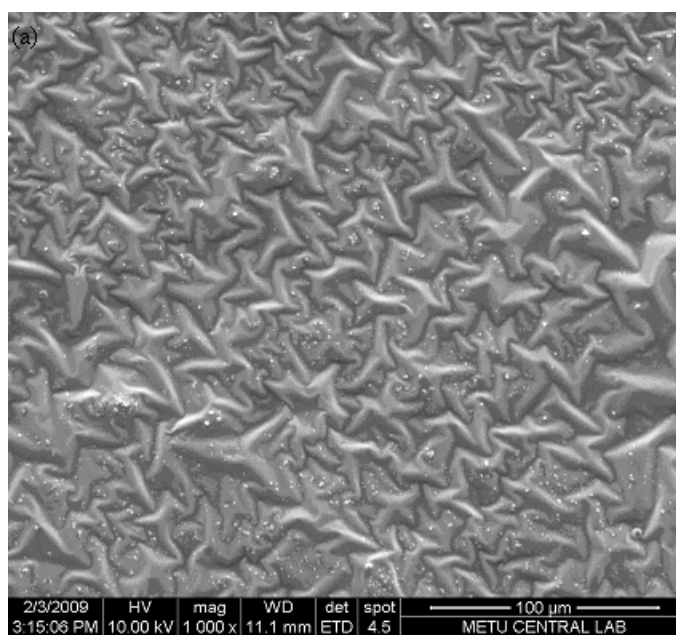


Figure 3.50 SEM micrographs of (a) $P_{4.6}H(8)_{air}$ and (b) $P_{16.1}H_{air}$ (after deprotection of trimethyl silyl groups)

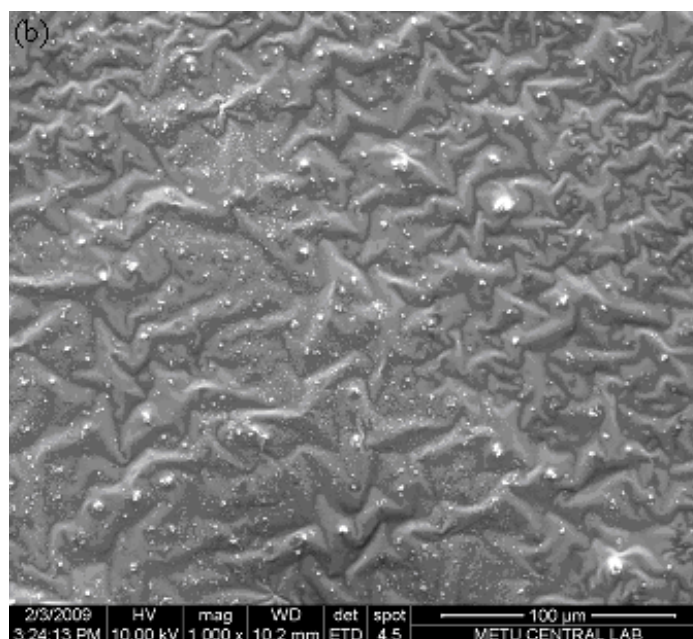


Figure 3.50 (cont'd)

3.4.7 DSC of Block Copolymers

3.4.7.1 P(DMS-b-MMA)

The DSC thermogram of P_{7.7}M(8) P(DMS-b-MMA) copolymer exhibits one glass transition temperature at around 137°C corresponding to PMMA block (Figure 3.51).

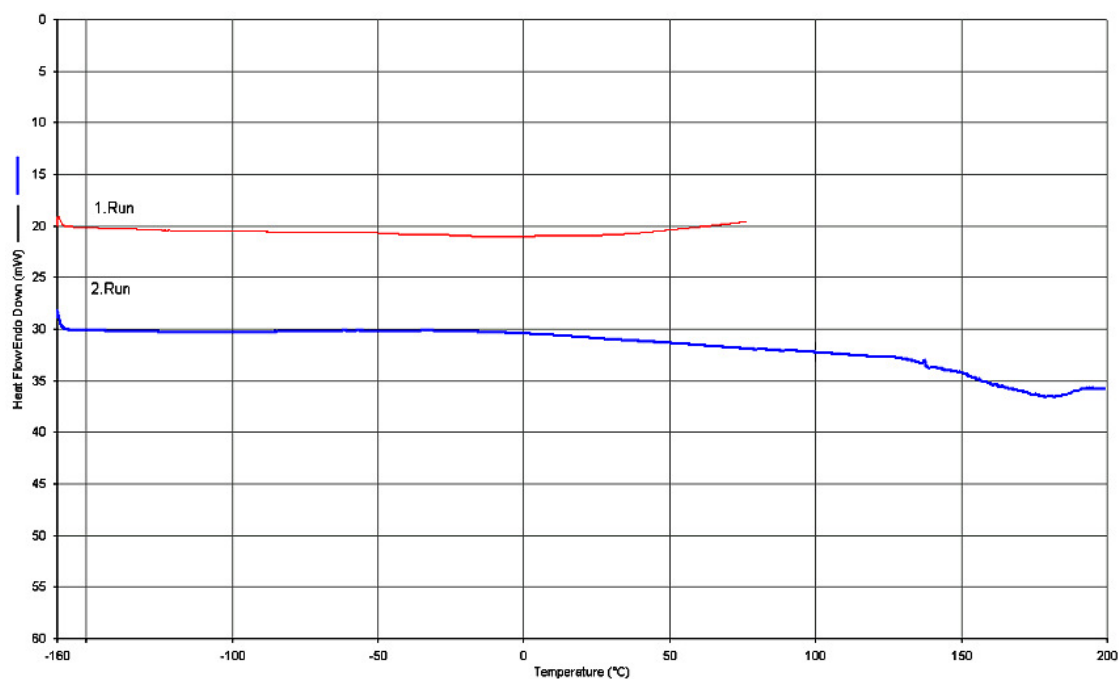


Figure 3.51 DSC thermogram of P_{7.7}M(8) copolymer

Characteristic PDMS transitions at low temperatures (glass transition, crystallization and melting) can not be observed in this copolymer composition. There is no evidence that the microphase separation occurred which agreed with XPS results. But a heterogeneous structure appeared when the DMS content increased from 7.7 to 14.3 in

P_{14.3}M(8) copolymer (% DMS was nearly twice). Figure 3.52 shows the glass transition (-125 °C), crystallization (-101°C) and double melting (-46 and -37°C) temperatures of PDMS block and another Tg (131°C) belongs to the PMMA block. The first melting peak is not very sharp and appeared as a shoulder.

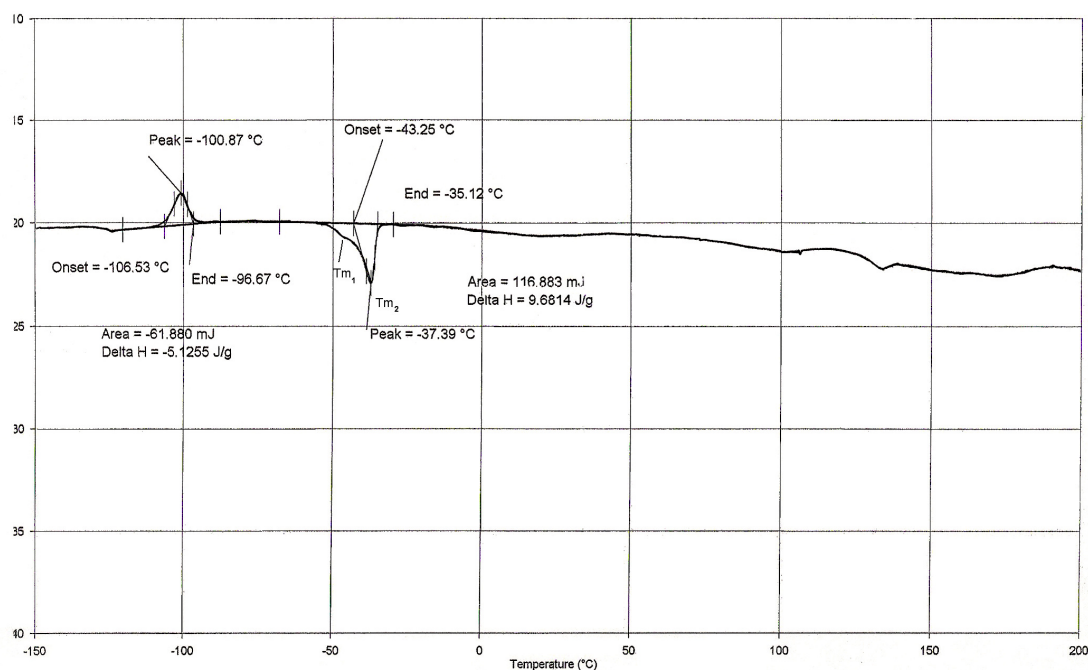


Figure 3.52 DSC thermogram of P_{14.3}M(8) copolymer

3.4.7.2 P(DMS-b-EMA)

All transition temperatures: glass transition (-125°C), crystallization (-93°C) and double melting (-50 and -36°C) of PDMS block and the Tg (90°C) of PEMA block can be seen in Figure 3.53. The existence of two separate Tg is evidence for the phase separation which is consistent with XPS result. The double melting behavior of some polymers has been explained by many research groups and they proposed different

mechanisms. Groeninckx et. al. [64] explained that the first melting peak in the PET from the amorphous state was associated with crystalline materials formed at the crystallization temperature and the second one was related to the melting of a fraction of the original crystalline material that was recrystallized during DSC. Basset et. al. [65] proposed that two melting peaks represent different morphologies with different lamella thicknesses. Lee and Porter explained that the double melting peaks observed in PEEK was caused by melting of most of the original crystals, their crystallization, remelting of the recrystallized part and melting of residual crystalline region [66]. While the P(DMS-b-EMA) copolymer was heated some rearrangements and crystallization occur from the amorphous phase. These crystals melted at -36°C (T_{m2}) and the first melting peak (T_{m1} at -50°C) corresponds to the original preceding crystal phase.

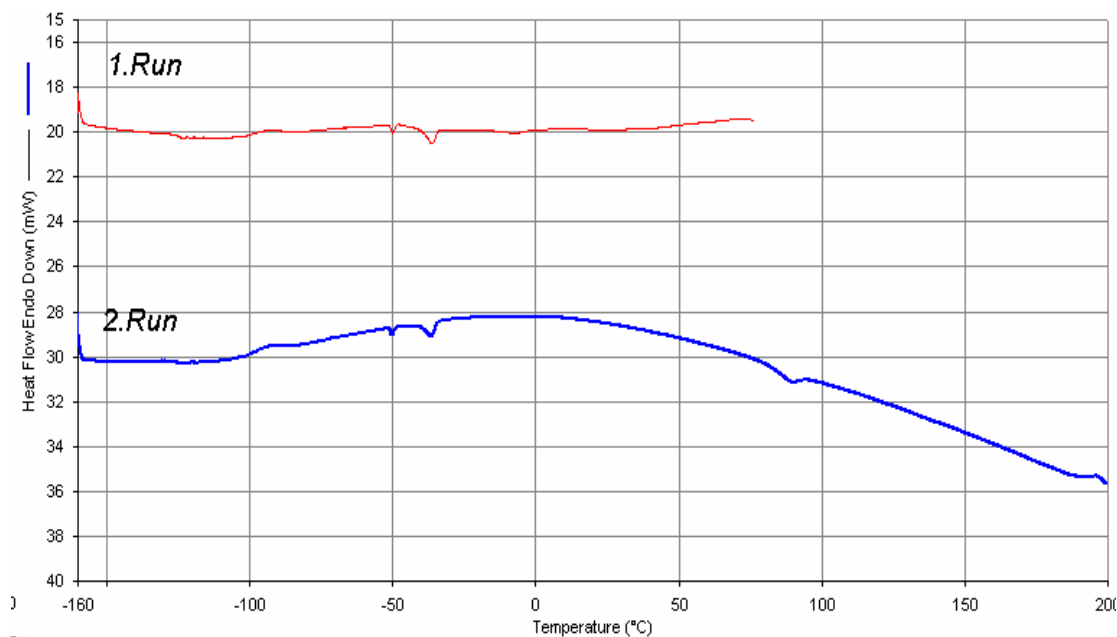


Figure 3.53 DSC thermogram of P_{6.8}E(8) copolymer

3.4.7.3 P(DMS-b-TMSHEMA)

The DSC thermogram of P(DMS-b-TMSHEMA) shows thermal transition temperatures of both PDMS (glass transition (-126°C), crystallization (-92°C) and double melting (-49 and -37°C)) and the P(TMS-HEMA) (T_g, 90°C) (Figure 3.54). These transitions imply that the phase separated morphology of the P(DMS-b-TMSHEMA) copolymer.

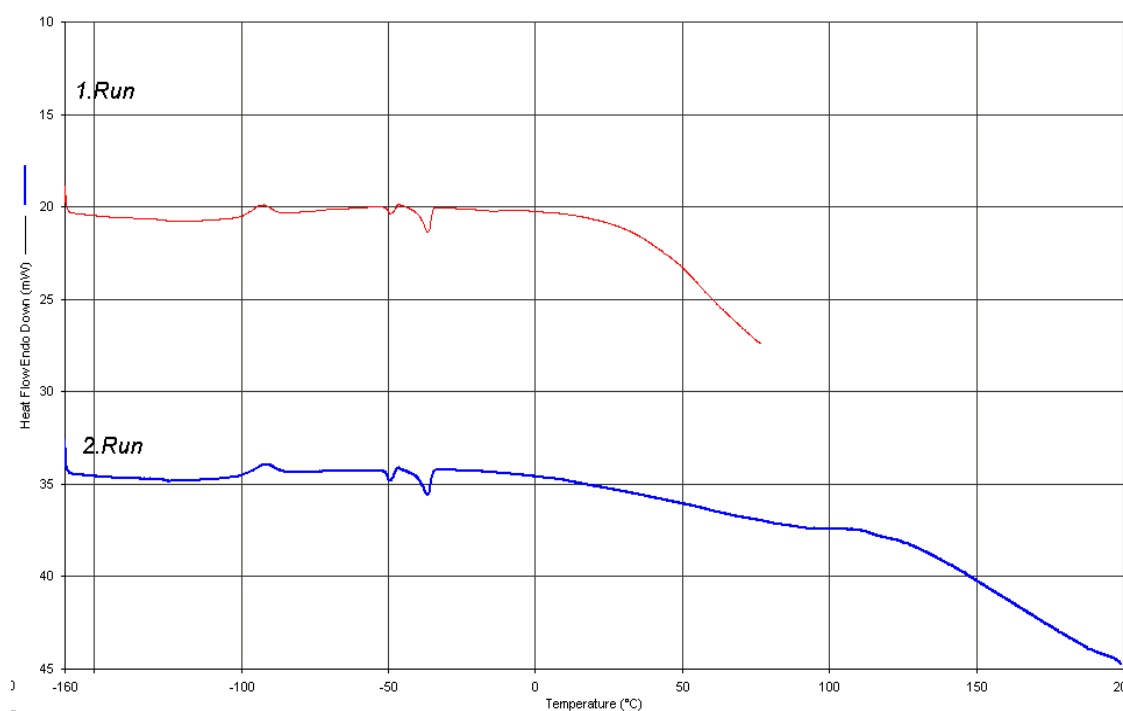


Figure 3.54 DSC thermogram of P_{8.7}TH(8)copolymer

CHAPTER 4

CONCLUSIONS

Poly(2-hydroxyethyl methacrylate), PHEMA, is the most widely used hydrogel because of water content is similar to that of living tissues, bio- and blood-compatibility and resistant to degradation. PDMS is also used as biomaterial due to the high oxygen permeability, high lubricity, thermal stability and chemically inert, elastomeric properties. HEMA based daily disposable soft contact lenses and silicone containing contact lenses share the market. Block copolymers containing both hydrophilic and hydrophobic segments have great interest and these amphiphilic copolymers also used as an emulsifying agent in polymer solutions and compatibilizer in polymer blends. The objective of this study is the synthesis of block copolymers involving 2-hydroxyethyl methacrylate (HEMA) and dimethyl siloxane (DMS) by appropriate methods. The results obtained in the current study are summarized as follows:

1. Aqueous solution polymerization of HEMA by gamma radiation:

- The polymerization of HEMA was carried out in aqueous solution to saturate –CH₂CH₂OH groups and that way to prevent intra- and intermolecular hydrogen bonding. In this case, the polymer might be linear. The conversion – time curve showed an autoacceleration character and the polymer obtained was insoluble in common solvents. Hence the polymerization did not take place in a controlled way with respect to the molecular weight.
- The thermal degradation mechanism of PHEMA obtained by gamma radiation was studied and the TGA and MS methods showed that the degradation is linkage and depolymerization with a combination of monomer fragmentation. The FT-IR of TGA fragments showed no monomer, which was degraded

further to give fragments. Mass analysis revealed that the fragments in the first two stages (at 48°C and 365°C) are corresponding to that of the monomer degradation, which are the same as the fragments obtained from GC-MS of monomer.

2. ATRP of HEMA:

- Various Cu(II) complexes were prepared before the ATRP of HEMA in order to shift the atom transfer equilibrium to the dormant species. Characterization of Cu(II) complexes were performed by UV-Vis and FTIR techniques and the Cu(II)O₂ complex was chosen for the ATRP of HEMA.
- The optimization of the polymerization process is of high importance in order to carefully control the block copolymer design. Ethyl-2-bromoisobutyrate (EBriB) initiator, CuCl/bipyridine catalyst and MEK/1-propanol solvent mixture were chosen for the ATRP of HEMA.
- Cl-end capped PHEMA was used as a macroinitiator for the copolymerization with PDMS via ATRP. However, the PDMS did not dissolve in the MEK/1-propanol mixture, the –OH groups were protected by trimethyl silyl group to decrease the hydrophilicity of HEMA. The newly formed monomer (TMSHEMA) was polymerized and copolymerized via ATRP. In this case, Cl-end capped P(TMSHEMA) could not be copolymerized with PDMS due to the difference in molecular weights. The second reason might be the PDMS polymer itself. Second block should be added as a sequential monomer instead of a polymer for the preparation of block copolymer via ATRP.

3. RAFT polymerization of HEMA:

- The effect of solvents on the RAFT polymerization of HEMA has been examined. MEK and ethyl acetate are much better solvents than toluene and they were used to improve the CTA solubility while performing the polymerizations.

- The polymerizations resulted in higher conversions in toluene due to the low solubility of CDB. RAFT polymerization of HEMA, under experimental condition such as $[RAFT]/[AIBN]=18$ at 80 °C in MEK, shows linear relationship between $\ln([M]_0/[M])$ and polymerization time meaning that the first-order kinetic up to the nearly 40 % conversion.
- The key requirements for achieving the well defined block copolymer consist of judicious choice of the reactive monomers and their concentrations and also the suitable solvent. Firstly prepared PHEMA block was used as a macroRAFT agent in the copolymerization with vinyl terminated PDMS via RAFT process. However, $^1\text{H-NMR}$ results of copolymers after deprotection revealed that the DMS units are absent in the copolymer structure. The reasons of the failure might be either the different hydrophilic/hydrophobic characters of the blocks or the lower reactivity of PDMS polymer than that of monomer. Also, PHEMA should has a high transfer constant in the subsequent polymerization step to give PDMS block.
- The comparison can be done between these three techniques that are free radicalic, ATRP and RAFT polymerization. In conventional free radical technique, it is not possible to obtain soluble polymer for the copolymerization reactions. Living radical polymerization process (ATRP and RAFT) allows us to prepare the predetermined molecular weight and architecture polymers and to have first-order kinetics.

4. Block copolymers with PDMS-MAI macroazoinitiator

- The chemical structures of P(DMS-b-MMA), P(DMS-b-EMA) and P(DMS-b-TMSHEMA) were analyzed by FTIR, $^1\text{H-NMR}$ and solid state NMR techniques and they all confirmed that the all block copolymers were synthesized successfully.

- XPS results of P(DMS-b-MMA), P(DMS-b-EMA) and P(DMS-b-TMSHEMA) copolymers revealed that:
 - i. in the air side of the P(DMS-b-MMA) film, as the siloxane content increases PDMS concentrations increases which means that the accumulation of PDMS segments on the surface of the film with increasing DMS content.
 - ii. Similar to the P(DMS-b-MMA) copolymer, in the P(DMS-b-EMA) film the PDMS concentration increases, as the DMS content increases on both sides (air and glass). On the contrary, the PDMS concentration on the glass side is more than that on air sides and this can be attributed to the PDMS segments inclined and moved to the glass surface.
 - iii. After the deprotection of TMS groups (DMS-b-HEMA) films shows that the PDMS segments tend to the air side of the film and this orientation to the air side becomes evident while increasing the DMS content.
- SEM analysis shows that that the microphase separation occurs between PEMA and PDMS domains and the segregation become clear with increasing DMS content and results obtained from XPS data are in consistent with SEM analysis. In SEM micrograph of P(DMS-b-HEMA) film (after deprotection) white PDMS particles appeared at the surface and this trend can be seen prominently by increasing the DMS content of copolymer.
- The DSC thermogram of P(DMS-b-TMSHEMA) shows thermal transition temperatures of both PDMS (T_g (-126°C), T_c (-92°C) and T_m (-49 and -37°C) and the P(TMS-HEMA) blocks (T_g , 90°C). These transition temperatures imply that the phase separated morphology of P(DMS-b-TMSHEMA) copolymer.

As a conclusion, P(DMS-b-HEMA) amphiphilic block copolymer was synthesized by PDMS macroazoinitiator. Hydrophilic PHEMA and the hydrophobic PDMS exist in

copolymer as phase separated and this morphology results in a special properties. The determination of contact angle and permeation of different gases of the films and also the other membrane properties of this multiblock copolymers are recommended for possible bioapplication.

REFERENCES

1. Montheard J.P., Chatzopoulos M., Chappard D., *J. of Macr. Sci.- Rev. in Macr. Chem. and Phys.* 1992, C32(1), 1-34.
2. Karlgard C.C.S., Sarkar D.K., Jones L.W., Moresoli C., Leung K.T., *Applied Surface Science*, 2004, 230, 106-114.
3. Hsiue G.H., Lee S.D., Chang P.C.T., *Artificial Organs*, 1996, 20(11), 1196-1207.
4. Lee S.D., Hsiue G.H., Kao C.Y., Chang P.C.T., *Biomaterials*, 1996, 17(6), 587-595.
5. Lee S.D., Hsiue G.H., Wang C.C. *Journal of Applied Polymer Science*, 1994, 54(9), 1279-1287.
6. Hsiue G.H., Lee S.D., Wang C.C. Shiue M.H., Chang P.C.T., *Biomaterials*, 1994, 15(3), 163-171.
7. Bodas D.S., Desai S.M., Gangal S.A., *Applied Surface Science*, 2005, 245, 186-190.
8. Abbasi F., Mirzadeh H., Katbab A.A., *Polymer International*, 2002, 51, 882-888.
9. Abbasi F., Mirzadeh H., *Journal of Polymer Science, Part B, Polymer Physics*, 2003, 41, 2145-2156.
10. Deng X.M., Castillo E.J., Anderson J.M., *Biomaterials*, 1986, 7, 247-251.
11. Hou Y., Tulevski G.S., Valint P.L., Gardella J.A., *Macromolecules*, 2002, 35, 5953-5962.
12. Kopecek J., Jokl J., Lim D.. *J. Polym. Sci. Part C* 1968; 16: 3877.
13. Fort R. J., Polyzoidis T. M.. *Eur. Polym. J.* 1976; 12(9):685-689.
14. Hirao A., Kato H., Yamaguchi K., Nakahama S. *Macromolecules*. 1986; 19(5), 1294-1299.

15. Mori H., Wakisaka O., Hirao A., Nakahama S. *Macromol. Chem. Phys.* 1994; 195, 3213-3224.
16. Beers K. L., Boo S., Gaynor S.G., Matyjaszewski. *Macromolecules.* 1999; 32(18): 5772-5776.
17. Robinson K.L., Khan M.A., Banez M.V.D., Wang X.S., Armes S.P. *Macromolecules.* 2001; 34 (10): 3155-3158.
18. Weaver J.V.M., Bannister I., Robinson K.L., Bories-Azeau X., Armes S.P., Smallridge M., McKenna P. *Macromolecules.* 2004; 37 (7): 2395-2403.
19. Chiefari J., Chong Y.K., Ercole F., Krstina J., Jeffery J., Le T.P.T., Mayadunne R.T.A., Meijs G.F., Moad C.L., Moad G., Rizzardo E., Thang S.H. *Macromolecules.* 1998; 31 (16): 5559-5562.
20. Kilian L. "Synthesis and characterization of responsive poly(alkyl methacrylate) topologies." Dissertation, VA Polytech. Inst. & State Uni., 2004.
21. Matyjaszewski K., Xia J. "Atom Transfer Radical Polymerization", *Chem. Rev.*, 2001, 101, 221-2990.
22. Matyjaszewski K., Davis T. P. 'Handbook of Radical Polymerization' John Wiley & Sons, Inc. Publication, 2002.
23. Kumakura M., Fujimura T., Kaetsu I., *European Polymer Journal*, 1983, 19(7), 621-626.
24. Kaetsu I., Ito A., Hayashi K., *Journal of Polymer Science, Polymer Chemistry Edition*, 1973, 11, 1811-1818.
25. Stol M., Cifkova I., Brynda E., *Biomaterials*, 1988, 9, 273-276.
26. Hill D.J.T., O'Donnell J.H., Pomery P.J., Saadat G., *Radiation Physics Chemistry*, 1996, 48(5), 605-612.
27. Razga J., Petranek J.. *Eur. Polym. J.* 1975, 11, 805-808.
28. Braun D., Steffan R., *Polymer Bulletin.* 1980, 3, 111-114.
29. Chandrasekhar T.M., White R.L. *J. Appl. Polym. Sci.* 1996, 60, 1209-1219.
30. Teijon C., Olmo R., Blanco M.D., Teijon J.M., Romero A.. *J. of Coll. and Int. Sci.* 2006; 295: 393-400.

31. Demirelli K., Coskun M., Kaya E. *Polym. Degr. and Stab.* 2001, 72: 75-80.
32. Caykara T., Ozyurek C., Kantoglu O., Erdogan B. *Polym. Degr. and Stab.* 2003, 80, 339-343.
33. Fischer H., *Macromolecules*, 1997, 30, 5666-5762.
34. Pintauer T., Matyjaszewski K., *Coordination Chemistry Reviews*, 2005, 249, 1155-1184.
35. Wang X., Luo N., Ying S., *Polymer*, 1999, 40, 4157-4161,.
36. Miller P.J., Matyjaszewski K., *Macromolecules*, 1999, 32, 8760-8767.
37. Moad G., Chiefari J., Chong Y.K.B., Krstina J., Mayadunne R. T.A., Postma A., Rizzardo E., Thang S.H., *Polym International*, 2000, 49, 993-1001.
38. Bai R.K., You Y.Z., Pan C.Y., *Polymer International*, 2000, 49, 898-902.
39. Saricilar S., Knott R., Barner-Kowollik C., Davis T.P., Heuts J.P.A., *Polymer*, 2003, 44, 5169-5176.
40. Eberhardt M., Theato P., *Macromolecular Rapid Communications*, 2005, 26, 1488-1493,
41. Tsujii Y., Ejaz M., Sato K., Goto A., Fukuda T., *Macromolecules*, 2001, 34, 8872-8878.
42. Destarac M., Charmot D., Franck X., Zard S. Z., *Macromolecular Rapid Communications*, 2000, 21, 1035.
43. Lutz J.F., Neugebauer D., Matyjaszewski K., *Journal of American Chemical Society*, 2003, 125, 6986-6993.
44. Boschmann D., Vana P., *Polymer Bulletin*, 2005, 53, 231-242.
45. Chiefari J., Chong Y.K., Ercole F., Krstina J., Jeffery J., Le T.P.T., Mayadunne R.T.A., Meijs G.F., Moad C.L., Moad G., Rizzardo E., Thang S.H., *Macromolecules*, 1998, 31, 5559-5562.
46. Chong Y.K., Le T.P.T., Moad G., Rizzardo E., Thang S.H., *Macromolecules*, 1999, 32, 2071-2074,.
47. Mayadunne R.T.A., Rizzardo E., Chiefari J., Krstina J., Moad G., Postma A., Thang S.H., *Macromolecules*, 33, 243-245, 2000.

48. Mertoglu M., Laschewski A., Skrabania K., Wieland C., *Macromolecules*, 38, 3601-3614, 2005.
49. Chang T.C., Chen H.B., Chen Y.C., Ho S.Y., *Journal of Polymer Science: Part A Polymer Chemistry*, 34, 2613-2620 (1996).
50. Deniz S., Baran N., Akgun M., Akgun N.A., Dincer S., *Turk J Chem*, 28, 645-657 (2004).
51. Lim K.T., Lee M.Y., Hwang H.S., Heo H., Hong S.S., Park J.M., *Polymer Bulletin* 2001, 47, 135-142.
52. Badische Anilin and Soda-Fabrik A.G., GB Patent No. 1219626, 1971.
53. Moore J.S., Stupps., *Macromolecules*, 1990, 23, 65-70.
54. Feng L., Fang H., Zhou S., Wu L., *Macromolecular Chem. and Phys.*, 2006, 207, 1575-1583.
55. Ando I. and Asakura T. 'Solid State NMR of Polymers', edited by Studies in Physical and Theoretical Chemistry, 1998, Vol. 84 Elsevier Science B.V., 1-21.
56. Kumar H., Kumar A.A., Siddar A., *Polymer Degradation and Stability*, 2006, 91, 1097-1104.
57. Matyjaszewski K., Shipp D.A., Wang J.L., Grimaud T., Patten T.E., *Macromolecules*, 1998, 31, 6836-6840.
58. Shipp D.A., Wang J.L., Matyjaszewski K., *Macromolecules*, 1998, 31, 8005-8008.
59. Beamson G., Clark D.T., Law D.S.L., *Surface and Interface Analysis*, 1999, 27, 76-86.
60. Salvati Jr.L., Hook T.J., Gardella J.A.Jr., Chin R.L., *Polymer Engineering and Science*, 1987, 27, 939-944.
61. Feng L., Fang H., Zhou S., Wu L., You B. *Journal of Applied Polymer Science*, 2007, 104, 3356-3366.
62. Chen H., Deng X., Hou X., Luo R., Liu B. *J. of Macromolecular Science Part A: Pure and Applied Chemistry*, 2009, 46, 83-89.

63. Chen L., Hook D.J., Valint P.L.Jr., Gardella J.A.Jr., J. of Vacuum Science and Tehnology, 2008, 26(4), 616-623.
64. Groeninckx G., Reynaers H., J. of Polymer Sci. Polymer Phys. Ed. 1980, 18, 1325-1341.
65. Bassett D.C., Olley R.H., AlRaheil I.A.M., Polymer, 1988, 29(10), 1745-1754.
66. Lee Y., Porter R.S., Macromolecules, 1988, 21, 2110-2776

APPENDIX A

UV-Vis Spectra of Cu(II) Complexes

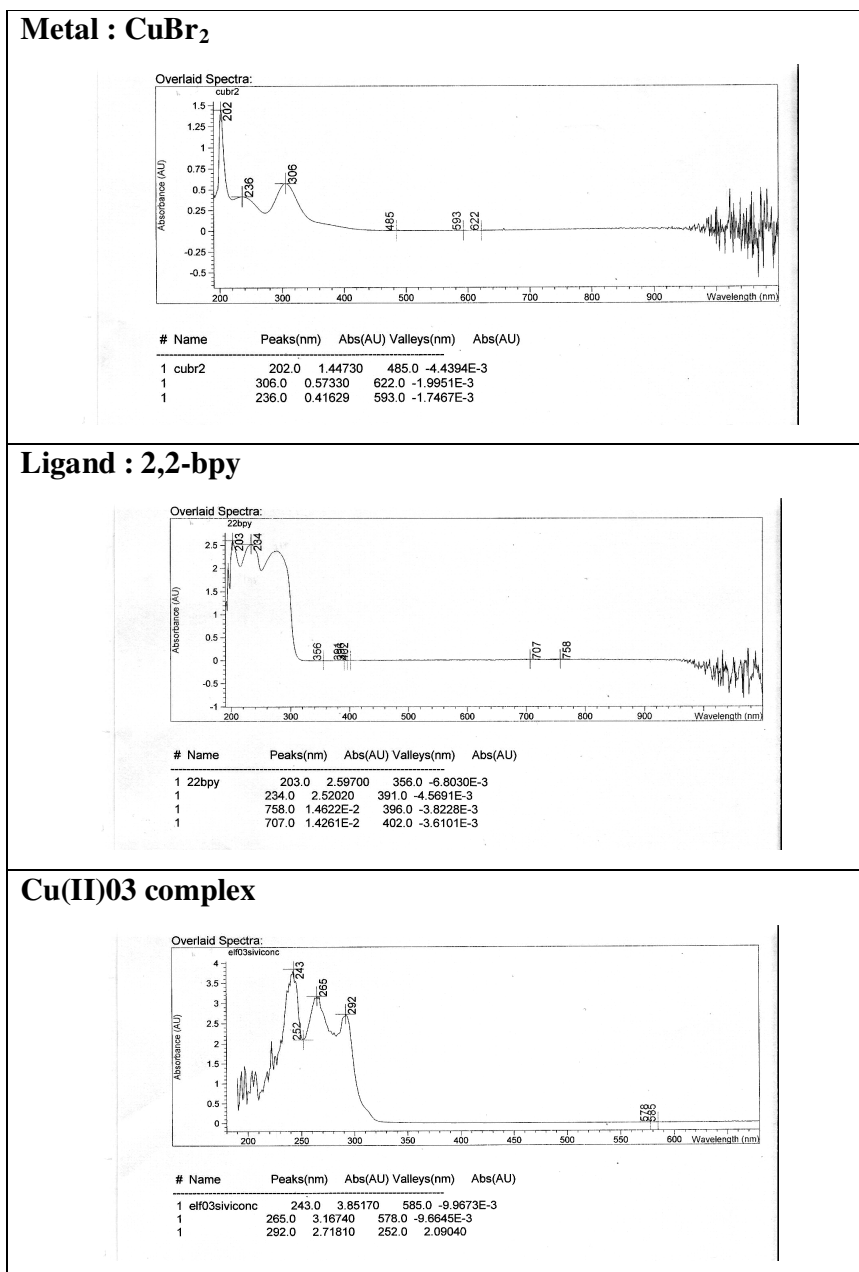
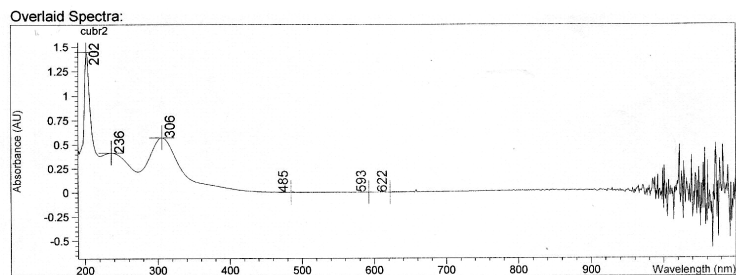


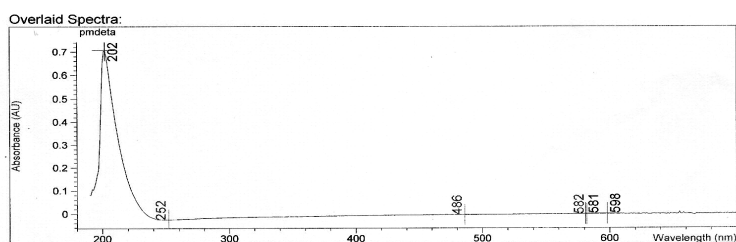
Figure A.1 UV-Vis spectrum of Cu(II)03 complex

Metal : CuBr₂



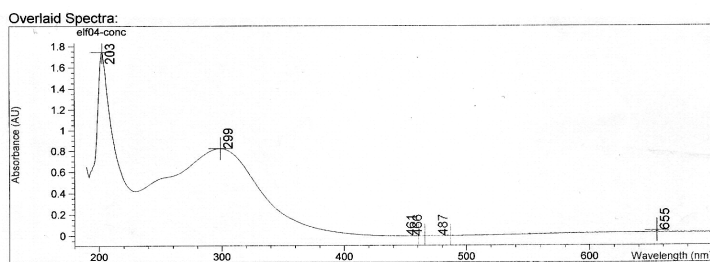
| # | Name | Peaks(nm) | Abs(AU) | Valleys(nm) | Abs(AU) |
|---|-------|-----------|---------|-------------|------------|
| 1 | cubr2 | 202.0 | 1.44730 | 485.0 | -4.4394E-3 |
| 1 | | 306.0 | 0.57330 | 622.0 | -1.9951E-3 |
| 1 | | 236.0 | 0.41629 | 593.0 | -1.7467E-3 |

Ligand : PMDETA



| # | Name | Peaks(nm) | Abs(AU) | Valleys(nm) | Abs(AU) |
|---|---------|-----------|------------|-------------|------------|
| 1 | pmdeata | 202.0 | 0.70642 | 252.0 | -2.5849E-2 |
| 1 | | 598.0 | -1.9155E-3 | 486.0 | -6.5956E-3 |
| 1 | | 581.0 | -2.3117E-3 | 582.0 | -4.5557E-3 |

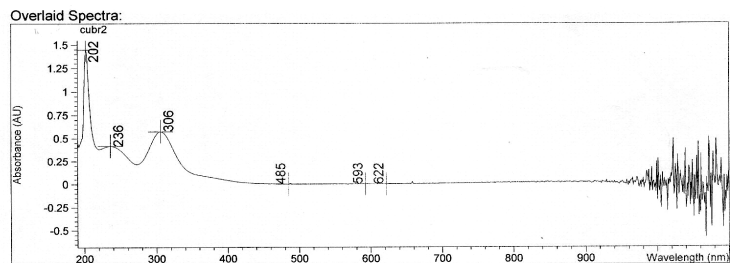
Cu(II)04 complex



| # | Name | Peaks(nm) | Abs(AU) | Valleys(nm) | Abs(AU) |
|---|------------|-----------|-----------|-------------|------------|
| 1 | elf04-conc | 203.0 | 1.74470 | 461.0 | -5.5027E-3 |
| 1 | | 299.0 | 0.82085 | 466.0 | -5.3134E-3 |
| 1 | | 655.0 | 4.0658E-2 | 487.0 | -5.3043E-3 |

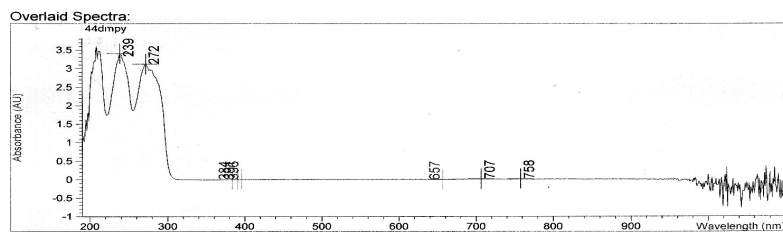
Figure A.2 UV-Vis spectrum of Cu(II)04 complex

Metal : CuBr₂



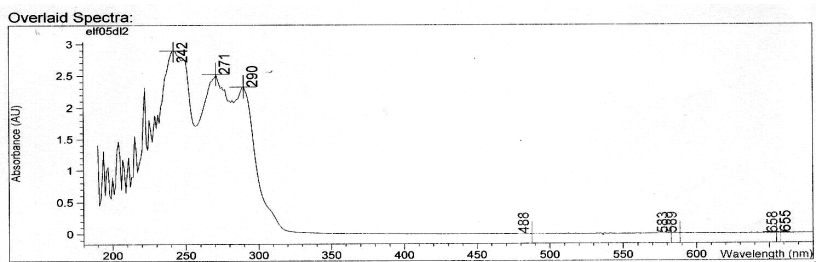
| # | Name | Peaks(nm) | Abs(AU) | Valleys(nm) | Abs(AU) |
|---|-------|-----------|---------|-------------|------------|
| 1 | cubr2 | 202.0 | 1.44730 | 485.0 | -4.4394E-3 |
| 1 | | 306.0 | 0.57330 | 622.0 | -1.9951E-3 |
| 1 | | 236.0 | 0.41629 | 593.0 | -1.7467E-3 |

Ligand : 4,4-Dmbpy



| # | Name | Peaks(nm) | Abs(AU) | Valleys(nm) | Abs(AU) |
|---|---------|-----------|-----------|-------------|------------|
| 1 | 44dmbpy | 239.0 | 3.39930 | 657.0 | -1.2693E-2 |
| 1 | | 272.0 | 3.11670 | 391.0 | -8.0533E-3 |
| 1 | | 707.0 | 7.7901E-3 | 384.0 | -7.9269E-3 |
| 1 | | 758.0 | 7.0767E-3 | 396.0 | -7.5936E-3 |

Cu(II)05 complex



| # | Name | Peaks(nm) | Abs(AU) | Valleys(nm) | Abs(AU) |
|---|----------|-----------|-----------|-------------|------------|
| 1 | elf05dl2 | 242.0 | 2.89260 | 658.0 | -1.4823E-2 |
| 1 | | 271.0 | 2.52210 | 583.0 | -1.0549E-2 |
| 1 | | 290.0 | 2.32200 | 589.0 | -1.0065E-2 |
| 1 | | 655.0 | 2.4080E-4 | 488.0 | -9.2731E-3 |

Figure A.3 UV-Vis spectrum of Cu(II)05 complex

APPENDIX B

GPC MW Distribution Plots

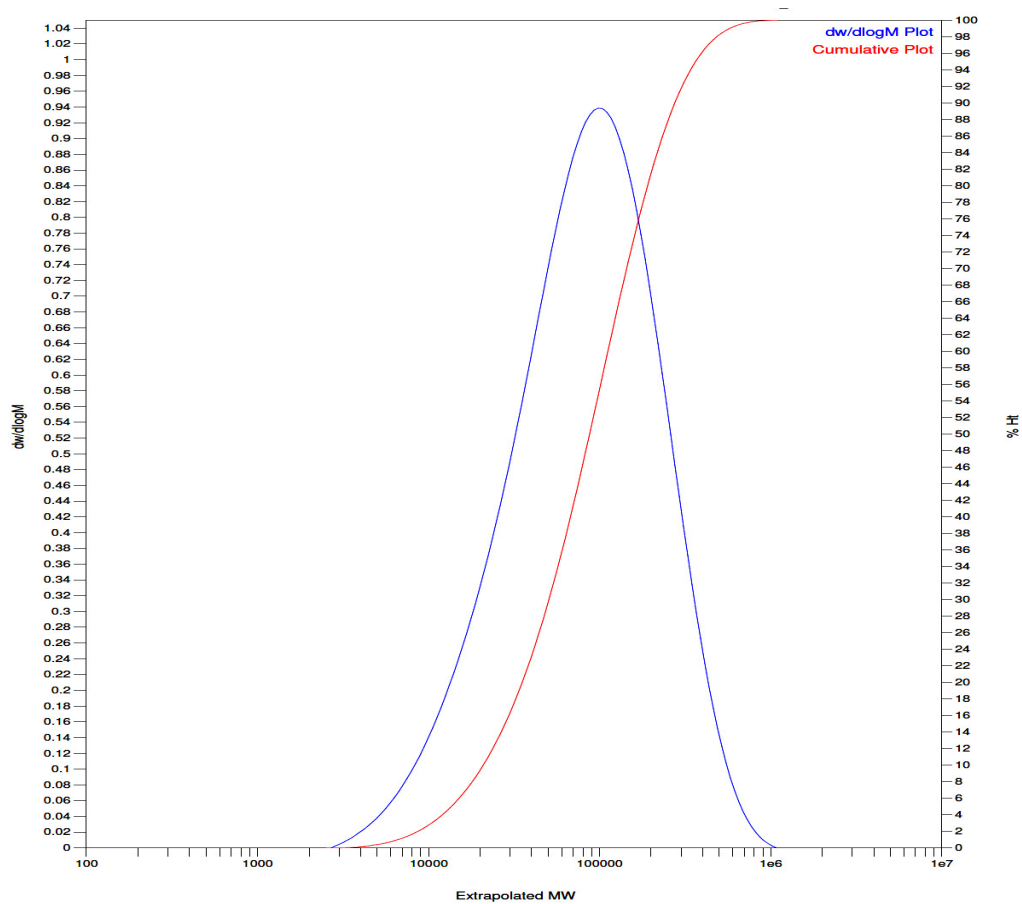


Figure B.1 Molecular weight distribution plot of P_{7.7}M(8) copolymer

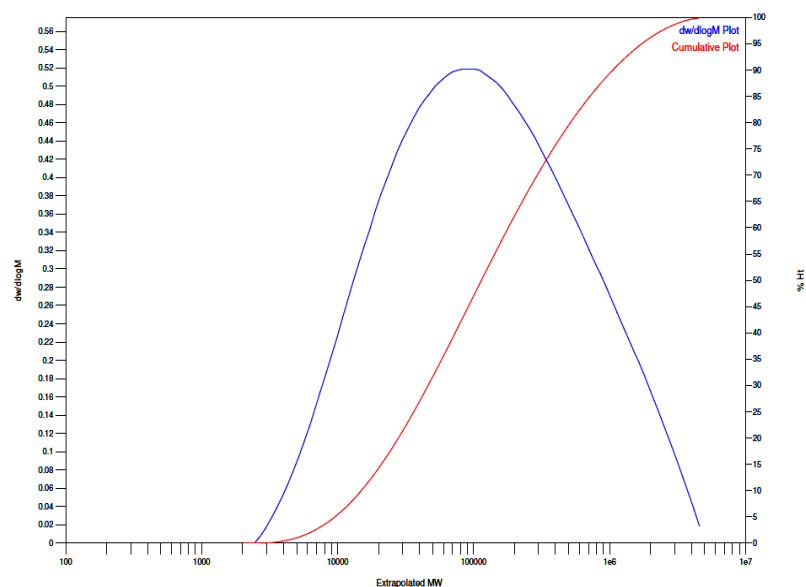


Figure B.2 Molecular weight distribution plot of PDMS-MAI macroazoinitiator

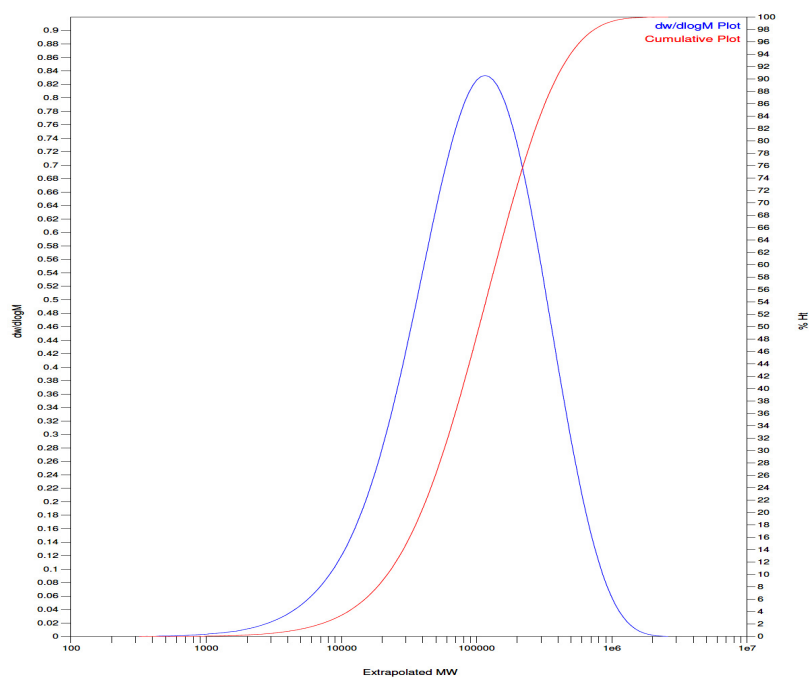


Figure B.3 Molecular weight distribution plot of P_{6.8}E(4) copolymer

APPENDIX C

XPS Results of copolymers

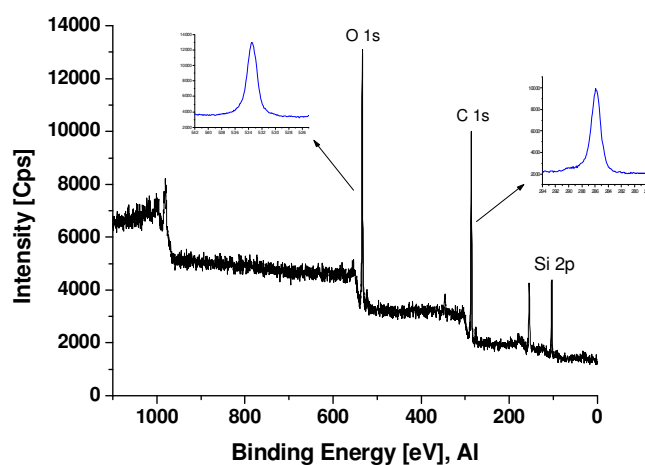


Figure C.1 Full scan XPS of P_{14.3}M(12) copolymer on air side

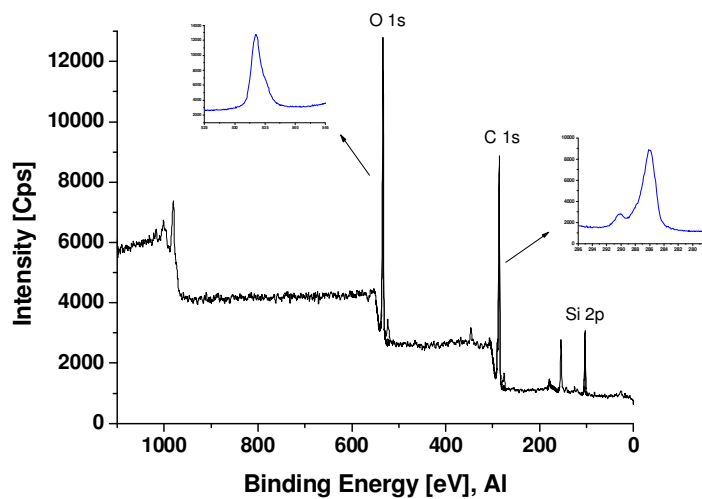


Figure C.2 Full scan XPS of P_{14.3}M(12) copolymer on glass side

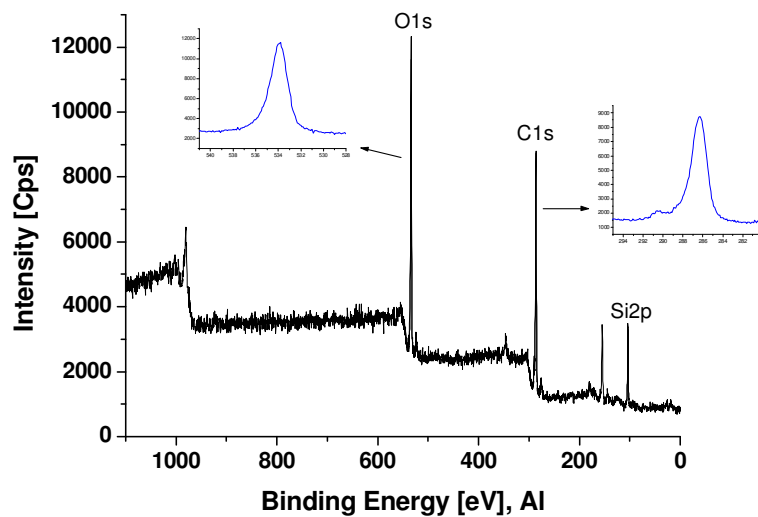


Figure C.3 Full scan XPS of P_{6.8}E(12) copolymer on air side

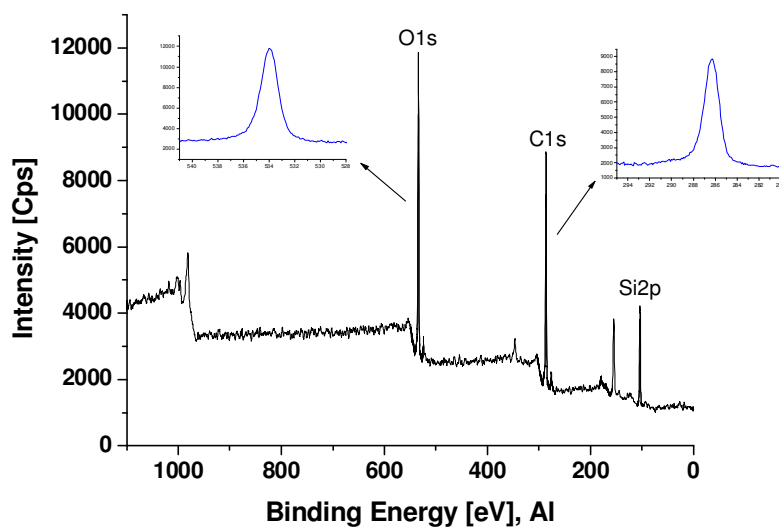
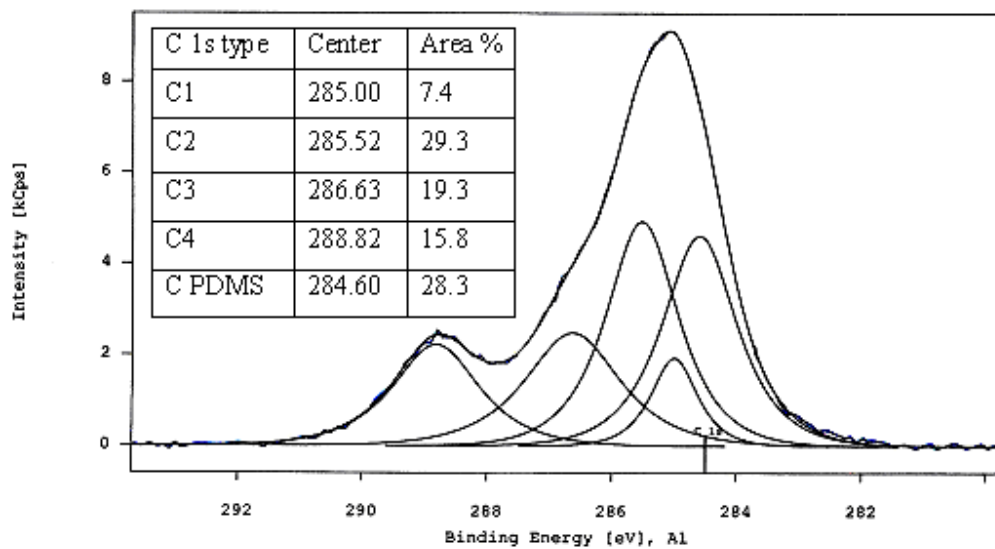
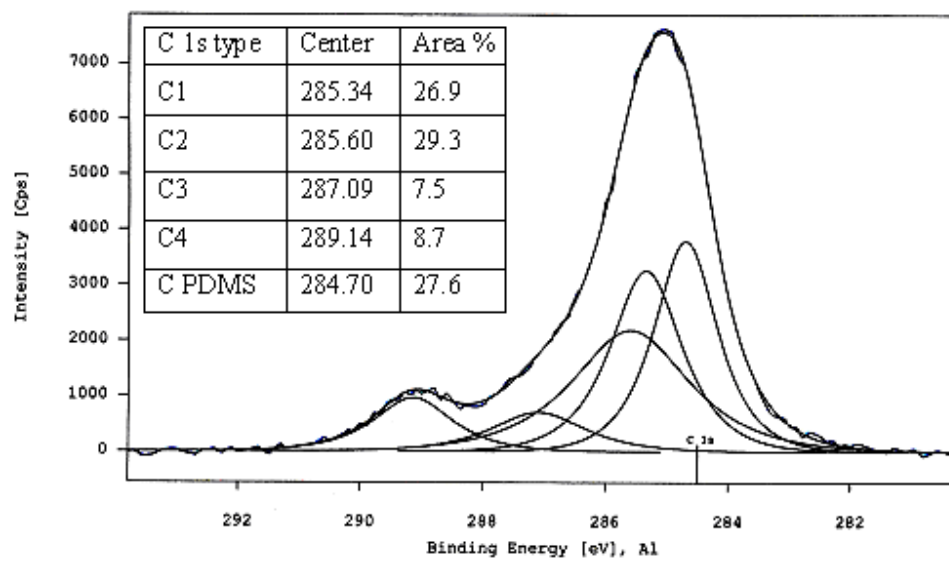


Figure C.4 Full scan XPS of P_{6.8}E(12) copolymer on glass side

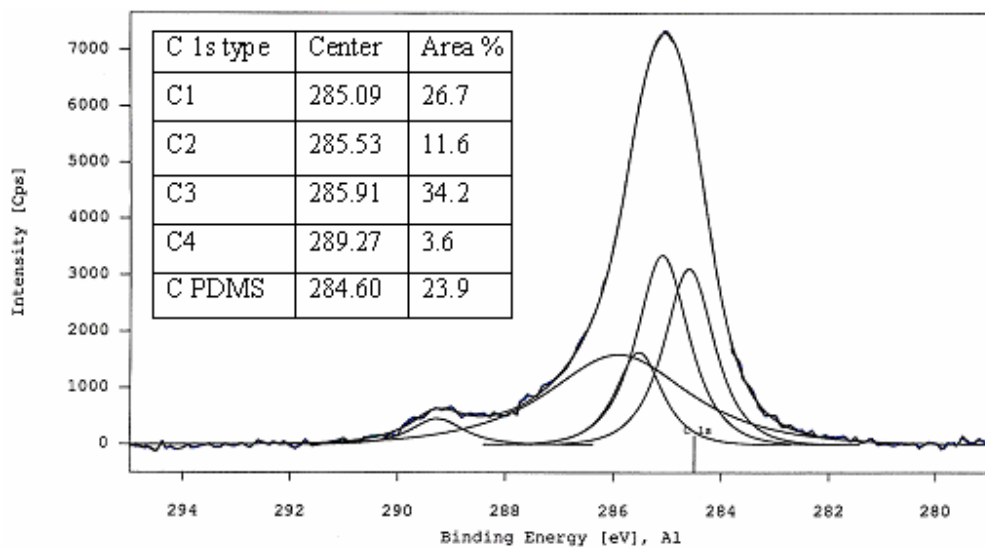
a)



b)



c)



d)

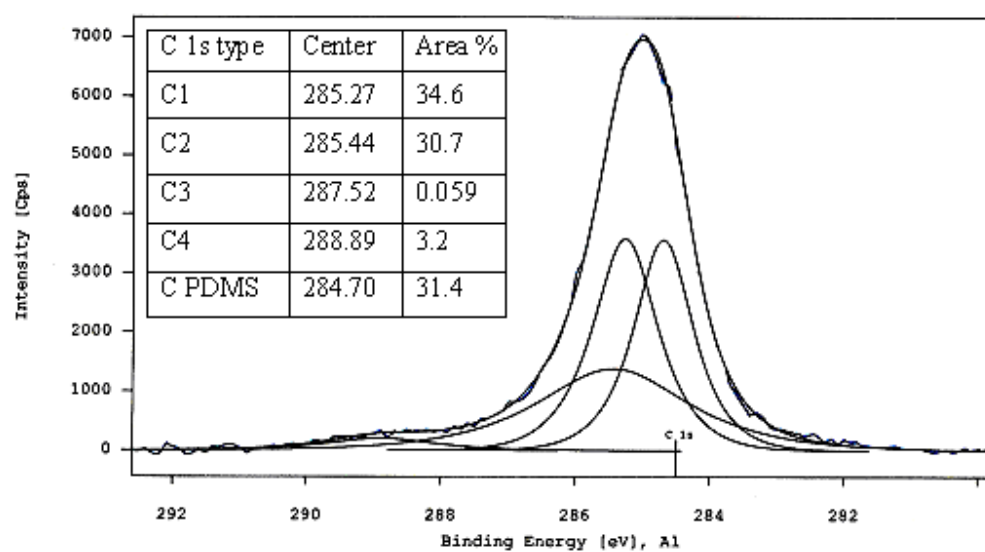


Figure C.5 C1s XPS spectra of P_{1.8}E(12) (a air side, b glass side) and P_{6.8}E(12) (c air side, d glass side) copolymers

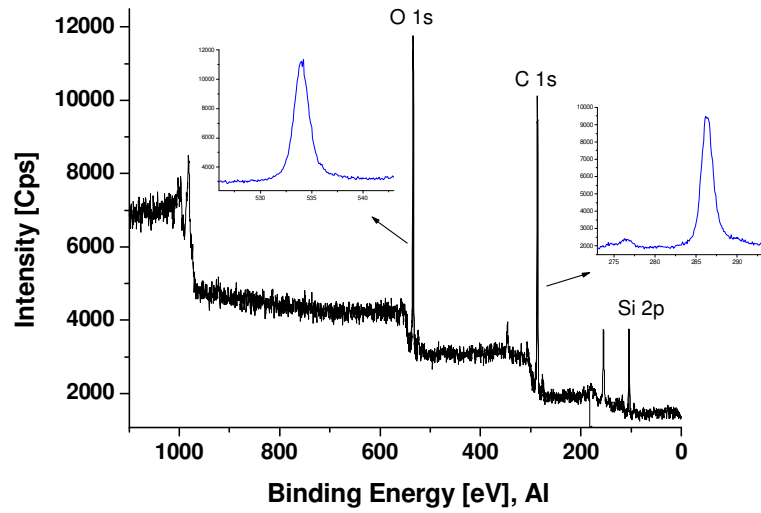


Figure C.6 Full scan XPS of P_{4.6}TH(12) copolymer on air side

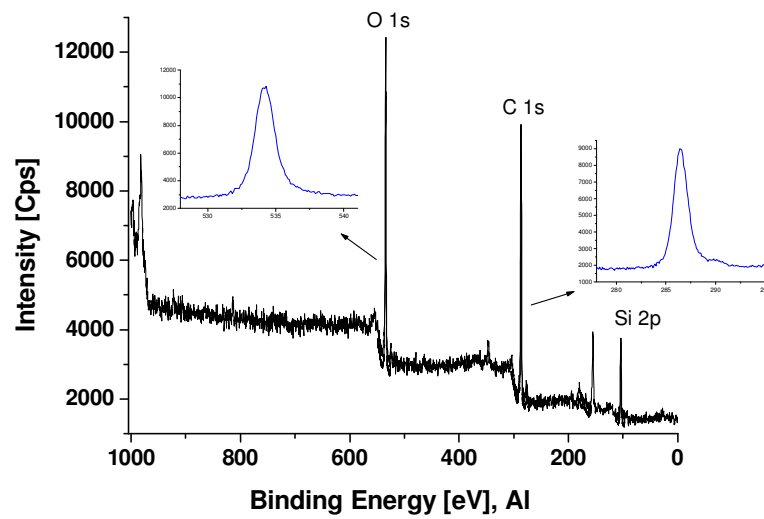
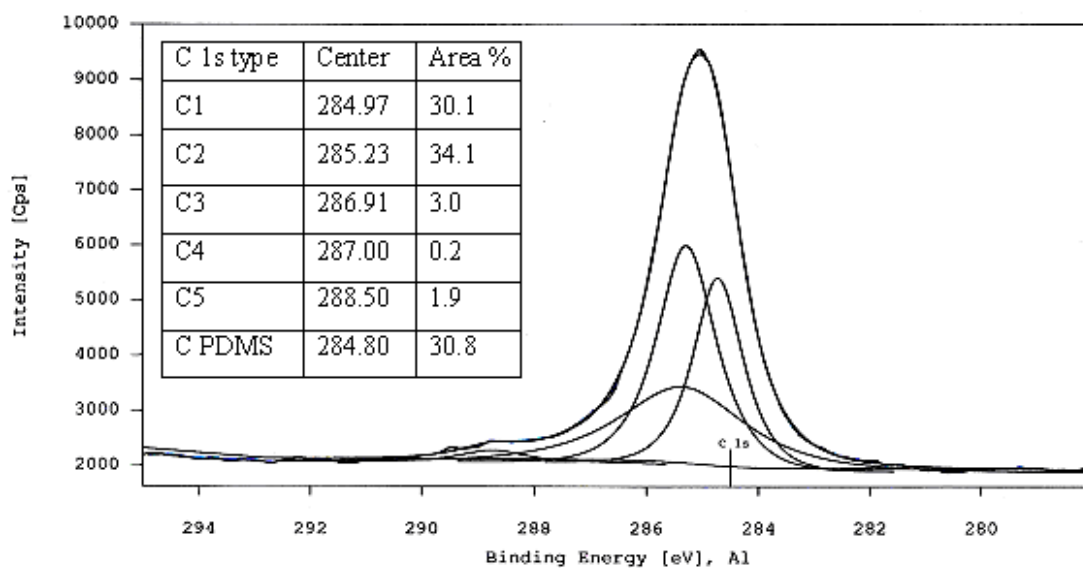
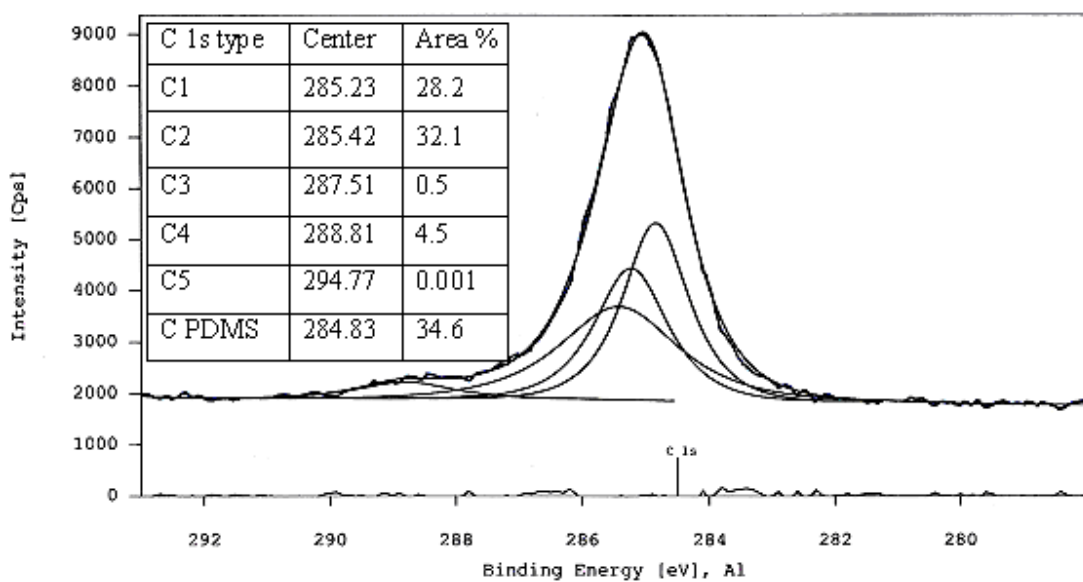


Figure C.7 Full scan XPS of P_{4.6}TH(12) copolymer on glass side

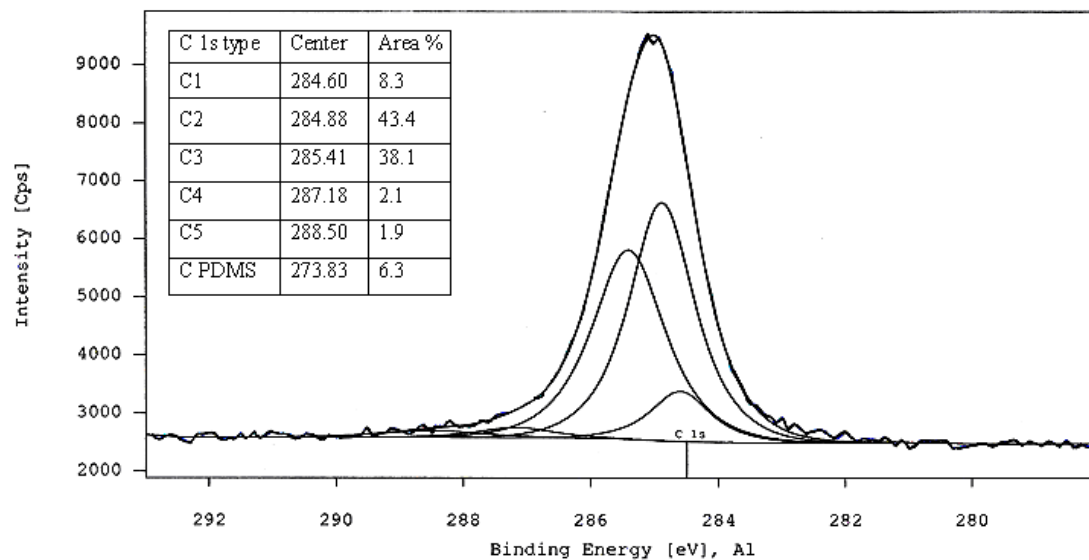
a)



b)



c)



d)

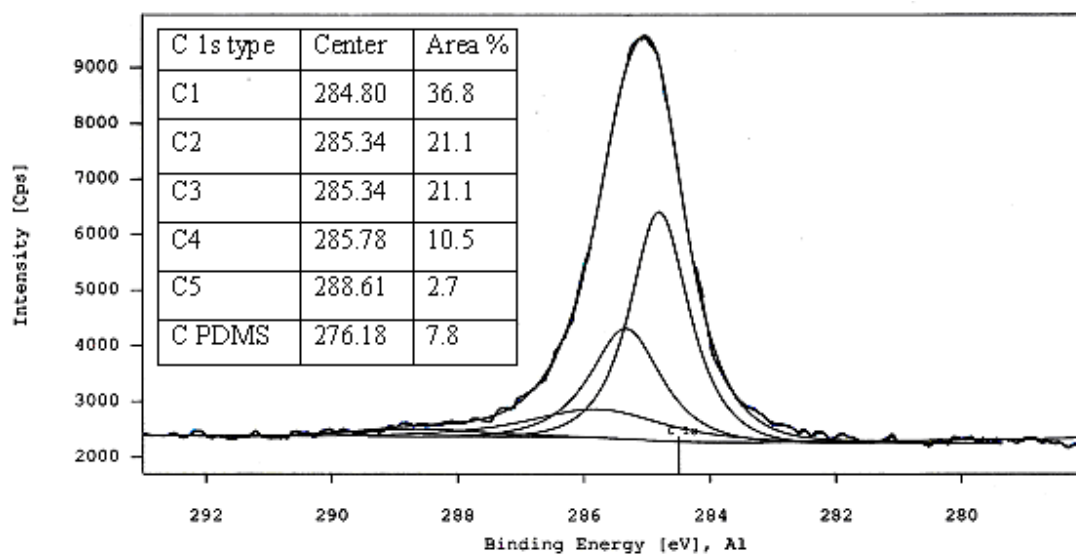


Figure C.8 C1s XPS spectra of P_{4.6}TH(12) (a air side, b glass side) and P_{8.7}TH(12) (c air side, d glass side) copolymers

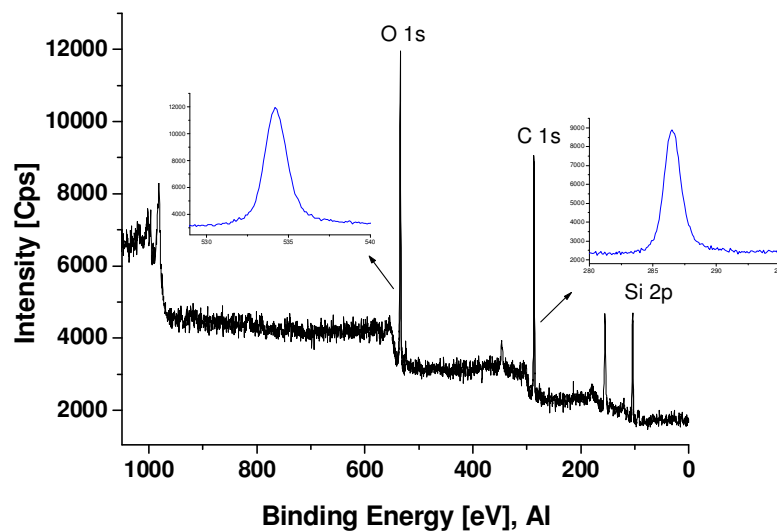


Figure C.9 Full scan XPS of P_{16.1}H copolymer (after deprotection) on air side

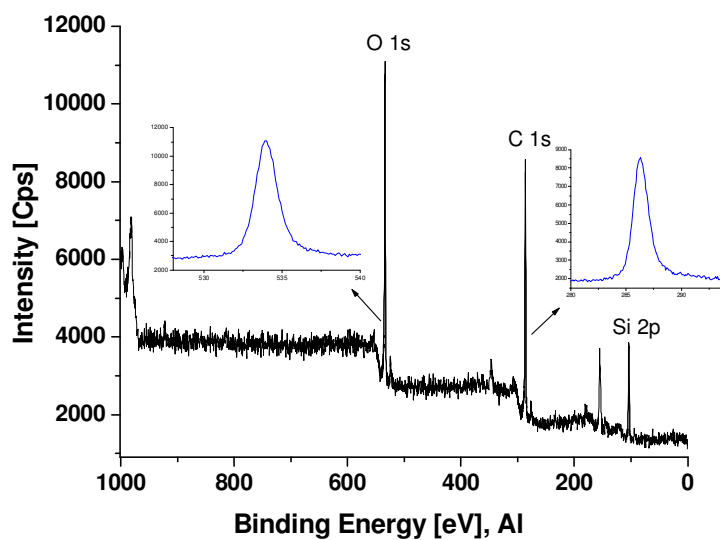
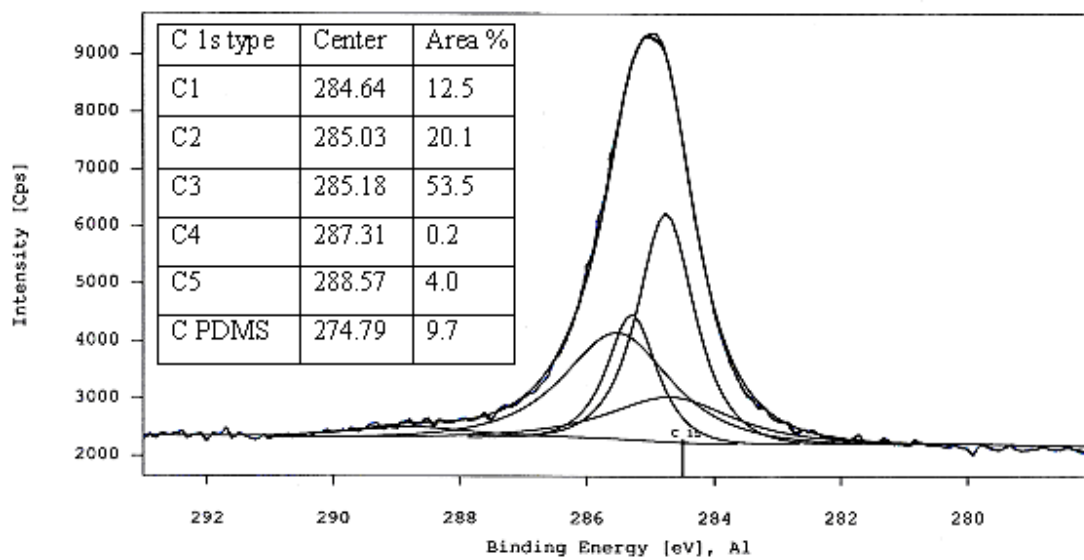
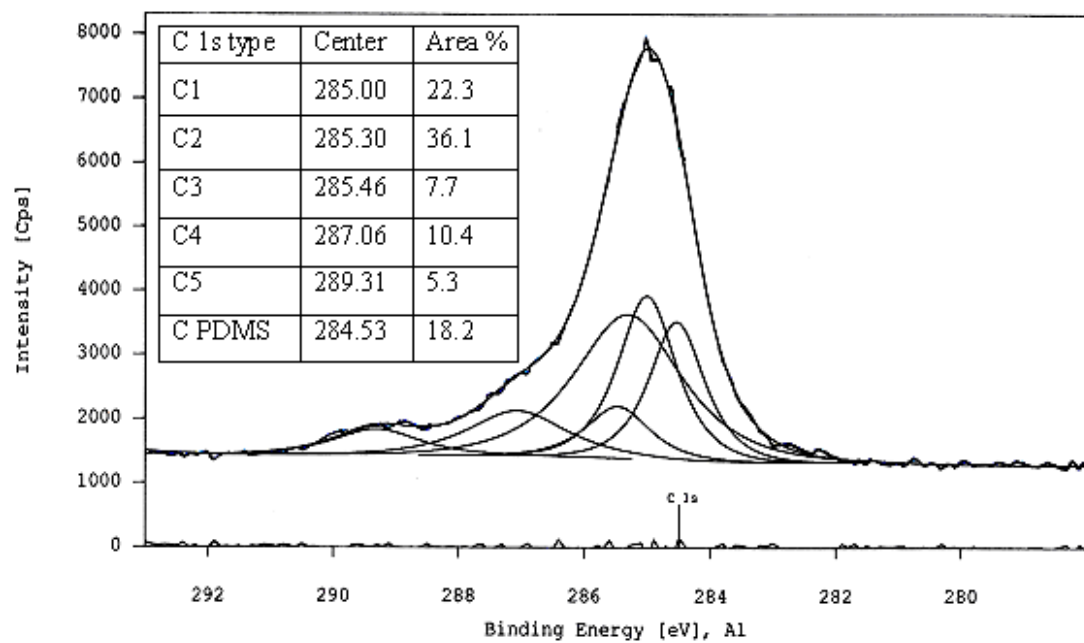


Figure C.10 Full scan XPS of P_{16.1}H copolymer (after deprotection) on glass side

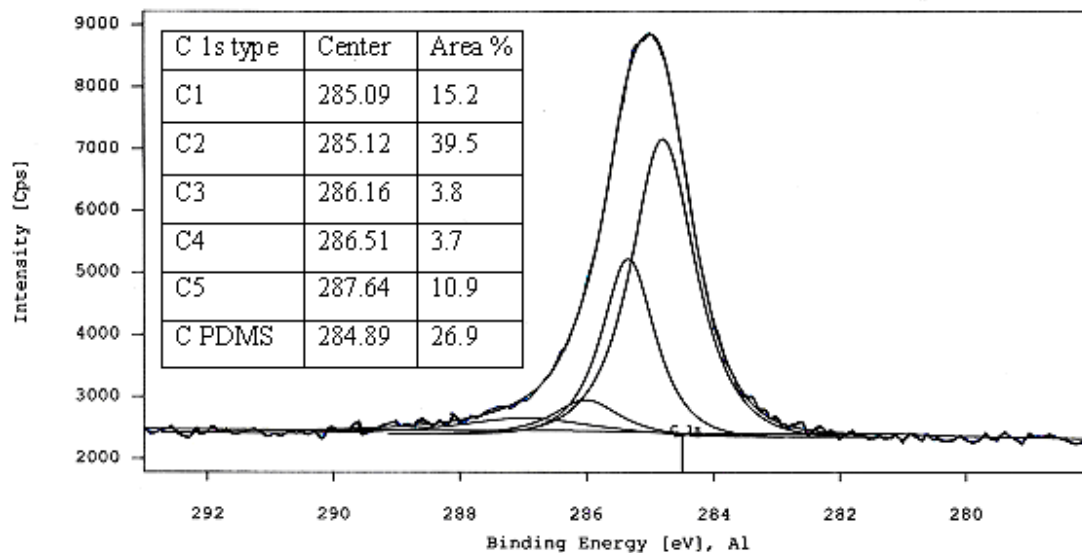
a)



b)



c)



d)

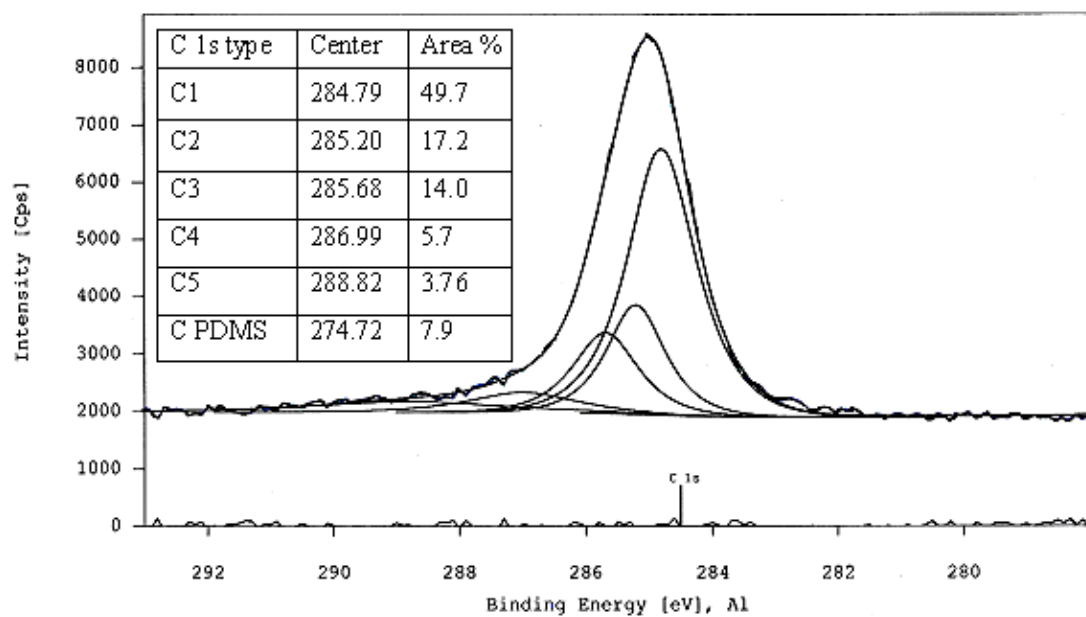


Figure C.11 C1s XPS spectra of P_{4.6}H(8) (a air side, b glass side) and P_{16.1}H(8) (c air side, d glass side) copolymers

CURRICULUM VITAE

PERSONAL INFORMATION

Surname, Name: Vargün, Elif

Nationality: Turkish (T.C.)

Date and Place of Birth: 08 August 1977, Ankara

Marital Status: Single

Phone: +90 312 210 3114

Fax: +90 312 210 3200

E-mail: evargun@metu.edu.tr

EDUCATION

| Degree | Institution | Year of Graduation |
|-------------|-------------------------------|--------------------|
| MS | METU Dept. of Chemistry | 2003 |
| BS | Gazi Uni. Dept. of Chem. Edu. | 1999 |
| High School | Bahçelievler Deneme | 1994 |

WORK EXPERIENCE

| Year | Place | Enrollment |
|-------|------------------------|--------------------|
| 2001- | METU Dept. of Chemistr | Research Assistant |

FOREIGN LANGUAGES: English

PUBLICATIONS

1. Vargün E., Usanmaz A., “Polymerization of 2-hydroxyethyl acrylate in bulk and solution by chemical initiator and by ATRP method”, *Jour. of Polym. Sci.: Part A, Polym. Chem.*, Vol 43, pp. 3957-3965, 2005.

2. Aran B., Sankır M., Vargün E., Sankır N.D., Usanmaz A. “Tailoring the swelling and glass transition temperature of the Acrylonitrile/Hydroxyethyl Acrylate copolymers” *Journal of Applied Polymer Science* (accepted).

ORAL PRESENTATIONS

1. Vargün Elif, Usanmaz Ali, Polymerization and Characterization of 2-Hydroxyethyl acrylate, National Chemistry Conference, Kars, 5-9 July 2004

POSTER PRESENTATIONS

1. Vargun, Elif; Usanmaz, Ali, Thermal degradation of poly(2-hydroxyethyl methacrylate) obtained by gamma radiation, 234th ACS National Meeting, Boston, MA, United States, 19-23 August, 2007
2. Vargun Elif, Usanmaz Ali, RAFT polymerization of HEMA in different solvents, Controlled/Living Polymerization: From Synthesis to Applications, CLP07, Antalya TURKEY, 25-29 October 2007